

Astrophysical Objects

Active Galaxies

Based on: An introduction to modern Astrophysics chapter 28

Helga Dénés 2023 S2 Yachay Tech
hdenes@yachaytech.edu.ec



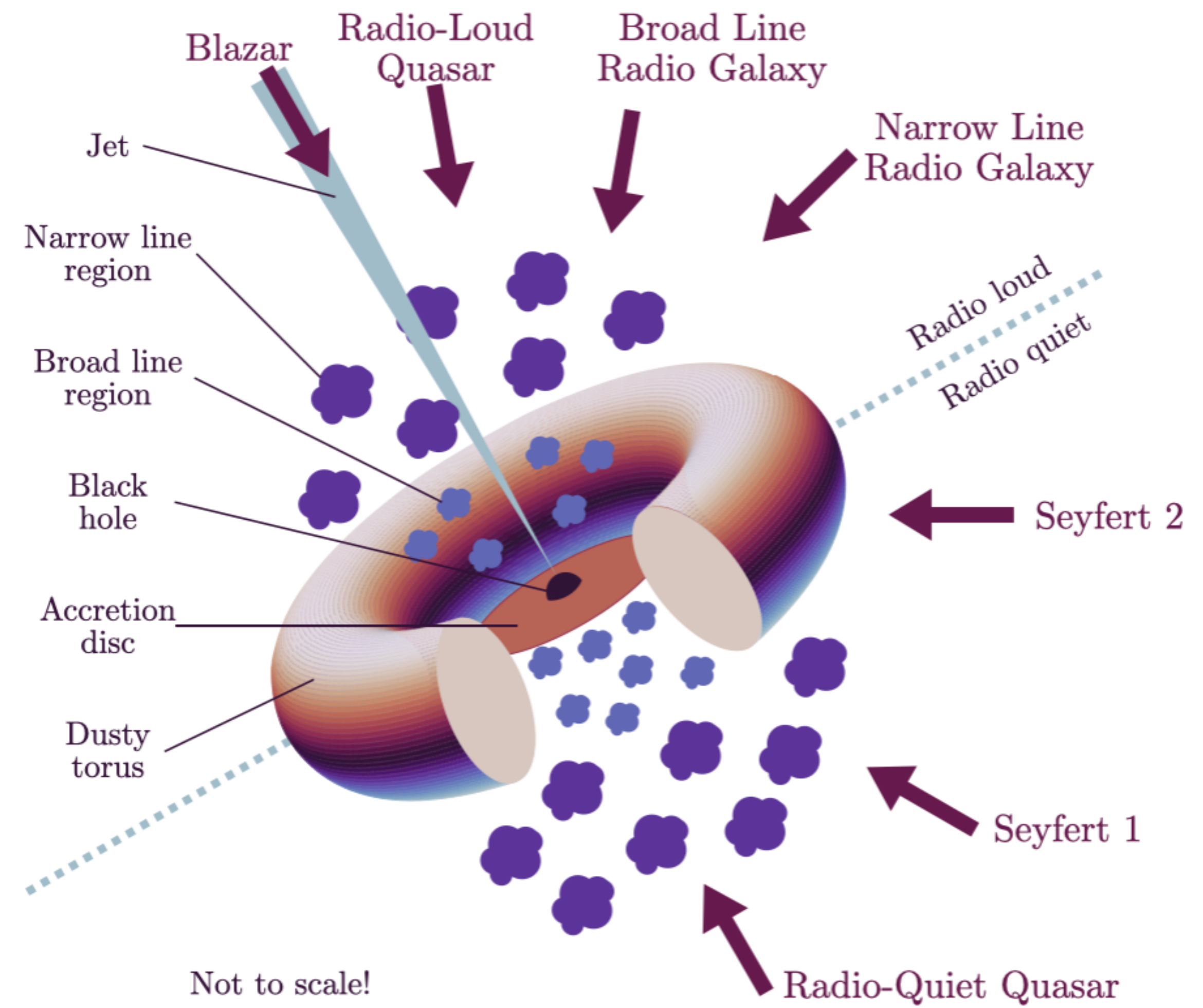
**SCHOOL OF
PHYSICAL SCIENCES
AND NANOTECHNOLOGY**

The unified model of AGN

Unified model of AGN adapted from Urry & Padovani (1995).

The thick arrows represent different viewing angles, and the observed object which results from them.

Note the asymmetry of the diagram; this is to demonstrate the two different possibilities of radio loud/quiet and is not representative of a single object.



Seyfert galaxies

NGC 1068

Edward A. Fath (1880– 1959), who in 1908 was observing the spectra of “**spiral nebulae**.”

Although most showed an absorption-line spectrum produced by the combined light of the galaxy’s stars, NGC 1068 displayed six **bright emission lines**.

In 1926 Edwin Hubble recorded the emission lines of this and two other galaxies.

Seventeen years later Carl K. Seyfert (1911–1960) reported that **a small percentage of galaxies have very bright nuclei** that are the source of **broad emission lines** produced by atoms in a **wide range of ionization states**. These nuclei are nearly stellar in appearance.



Seyfert galaxies

Today these objects are known as **Seyfert galaxies**, with spectra that are categorized into one of two classes. **Seyfert 1** galaxies have **very broad emission lines** that include both allowed lines (H I, He I, He II) and narrower forbidden lines (such as [O III]). Seyfert 1 galaxies generally have “narrow” allowed lines as well, although even the narrow lines are broad compared to the spectral lines exhibited by normal galaxies. The width of the lines is attributed to **Doppler broadening**, indicating that the allowed lines originate from sources with **speeds typically between 1000 and 5000 km s⁻¹**, while the forbidden lines correspond to speeds of around 500 km s⁻¹.

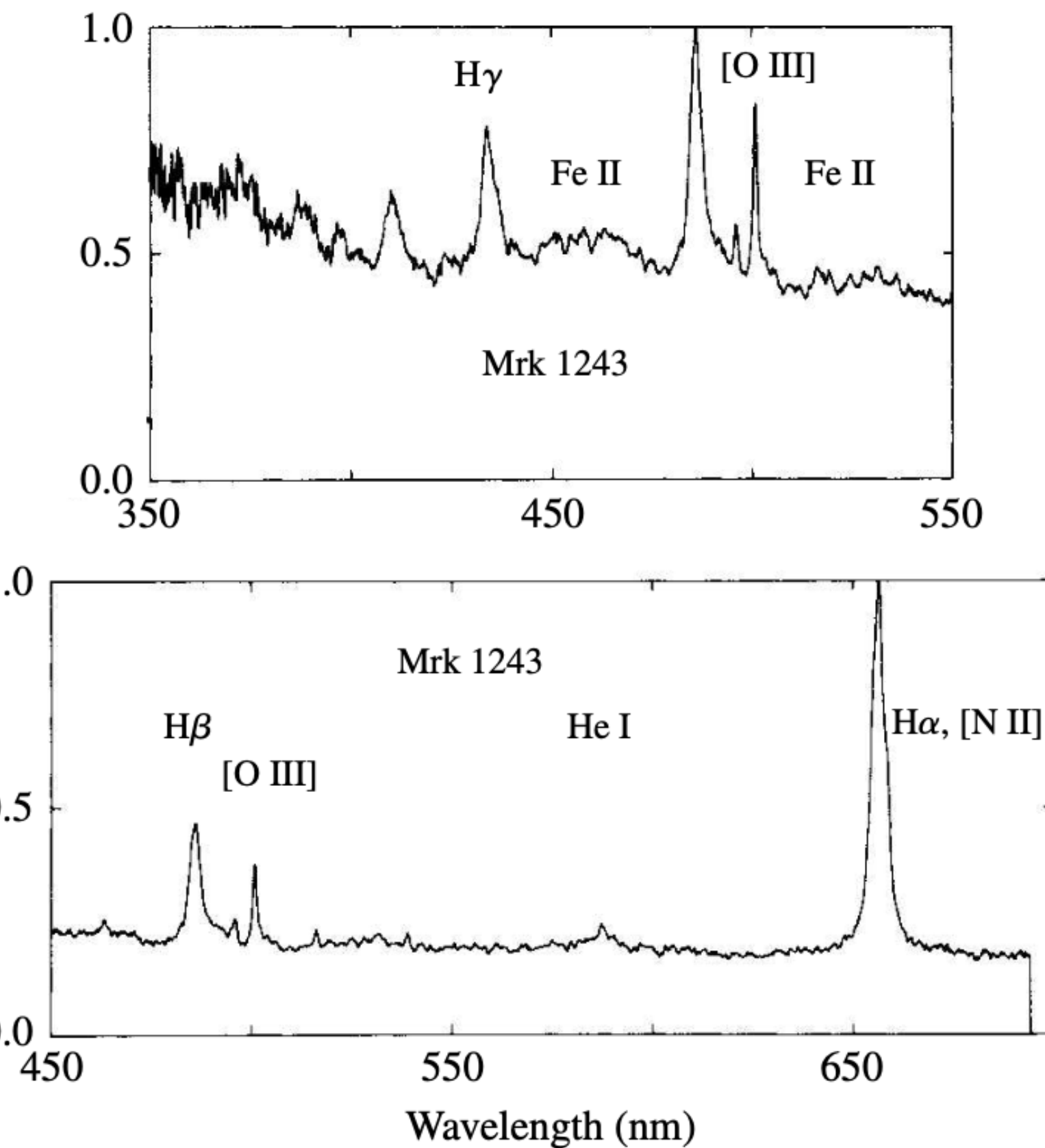


FIGURE 1 The visible spectrum of Mrk 1243, a Seyfert 1 galaxy. (Figure adapted from Osterbrock, *QJRAS*, 25, 1, 1984.)

Seyfert galaxies

Mrk 1243 - PanSTARS image

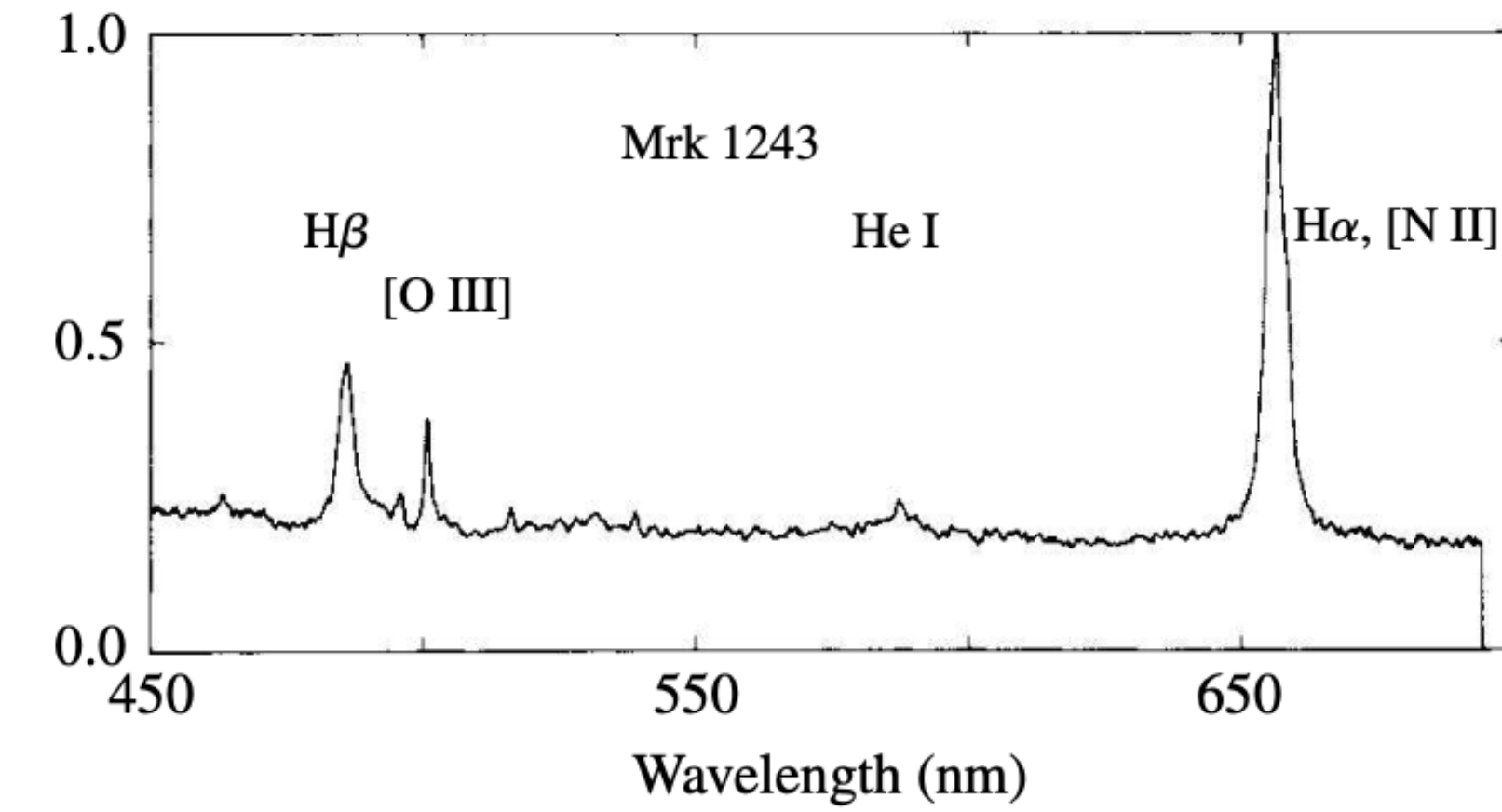
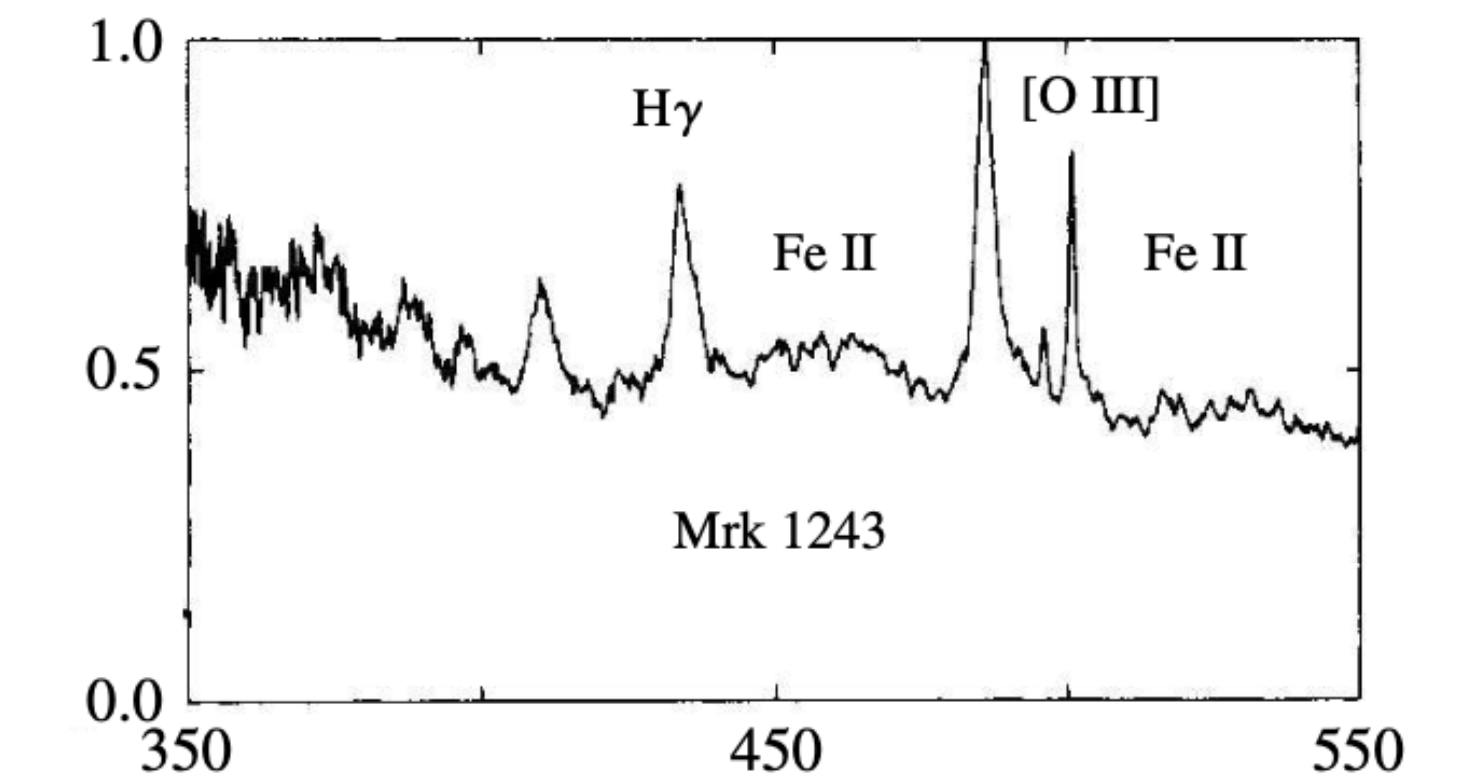


FIGURE 1 The visible spectrum of Mrk 1243, a Seyfert 1 galaxy. (Figure adapted from Osterbrock, *QJRAS*, 25, 1, 1984.)

Seyfert galaxies

Seyfert 2 galaxies have **only narrow lines** (both permitted and forbidden), with characteristic **speeds of about 500 km s⁻¹**. Every spectrum also shows a **featureless continuum** that is devoid of lines, originating from a small central source. The **great luminosity** of a Seyfert 1 galaxy arises from this continuum, which often overwhelms the combined light of all of the galaxy's stars. The continuum observed for a Seyfert 2 is significantly less luminous.

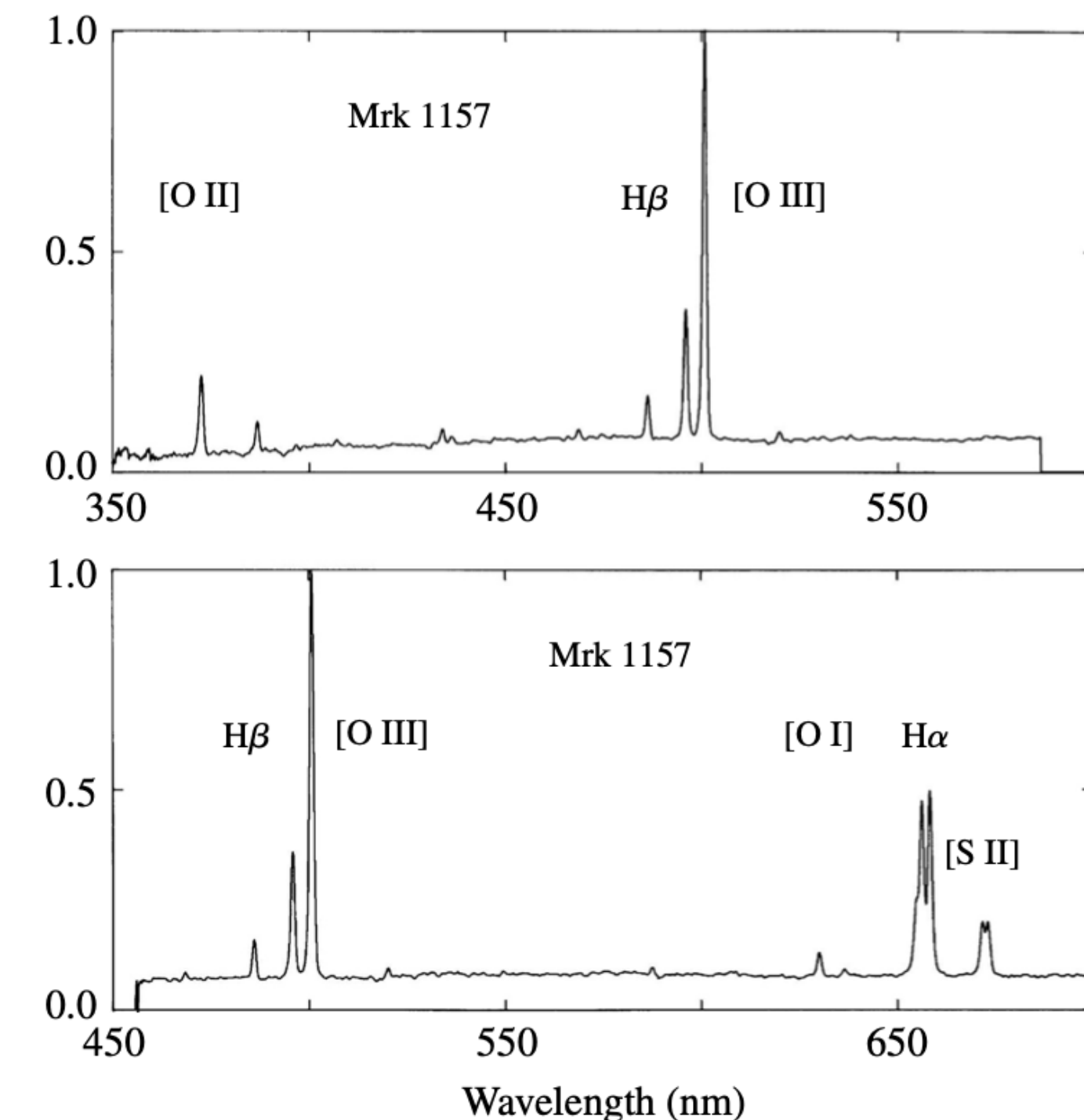


FIGURE 2 The visible spectrum of Mrk 1157, a Seyfert 2 galaxy. (Figure adapted from Osterbrock, *QJRAS*, 25, 1, 1984.)

Seyfert galaxies

Mrk 1157 - PanSTARS image

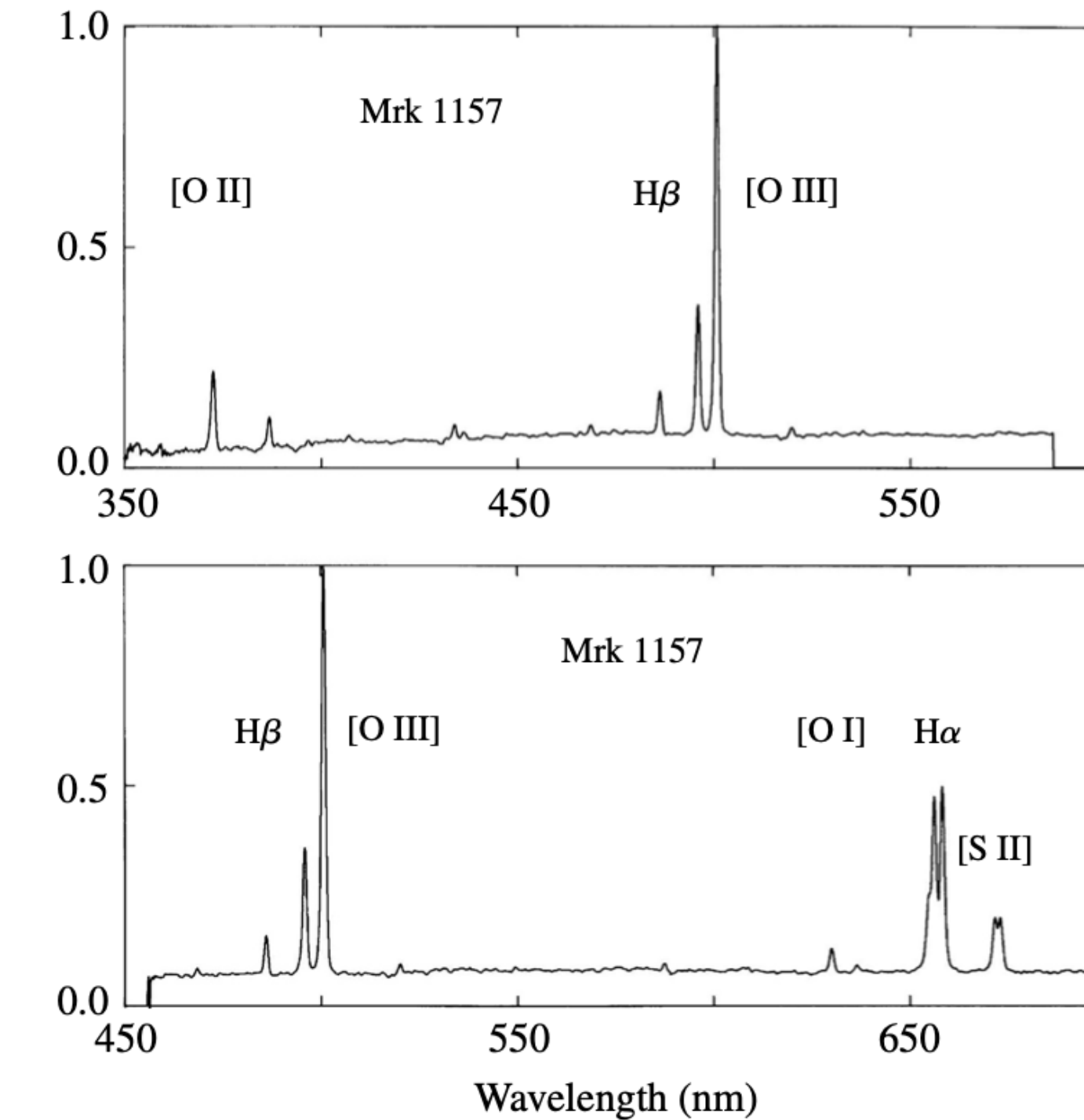
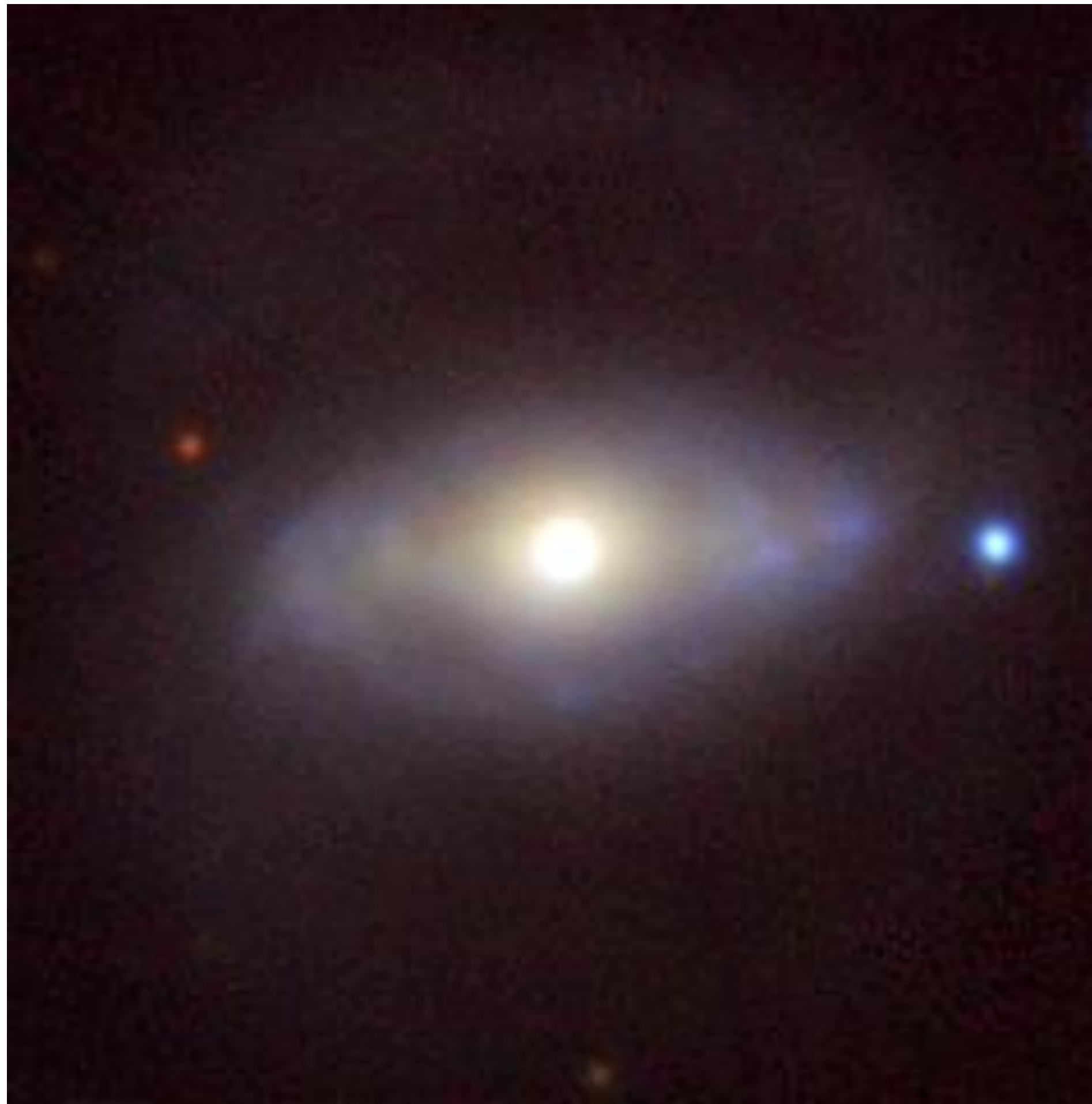


FIGURE 2 The visible spectrum of Mrk 1157, a Seyfert 2 galaxy. (Figure adapted from Osterbrock, *QJRAS*, 25, 1, 1984.)

Seyfert galaxies

The black hole-powered core of a nearby active galaxy appears in this colorful Hubble image. The galaxy lies 13 million light-years away in the southern constellation Circinus. This galaxy is designated a **type 2 Seyfert**.

AGN have the ability to remove gas from the centers of their galaxies by blowing it out into space at phenomenal speeds. Much of the gas in the disk of the Circinus spiral is concentrated in two specific rings — a larger one of diameter 1,300 light-years, and a previously unseen ring of diameter 260 light-years.

The smaller **inner ring is located on the inside of the green disk**. The **larger outer ring extends off the image** and is in the plane of the galaxy's disk. Both rings are home to large amounts of gas and dust as well as areas of major "**starburst**" activity, where new stars are rapidly forming on timescales of 40 - 150 million years, much shorter than the age of the entire galaxy.

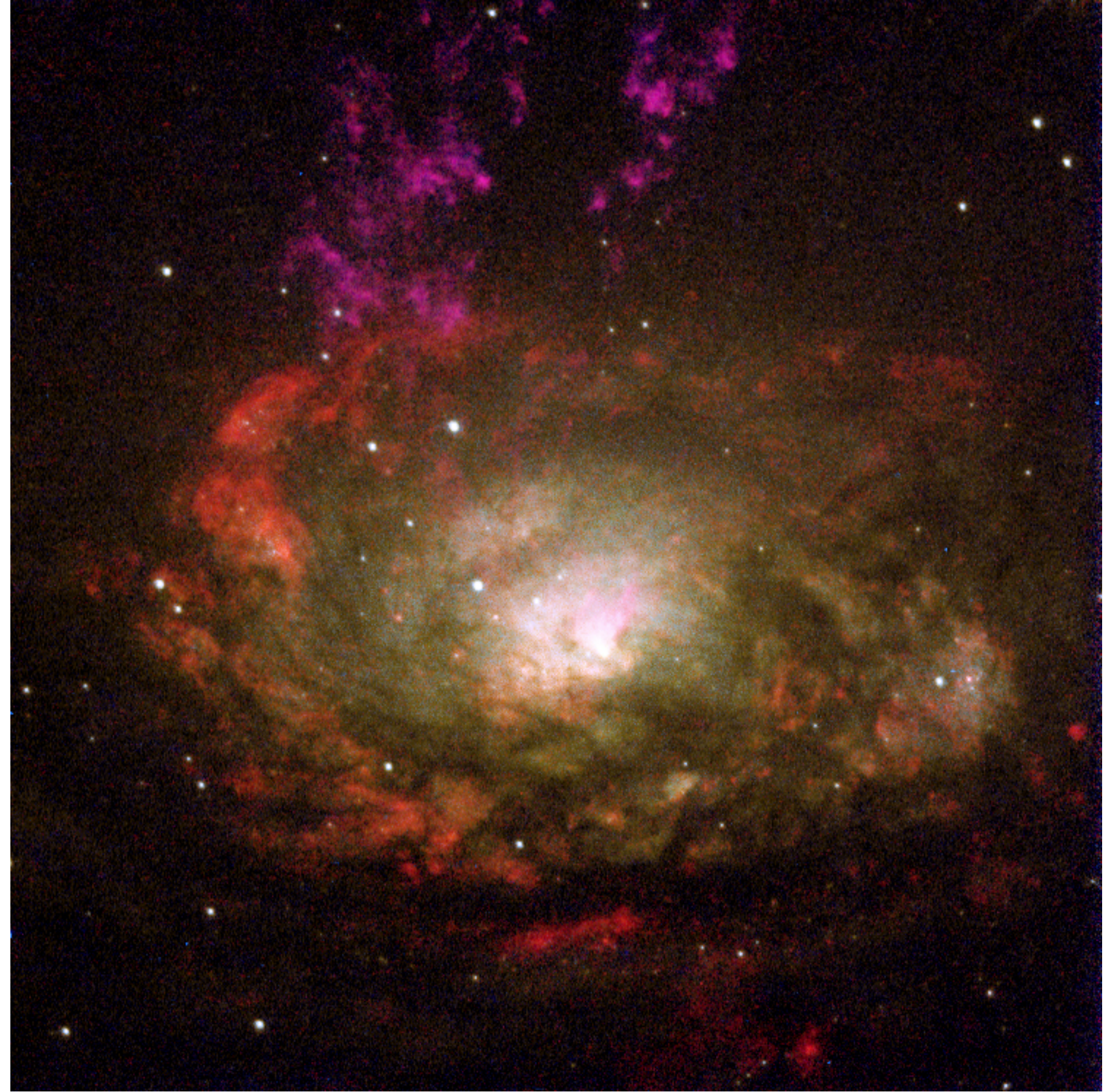


Seyfert galaxies

At the center of the starburst rings is the Seyfert nucleus, the supermassive black hole that is accreting. The black hole and its accretion disk are **expelling gas out of the galaxy's disk** and into its halo (the region above and below the disk). This gas is seen as **magenta-colored streamers** extending towards the top of the image.

In the center of the galaxy and within the inner starburst ring is a **V-shaped structure of gas**. The structure appears whitish-pink in this composite image. This region, which is the projection of a **three-dimensional cone** extending from the nucleus to the galaxy's halo, contains gas that has been heated by radiation emitted by the accreting black hole. A "**counter-cone**," believed to be present, is obscured from view by dust in the galaxy's disk.

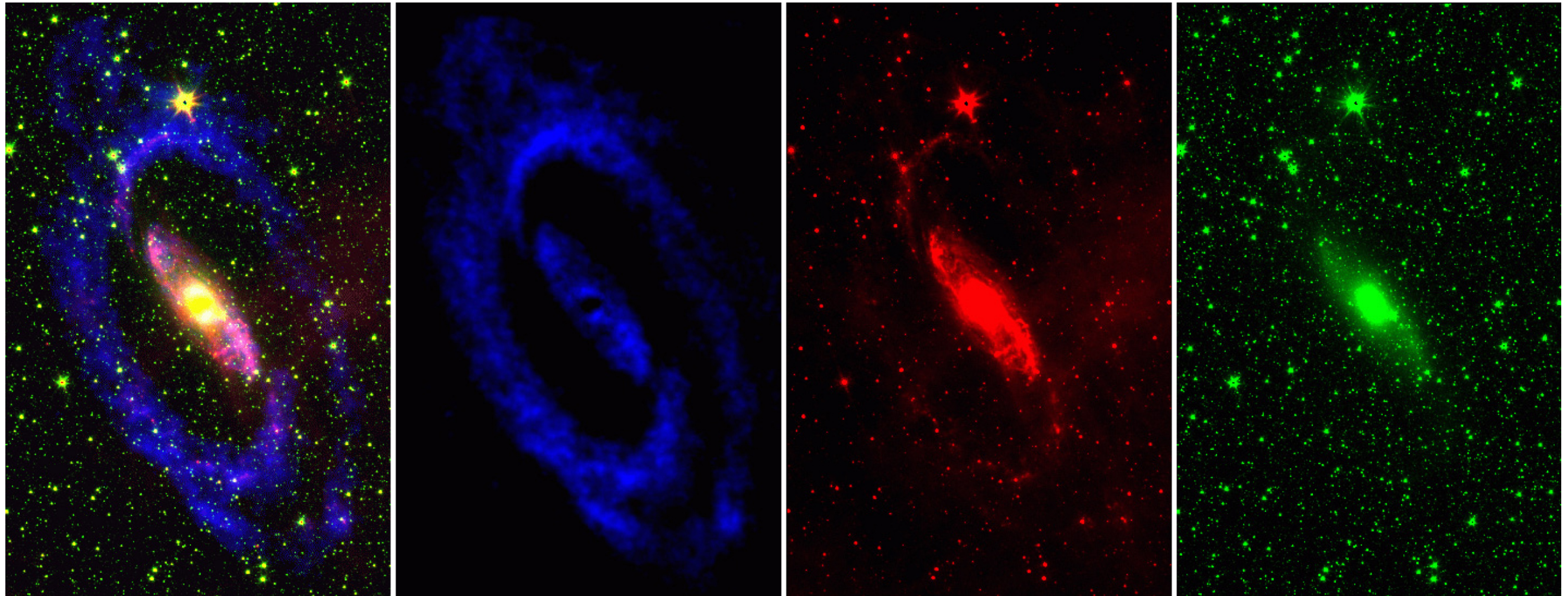
Ultraviolet radiation emerging from the central source excites nearby gas causing it to glow. **The excited gas is beamed into the oppositely directed cones** like two giant searchlights.



Seyfert galaxies

The **Circinus Galaxy** as seen at different wavelengths. The three single-color panels show the **ATCA HI gas distribution** at an angular resolution of 15 arcsec (only the inner disk is shown here), the **Spitzer 8 micron image** (PAH emission + stars) and the **Spitzer 3.6 micron image** (stars).

For et al 2012



Seyfert galaxies

Some spectra display **both broad and narrow permitted lines**, and so they are classified as an **intermediate type** such as Seyfert 1.5. However, it is important to emphasize that this is a spectral classification. The **spectra of a few Seyfert galaxies have changed nearly from type 1.5 to type 2 in a matter of years**, although the broad H α emission line has rarely if ever completely disappeared.

The galaxies known to emit the **most X-ray energy are Seyferts of types 1 and 1.5**. The X-ray emission is quite **variable**, and can change appreciably on **timescales ranging from days to hours**.

In contrast, **X-rays are less frequently measured for Seyfert 2** galaxies. An analysis of the hard X-rays that are observed for Seyfert 2s indicates that the “missing” X-rays have been **absorbed by intervening material with huge hydrogen column densities** of between 10^{26} and 10^{28} m^{-2} .

Seyferts make up only a few tenths of a percent of all field galaxies.

It is interesting that at least **90%** of the Seyferts close enough to be resolved by telescopes are **spiral galaxies**, typically of types Sb or SBb.

Seyfert galaxies

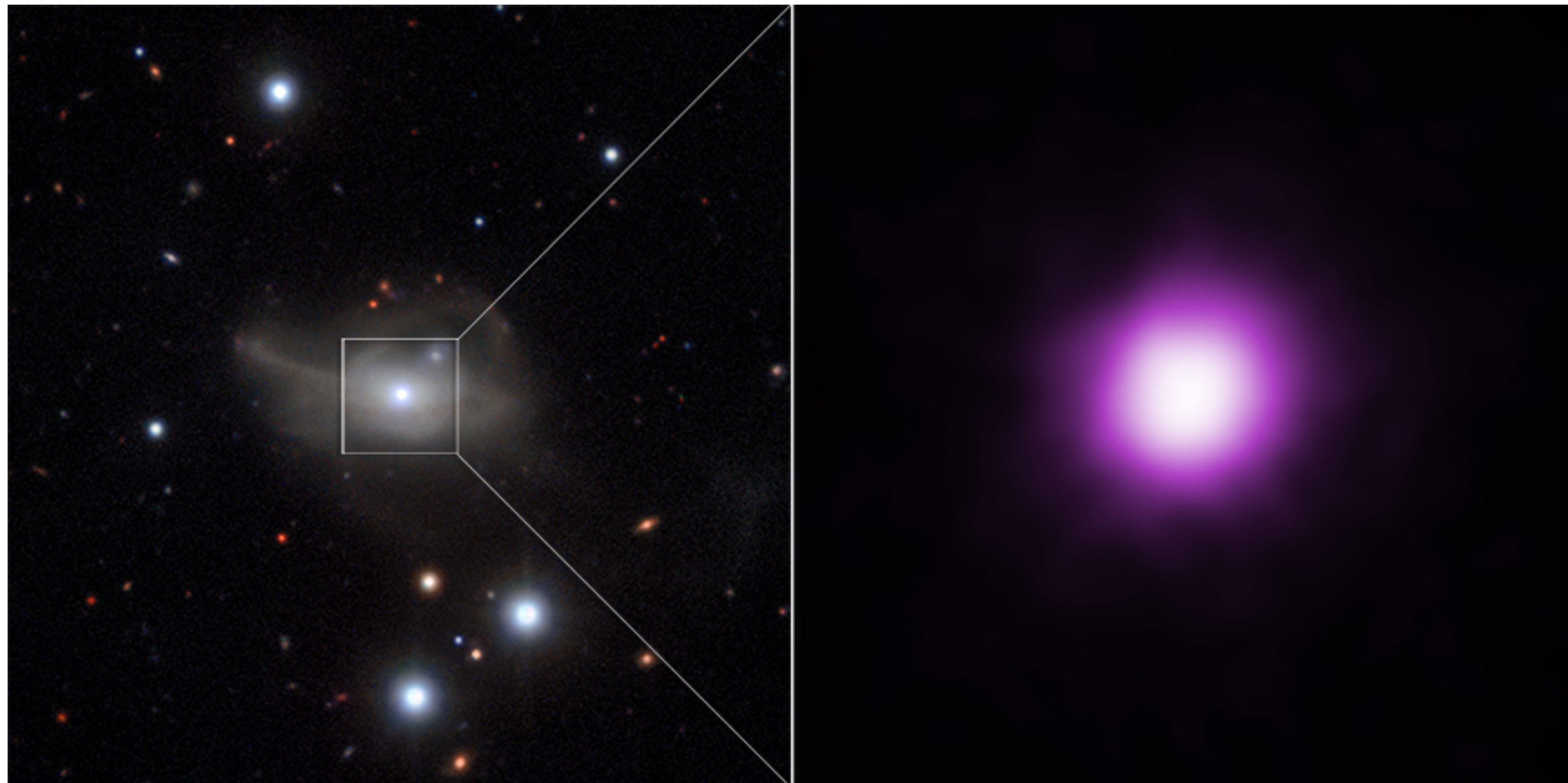
They are **frequently accompanied by other galaxies** with which they may be gravitationally interacting.
Seyfert galaxy **NGC 4151** (type Sab) with a galactic disk around its bright nucleus + some outer spiral arms.



Seyfert galaxies

The galaxy Markarian 1018 stands out by changing type twice, from a faint to a bright AGN in the 1980s and then changing back to a faint AGN within the last five years. A handful of AGN have been observed to make this full-cycle change. During the second change in type the Markarian 1018 AGN became eight times fainter in [X-rays](#) between 2010 and 2016.

The AGN had faded because the black hole was being starved of infalling material. This starvation also explains the fading of the AGN in X-rays.



The spectra

Seyferts belong to the general class of galaxies with **active galactic nuclei**, or AGN for short. Other members of this class, such as radio galaxies, quasars, and blazars.

Figure 4 is a rough schematic of the continuum observed for many types of AGNs (note that the logarithm of the product νF_ν is plotted on the figure's vertical axis). The most notable feature of this **spectral energy distribution (SED)** is its persistence over some **10 orders of magnitude in frequency**. This wide spectrum is markedly **different from the thermal (blackbody) spectrum** of a star or the combined spectra of a galaxy of stars.

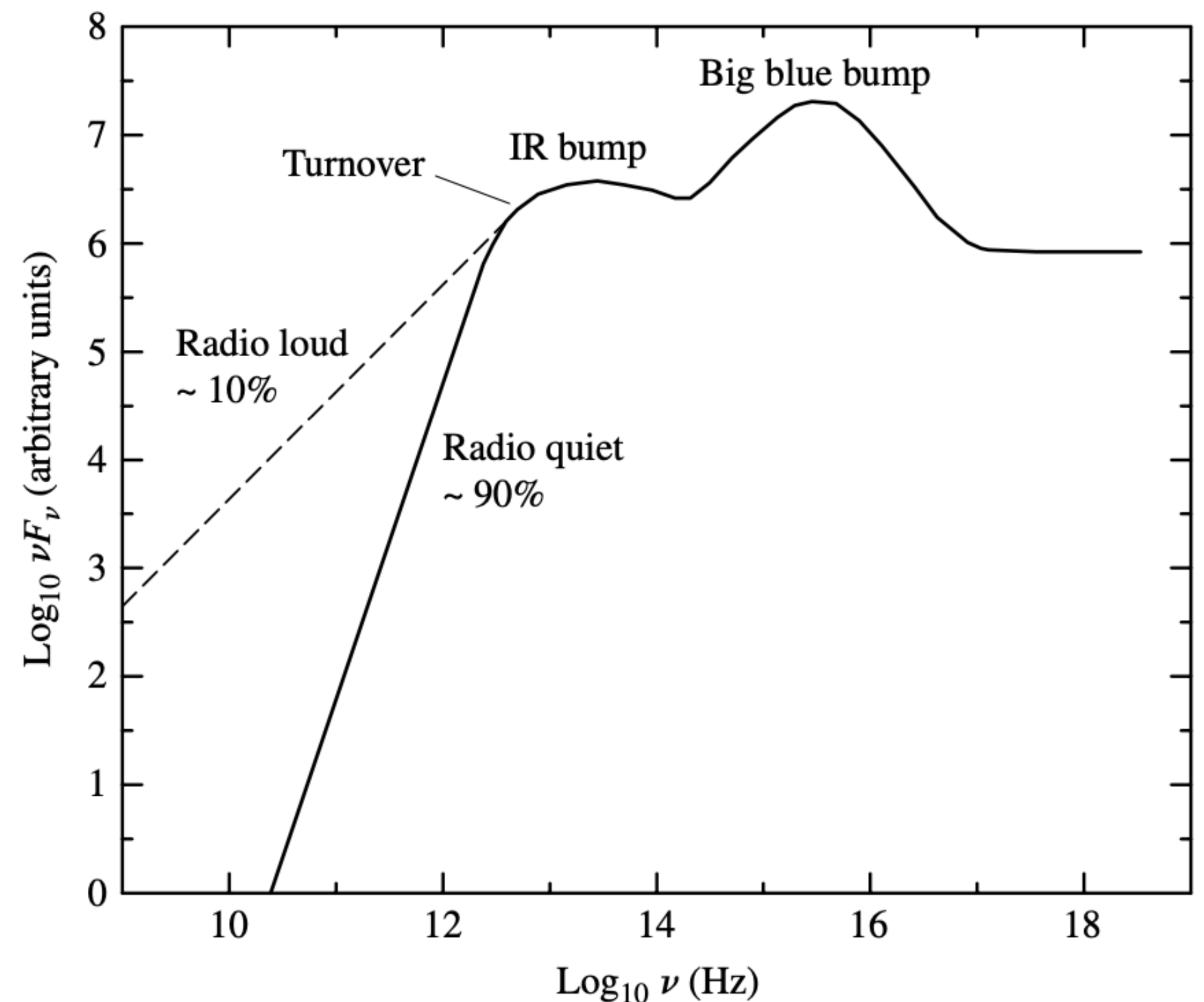


FIGURE 4 A sketch of the continuum observed for many types of AGNs.

The spectra

When AGNs were first studied, it was thought that their spectra were quite flat. Accordingly, a power law of the form

$$F_\nu \propto \nu^{-\alpha}$$

was used to describe the monochromatic energy flux, F_ν . The **spectral index**, α , was believed to have a value of $\alpha \approx 1$.

The power received within any frequency interval between ν_1 and ν_2 is

$$L_{\text{interval}} \propto \int_{\nu_1}^{\nu_2} F_\nu d\nu = \int_{\nu_1}^{\nu_2} \nu F_\nu \frac{d\nu}{\nu} = \ln 10 \int_{\nu_1}^{\nu_2} \nu F_\nu d \log_{10} \nu,$$

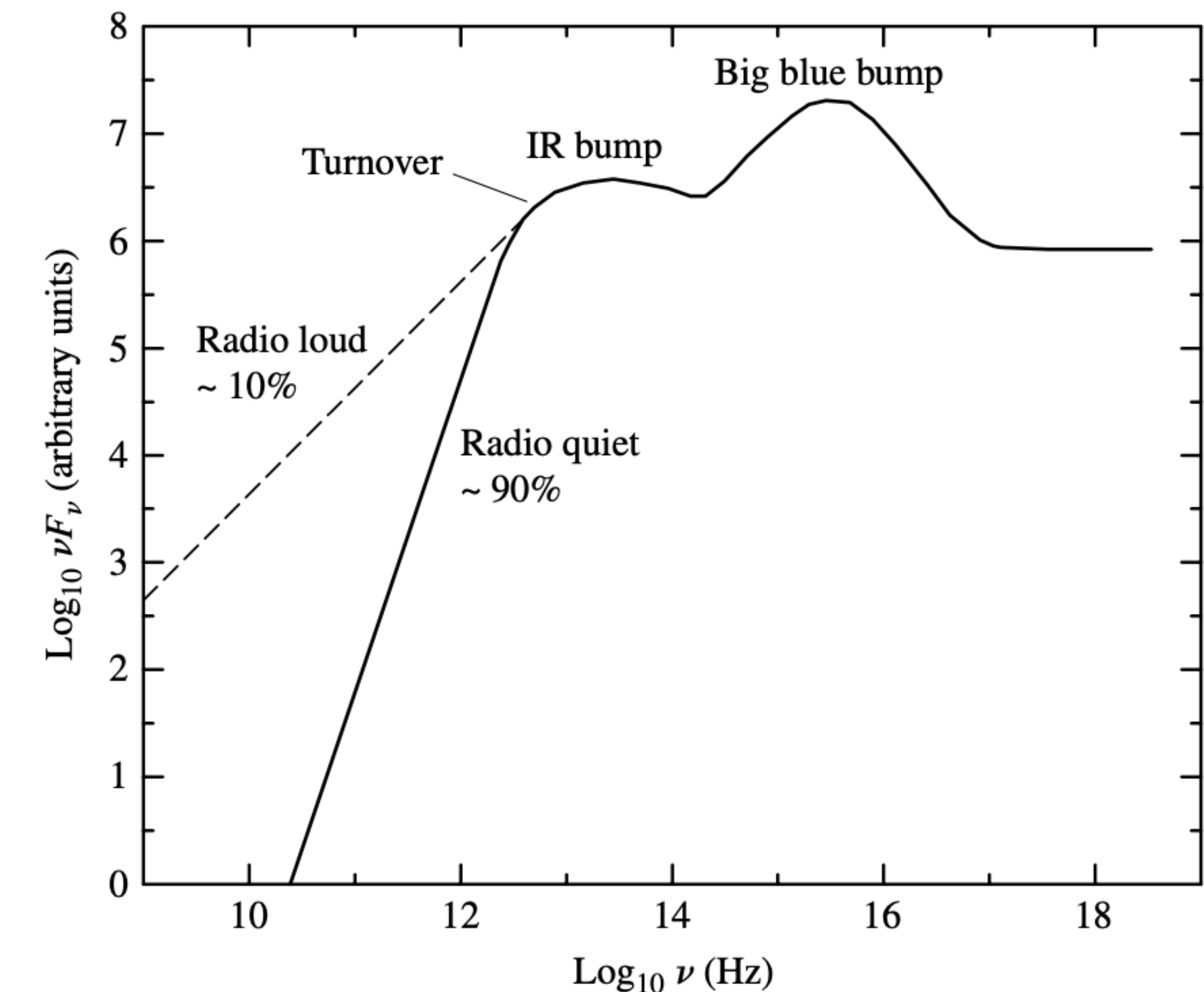


FIGURE 4 A sketch of the continuum observed for many types of AGNs.

The spectra

so that **equal areas under a graph of νF_ν vs. $\log_{10} \nu$** correspond to **equal amounts of energy**; hence the reason for plotting $\log_{10} \nu F_\nu$ on the ordinate in Fig. 4.

A value of $\alpha \approx 1$ reflects the **horizontal trend** seen to the right of the turnover in Fig. 4.

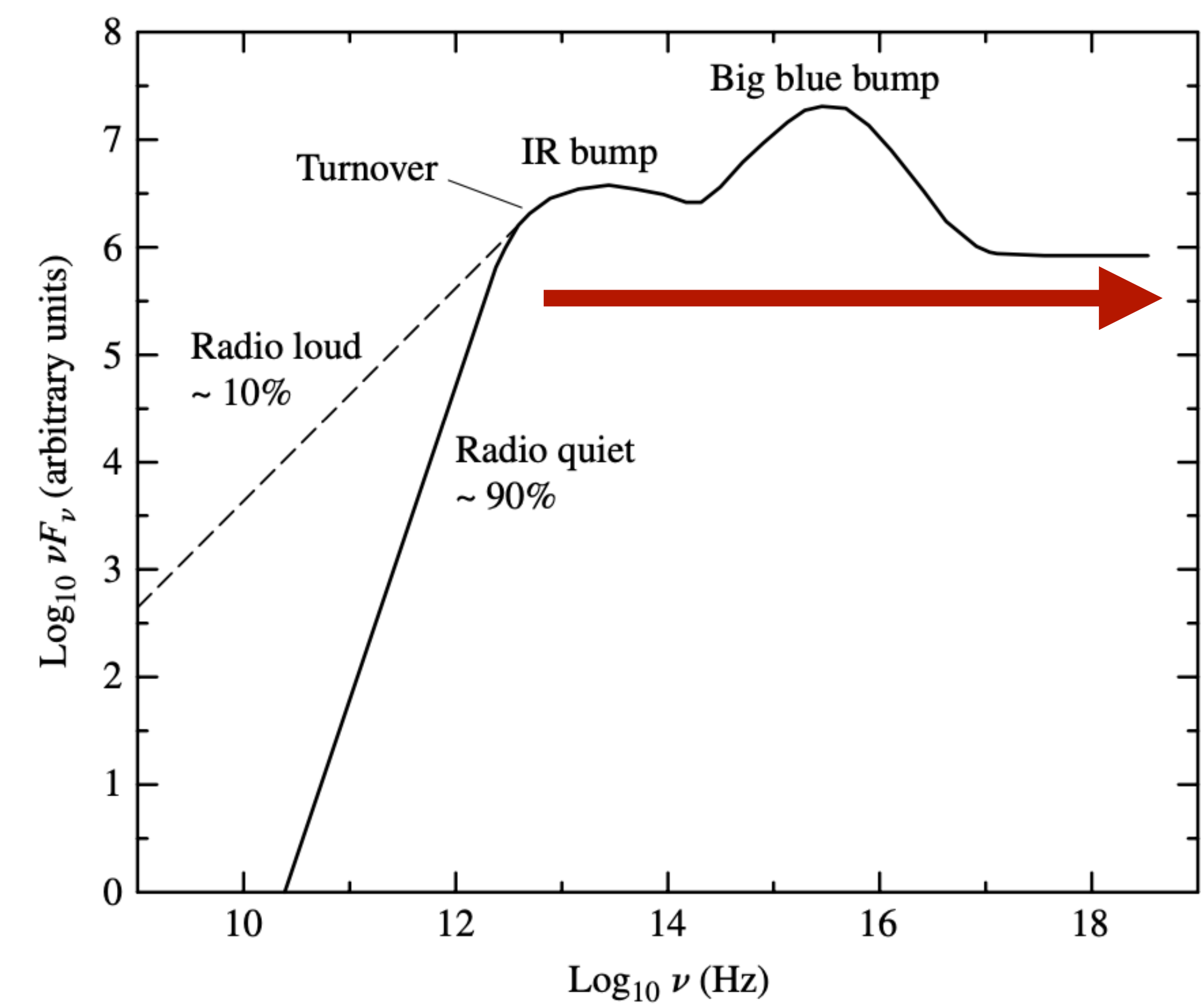


FIGURE 4 A sketch of the continuum observed for many types of AGNs.

The spectra

The continuous spectra of AGNs are now known to be more complicated, involving a mix of thermal and nonthermal emission. However, this is still used to *parameterize* the continuum.

The **spectral index typically has a value between 0.5 and 2 that usually increases with increasing frequency**, so the curve of $\log_{10} \nu F_\nu$ vs. $\log_{10} \nu$ in Fig. 4 is generally concave downward.

In fact, the value of α is **constant over only a limited range of frequencies**, such as in the infrared and visible regions of the spectrum. The shape and polarization of the visible-UV spectrum indicates that it can sometimes be decomposed into contributions from thermal sources (**blackbody spectrum, low polarization**) and nonthermal sources (**power-law spectrum, significant polarization**).

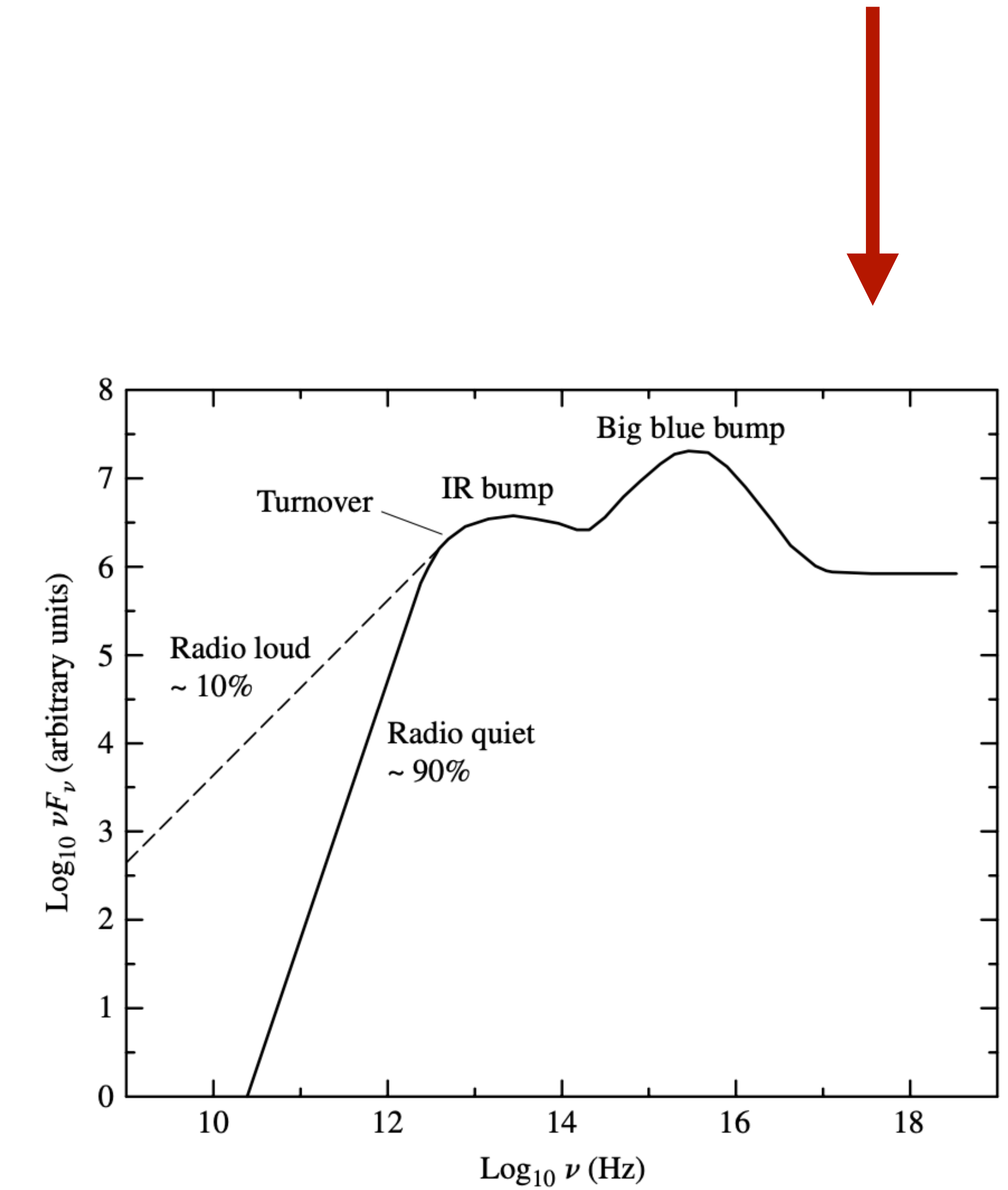


FIGURE 4

A sketch of the continuum observed for many types of AGNs.

The spectra

The **thermal component** appears as the **big blue bump** in Fig. 4, which can contain an appreciable amount of the bolometric luminosity of the source.

It is generally believed that the emission from the big blue bump is **due to an optically thick accretion disk**, although some researchers have suggested that free-free emission may be responsible.

Also evident is a thermal **infrared bump** to the left of the big blue bump; it is probably due to emission from warm ($T < 2000$ K) dust grains.

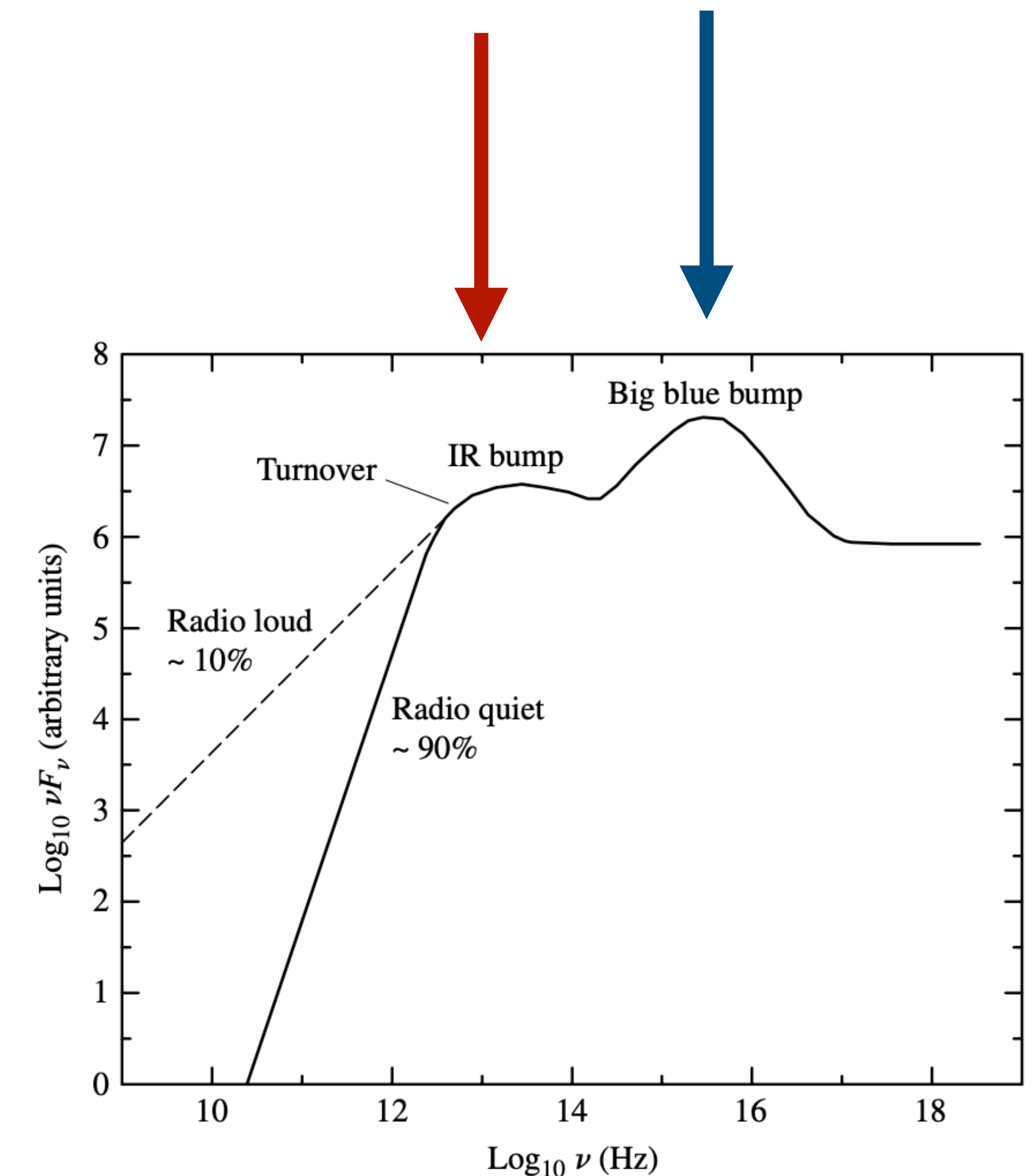


FIGURE 4 A sketch of the continuum observed for many types of AGNs.

The spectra

A pure power-law spectrum (with constant α) is the signature of synchrotron radiation, which is frequently encountered in astronomical situations involving relativistic electrons and magnetic fields.

As shown in Fig. 5, a synchrotron spectrum is produced by the combined radiation emitted by individual electrons as they spiral around magnetic field lines. If the distribution of the individual electron energies obeys a power law, then the resulting synchrotron spectrum is described by Eq. (1).

However, the synchrotron spectrum does not continue to rise without limit as the frequency decreases. **At a transition frequency, the spectrum turns over** and varies as $\nu^{5/2}$ (spectral index $\alpha = -2.5$). This occurs because **the plasma of spiraling electrons becomes opaque to its own synchrotron radiation**, an effect known as **synchrotron self-absorption**.

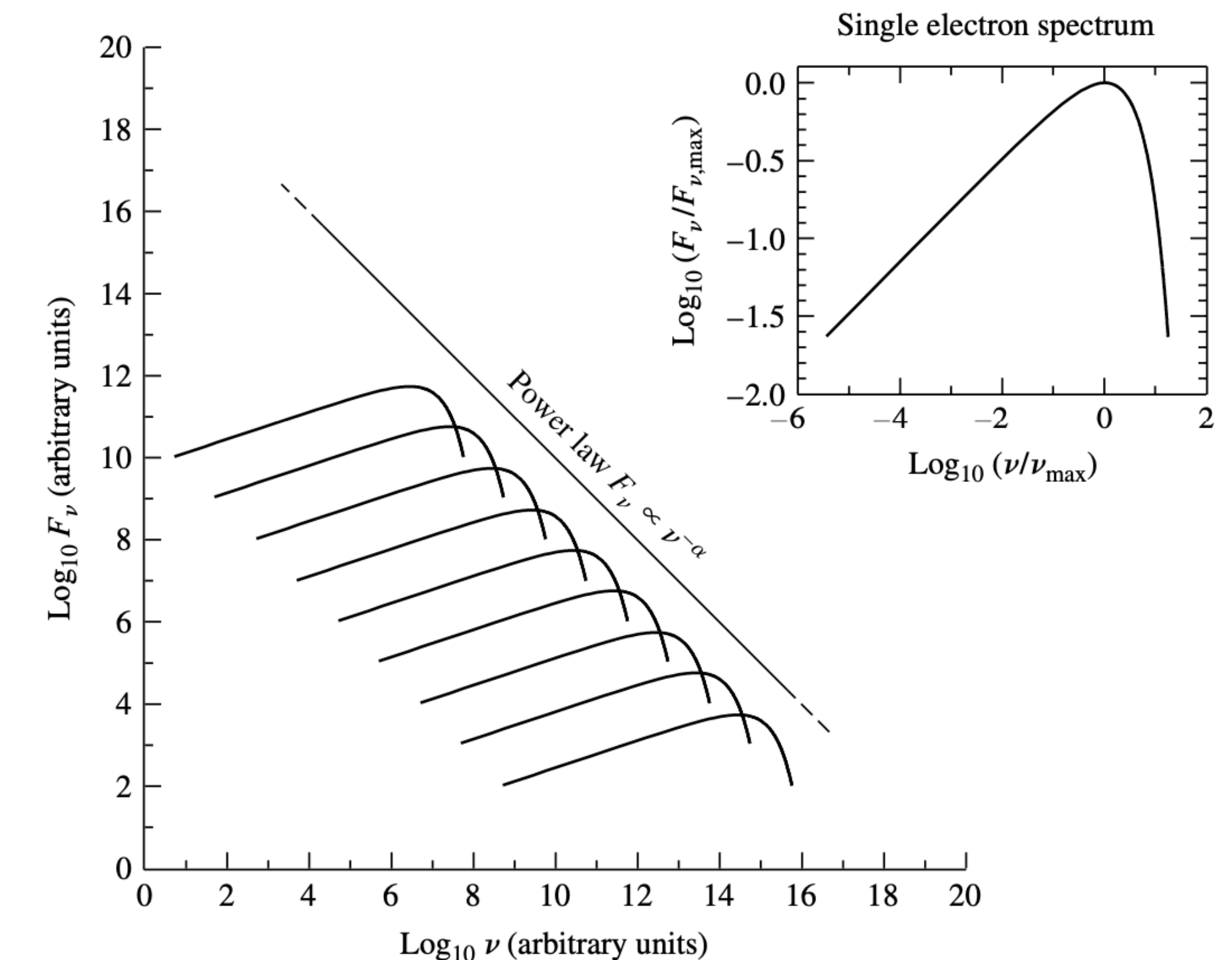


FIGURE 5 The power-law spectrum of synchrotron radiation, shown as the sum of the radiation produced by individual electrons as they spiral around magnetic field lines. The spectrum of a single electron is at the upper right. The turnover at low frequencies is not shown.

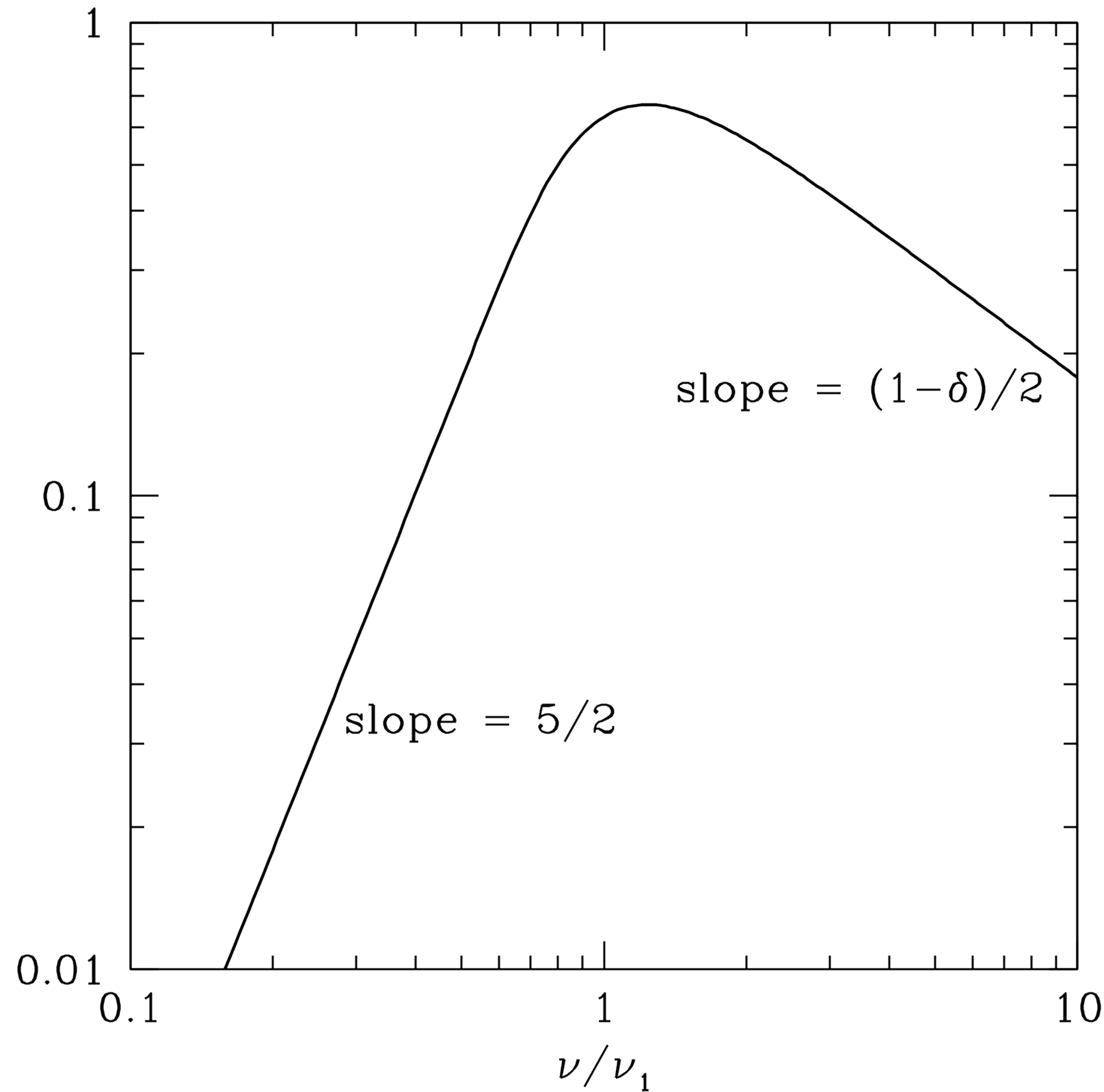
The spectra

A pure power-law spectrum (with constant α) is the signature of synchrotron radiation, which is frequently encountered in astronomical situations involving relativistic electrons and magnetic fields.

As shown in Fig. 5, a synchrotron spectrum is produced by the combined radiation emitted by individual electrons as they spiral around magnetic field lines. If the distribution of the individual electron energies obeys a power law, then the resulting synchrotron spectrum is described by Eq. (1).

However, the synchrotron spectrum does not continue to rise without limit as the frequency decreases. **At a transition frequency, the spectrum turns over** and varies as $\nu^{5/2}$ (spectral index $\alpha = -2.5$). This occurs because **the plasma of spiraling electrons becomes opaque to its own synchrotron radiation**, an effect known as **synchrotron self-absorption**.

homogeneous cylindrical synchrotron source in terms of the frequency at ν_1 at which $\tau = 1$. Real astrophysical sources are inhomogeneous, so their low-frequency spectral slopes are smaller than 5/2 and their spectral peaks are not so sharp.



The spectra

In some SEDs (Spectral energy distribution), the “turnover” evident in the schematic continuum spectrum in Fig. 4 may be due to synchrotron self-absorption.

However, the **thermal contributions to the continuum spectrum evident in the infrared bump suggest** that in other cases, the turnover may be due to the long-wavelength Rayleigh–Jeans portion of the blackbody spectrum produced by the warm dust grains.

It is possible that the steeper, low-frequency spectra of radio-quiet AGNs are due to the thermal spectrum of dust grains, while the shallower, low-frequency spectra of radio-loud AGNs **may be due to a combination of thermal and nonthermal emission.**

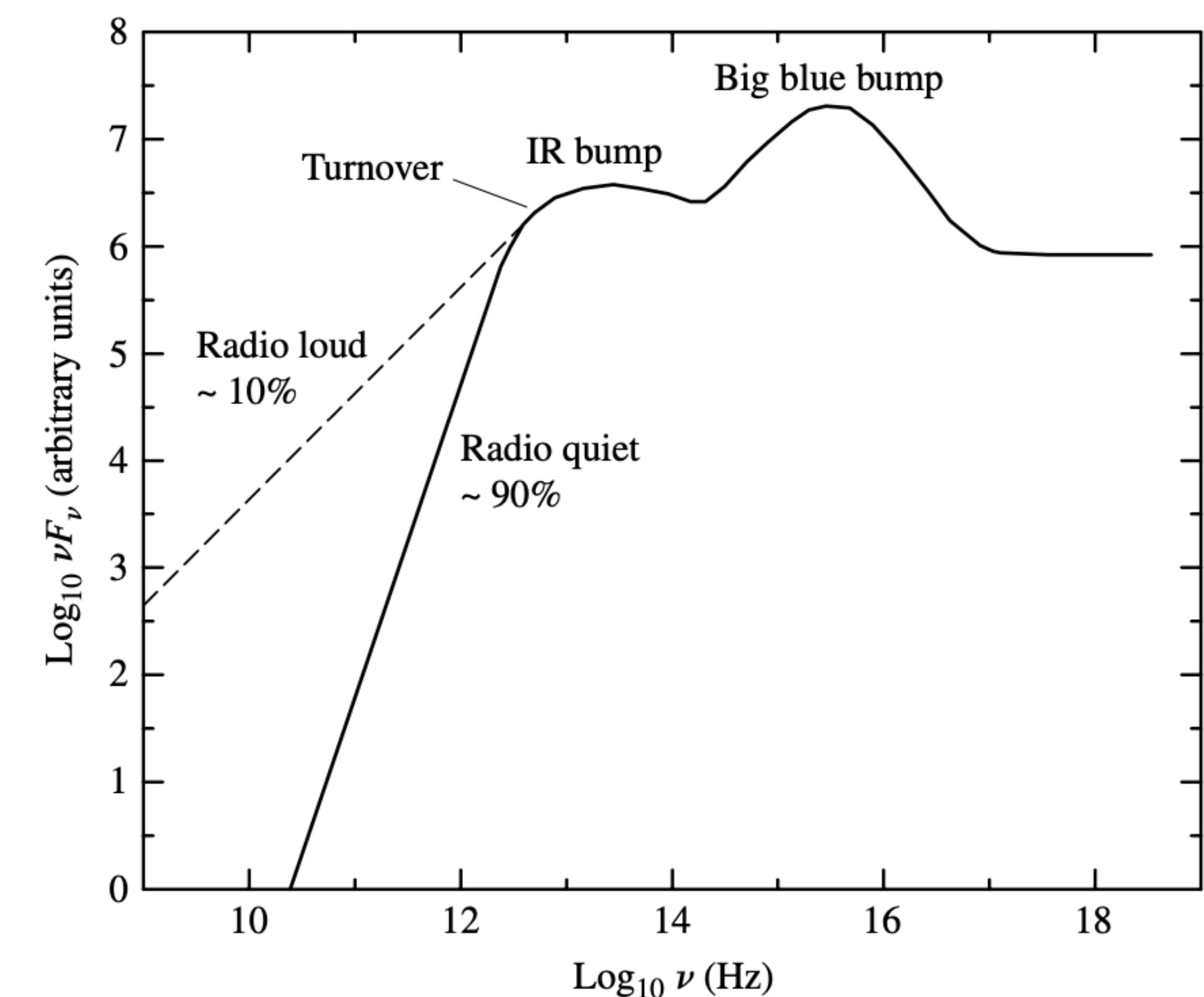
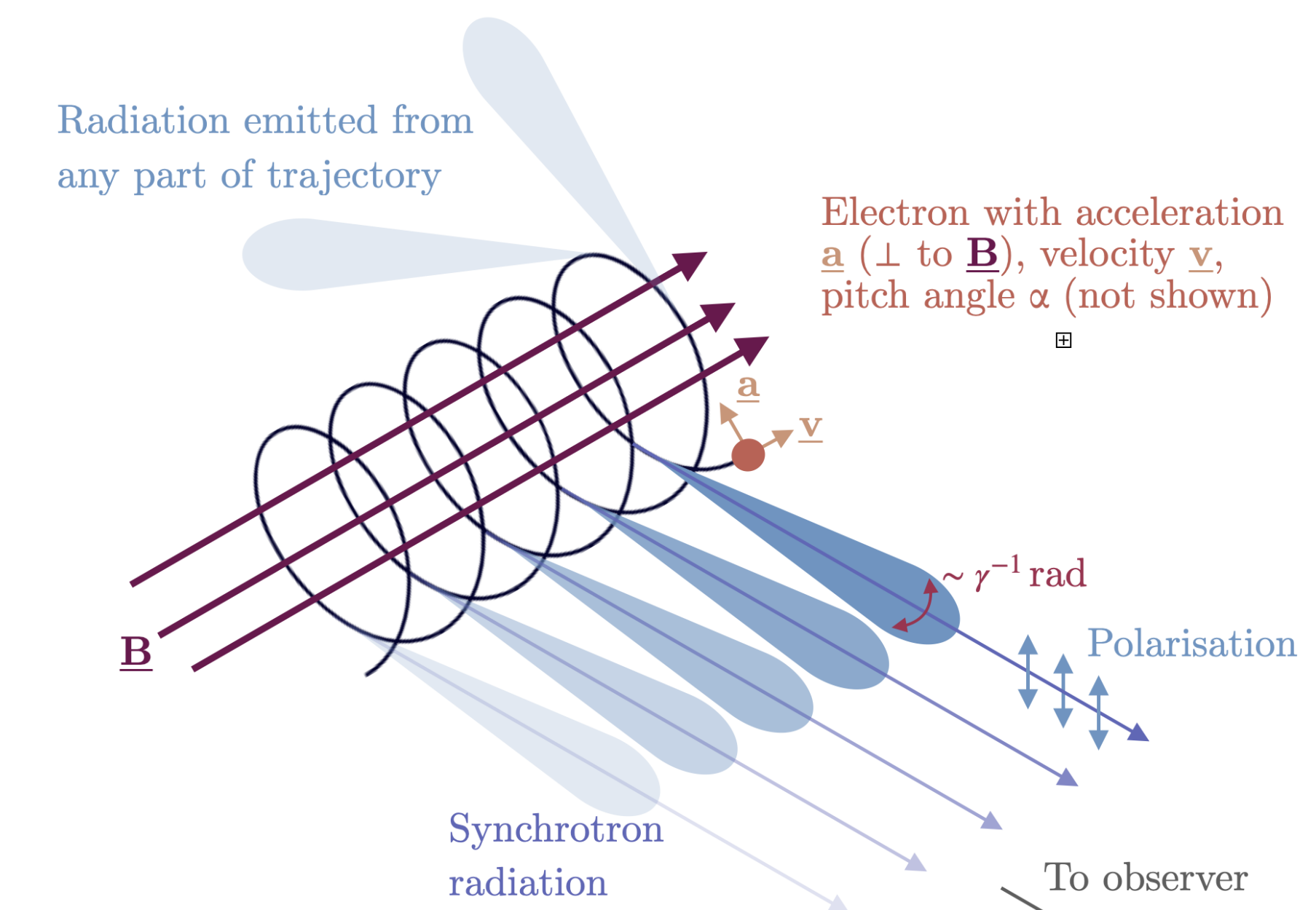


FIGURE 4 A sketch of the continuum observed for many types of AGNs.

Synchrotron radiation

- **Synchrotron radiation is the electromagnetic radiation emitted when relativistic charged particles are subject to an acceleration perpendicular to their velocity.** It is produced naturally by fast electrons moving through magnetic fields. The radiation produced in this way has a characteristic polarization and the frequencies generated can range over a large portion of the electromagnetic spectrum.
- Synchrotron radiation is similar to bremsstrahlung radiation, which is emitted by a charged particle when the acceleration is parallel to the direction of motion.
- The **general term for radiation emitted by particles in a magnetic field is gyromagnetic radiation**, for which synchrotron radiation is the ultra-relativistic special case. Radiation emitted by charged particles moving non-relativistically in a magnetic field is called cyclotron emission. For particles in the mildly relativistic range ($\approx 85\%$ of the speed of light), the emission is termed gyro-synchrotron radiation.



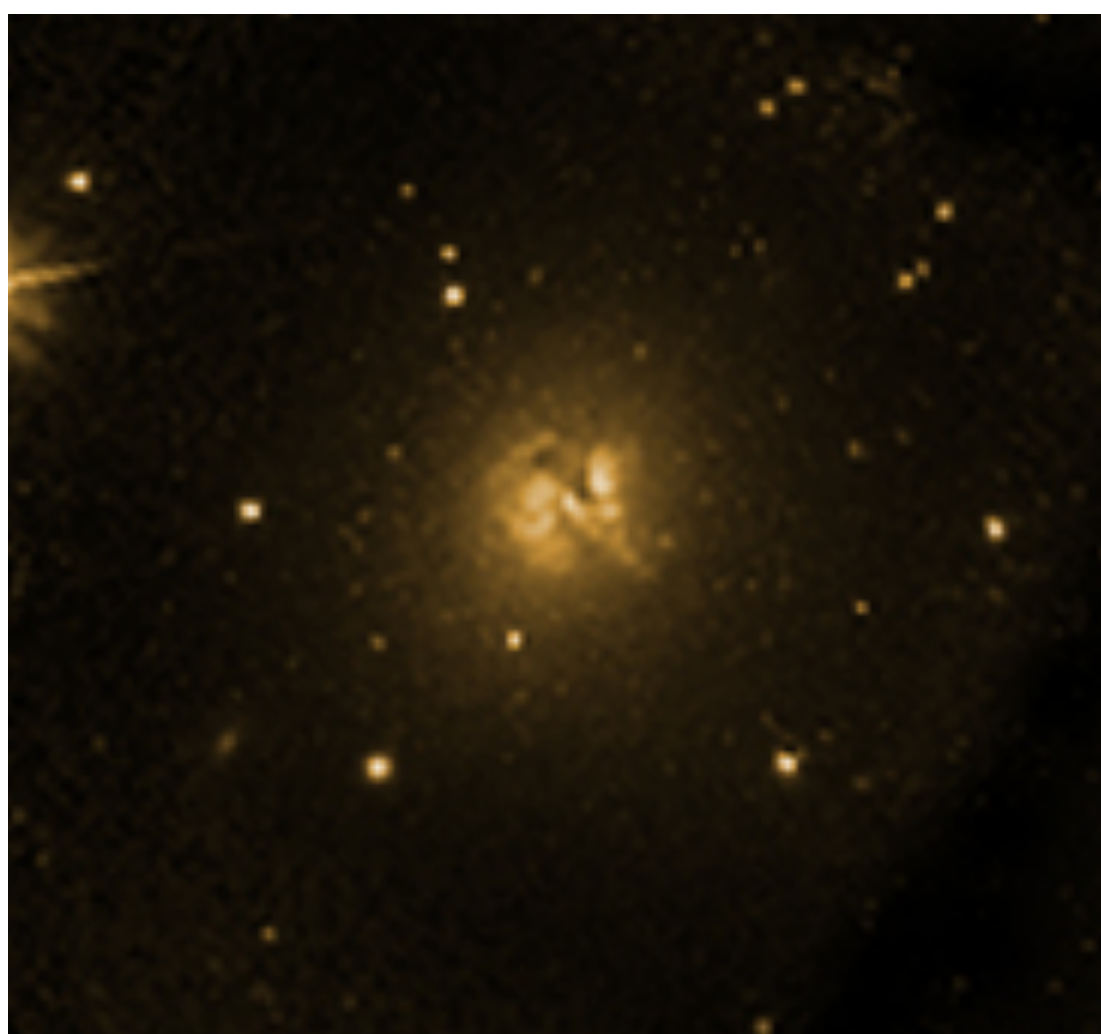
Radio Galaxies

The first discrete source of strong radio waves (other than the Sun) was discovered in the constellation Cygnus and was named Cygnus A.

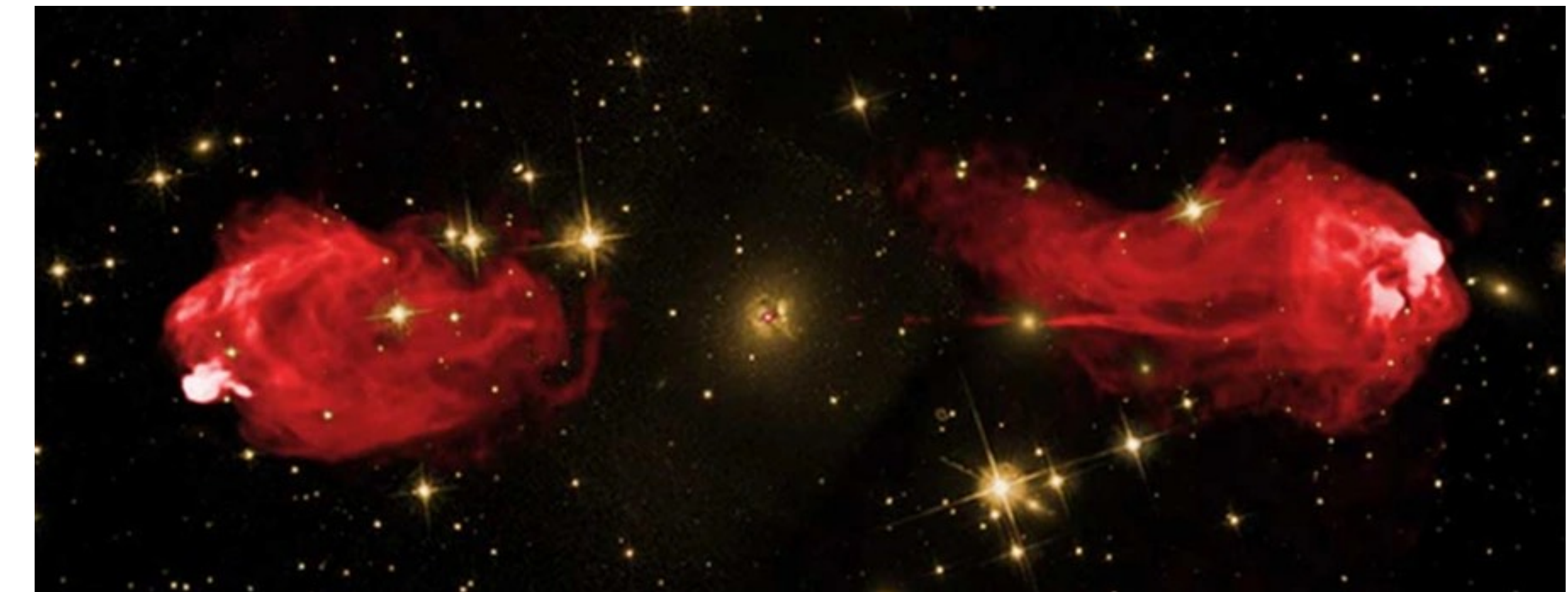
Using the accurate position provided by radio astronomy the optical counterpart of Cyg A. It is a **peculiar-looking cD galaxy** whose center is apparently encircled by a **ring of dust**.

Cyg A's spectrum shows a redshift of $z = \Delta\lambda/\lambda_{rest} = 0.057$, corresponding to a recessional velocity of 16,600 km s⁻¹. From Hubble's law, the distance to Cyg A is about 170h⁻¹ Mpc (implying a distance of 240 Mpc if h = [h]_{WMAP}).

Considering that Cyg A is the brightest radio source beyond the Milky Way, this **distance is surprisingly large**.



Cyg A - radio galaxy (AGN)

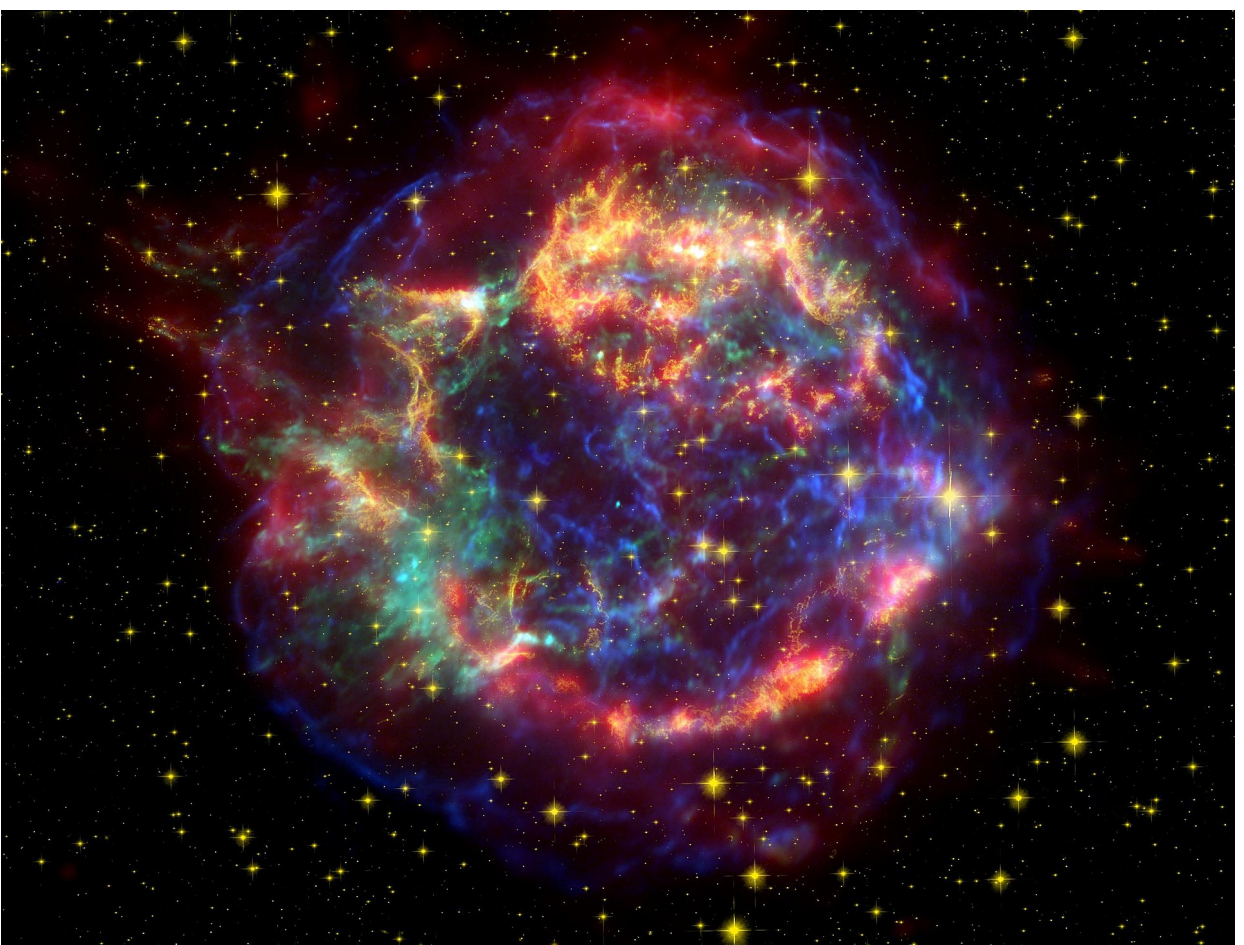


Radio Galaxies

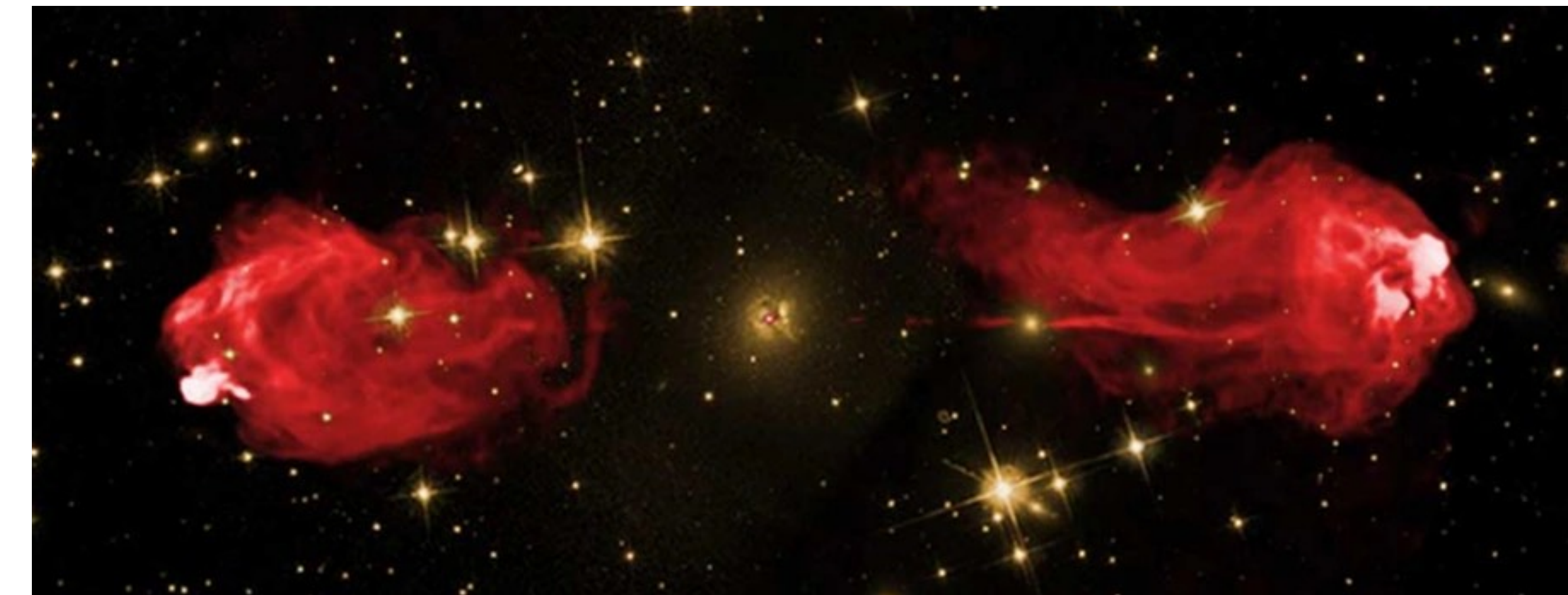
In fact, the only discrete radio sources brighter than Cyg A are the Sun and Cassiopeia A, the nearby (3 kpc) remnant of a Type II supernova. **To be detected so far away, Cyg A must pour out enormous amounts of radio energy.**

Cyg A is one example of a class of galaxies, called **radio galaxies**, that are **extremely bright at radio wavelengths**.

Cas A - Supernova remnant



Cyg A - radio galaxy (AGN)



Radio Galaxies



Example 1.1. The radio energy emitted by Cygnus A can be estimated by using its distance of $d = 170h^{-1}$ Mpc together with the observed value of the monochromatic flux at a radio frequency of 1400 MHz,

$$F_{1400} = 1.255 \times 10^{-23} \text{ W m}^{-2} \text{ Hz}^{-1} = 1255 \text{ Jy}.$$

The radio spectrum follows the power law of Eq. (1) with $\alpha \approx 0.8$, so $F_\nu \propto \nu^{-0.8}$. That is, we can write

$$F_\nu = F_{1400} \left(\frac{\nu}{1400 \text{ MHz}} \right)^{-0.8}.$$

The radio luminosity can be found by integrating the monochromatic flux over the range of radio frequencies. The upper frequency limit is taken to be $\nu_2 = 3 \times 10^9$ Hz, corresponding to a radio wavelength of 0.1 m. The power-law behavior of the radio spectrum does not continue to $\nu = 0$. Instead, the flux received from Cygnus A declines when the frequency falls below about $\nu_1 = 10^7$ Hz.

Radio Galaxies



With these limits, the radio luminosity is approximately

$$L_{\text{radio}} = 4\pi d^2 \int_{\nu_1}^{\nu_2} F_{\nu} d\nu = 4\pi d^2 F_{1400} \int_{\nu_1}^{\nu_2} \left(\frac{\nu}{1400 \text{ MHz}} \right)^{-0.8} d\nu = 2.4 \times 10^{37} h^{-2} \text{ W.}$$

Using the WMAP value of $[h]_{\text{WMAP}} = 0.71$, the radio luminosity of Cygnus A is estimated to be $L_{\text{radio}} = 4.8 \times 10^{37}$ W. This is **several million times more radio energy than is produced by a normal galaxy** such as M31 and is roughly three times the energy produced at *all* wavelengths by the Milky Way.



M31 - Andromeda galaxy

Radio Galaxies



Like Seyfert galaxies, radio galaxies may also be divided into two classes:

- **broad-line radio galaxies** (BLRGs, corresponding to Seyfert 1s) and
- **narrow-line radio galaxies** (NLRGs, corresponding to Seyfert 2s).

BLRGs have bright, starlike nuclei surrounded by very faint, hazy envelopes.

NLRGs, on the other hand, are giant or supergiant elliptical galaxies (types cD, D, and E); Cyg A is a NLRG.

Despite their similarities, there are obvious differences between Seyferts and radio galaxies. Although **Seyfert nuclei emit some radio energy**, they are **relatively quiet at radio wavelengths** compared with radio galaxies. Furthermore, while nearly all **Seyferts are spiral galaxies**, **none of the strong radio galaxies are spirals**.

Radio lobes and jets



A radio galaxy may display extended **radio lobes**, or it may radiate its energy both from a compact **core** in its nucleus and from a **halo** that is about the size of the visible galaxy or larger.

Cyg A -> The optical galaxy is flanked by two huge radio lobes that are the sources of the tremendous radio luminosity estimated in Example 1.1. Each of the lobes has a diameter of about 17h^{-1} kpc.

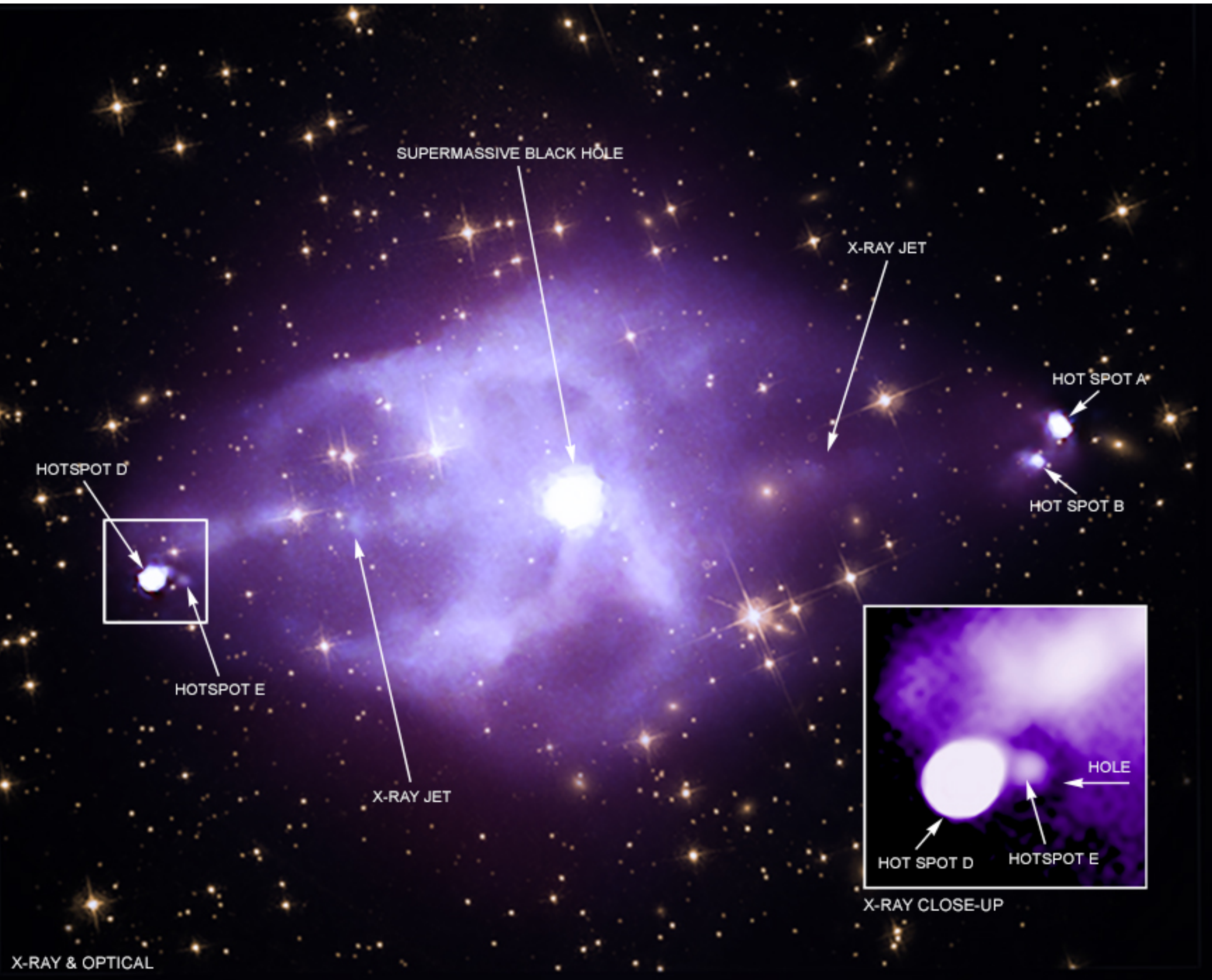
Observations reveal that one of the lobes is connected to the central galaxy of Cyg A by a collimated **jet** that spans the roughly 50h^{-1} kpc of space separating the galaxy from the lobe. (Since the orientations of jets and radio lobes are not well determined, the values for their sizes quoted here are projected distances on the plane of the sky.)

At least half of the stronger radio galaxies have detectable jets, as do more than three-quarters of the weaker sources. The jets associated with the powerful sources tend to be one-sided (like Cyg A's), while those found in less luminous radio galaxies are typically two-sided. One reason for this is that the **stronger radio galaxies can be seen at greater distances, and so a dim counterjet may go undetected.**

Radio lobes and jets

In this composite image of Cygnus A, X-rays from Chandra (red, green, and blue that represent **low, medium and high energy X-rays**) are combined with an optical view from the HST of the galaxies and stars in the same field of view. Chandra's data reveal the presence of **powerful jets of particles and electromagnetic energy** that have shot out from the black hole. The jet on the left has slammed into a **wall of hot gas**, then bounced to **punch a hole** in a cloud of energetic particles, before it **collides with another part of the gas wall**.

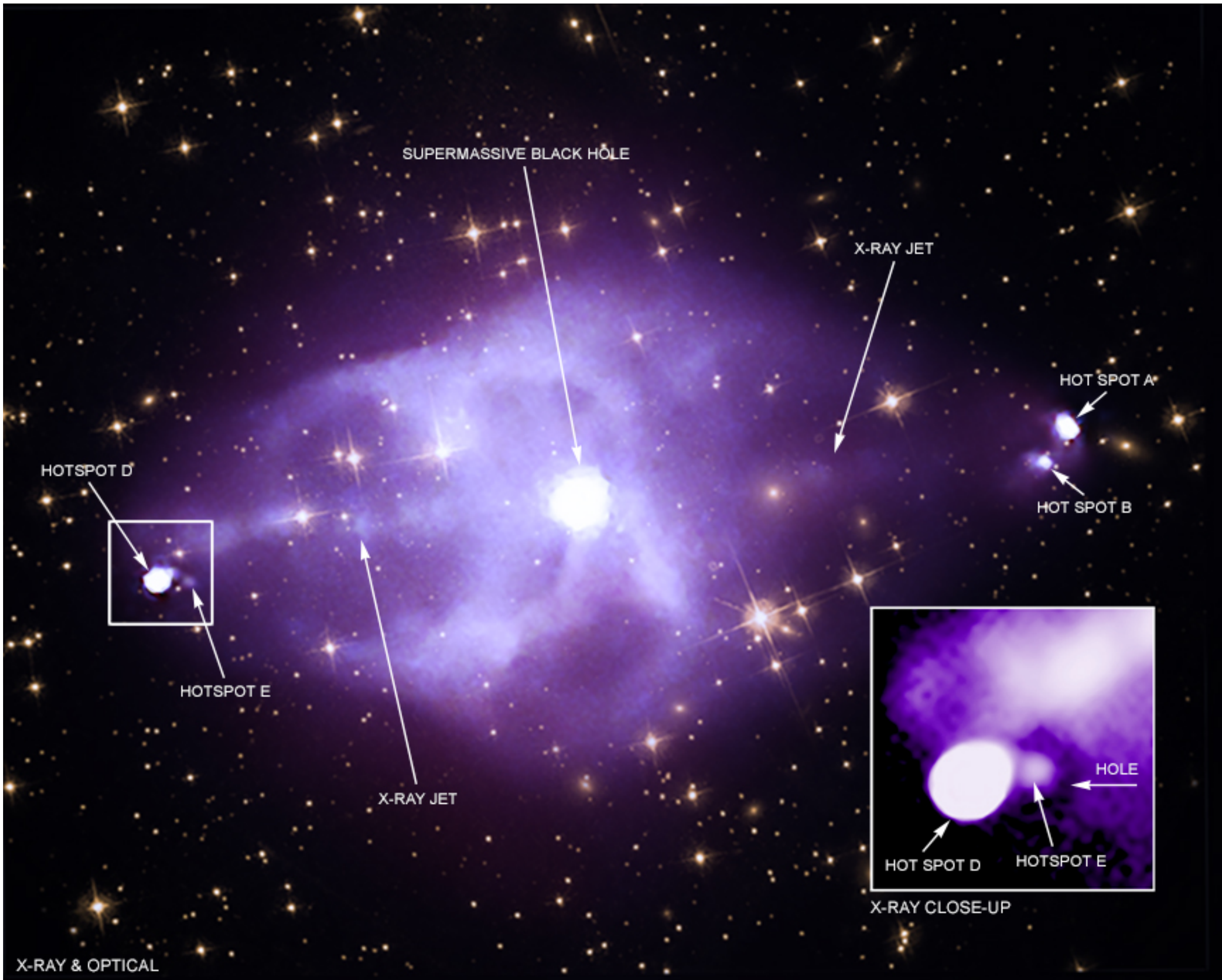
The point that the jet on the left ricocheted off a wall of intergalactic gas ("hotspot E"), and the point where the jet then struck the intergalactic gas a second time ("hotspot D").



Radio lobes and jets

The inset contains a close-up view of the hotspots on the left and the hole punched by the rebounding jet, which surrounds hotspot E. Cygnus A is a large galaxy that sits **in the middle of a cluster of galaxies** about 760 million light years from Earth. Jets can significantly affect how the galaxy and its surroundings evolve.

Energy produced by jets from black holes can **heat intergalactic gas in galaxy clusters and prevent it from cooling** and forming large numbers of stars in a central galaxy like Cygnus A.



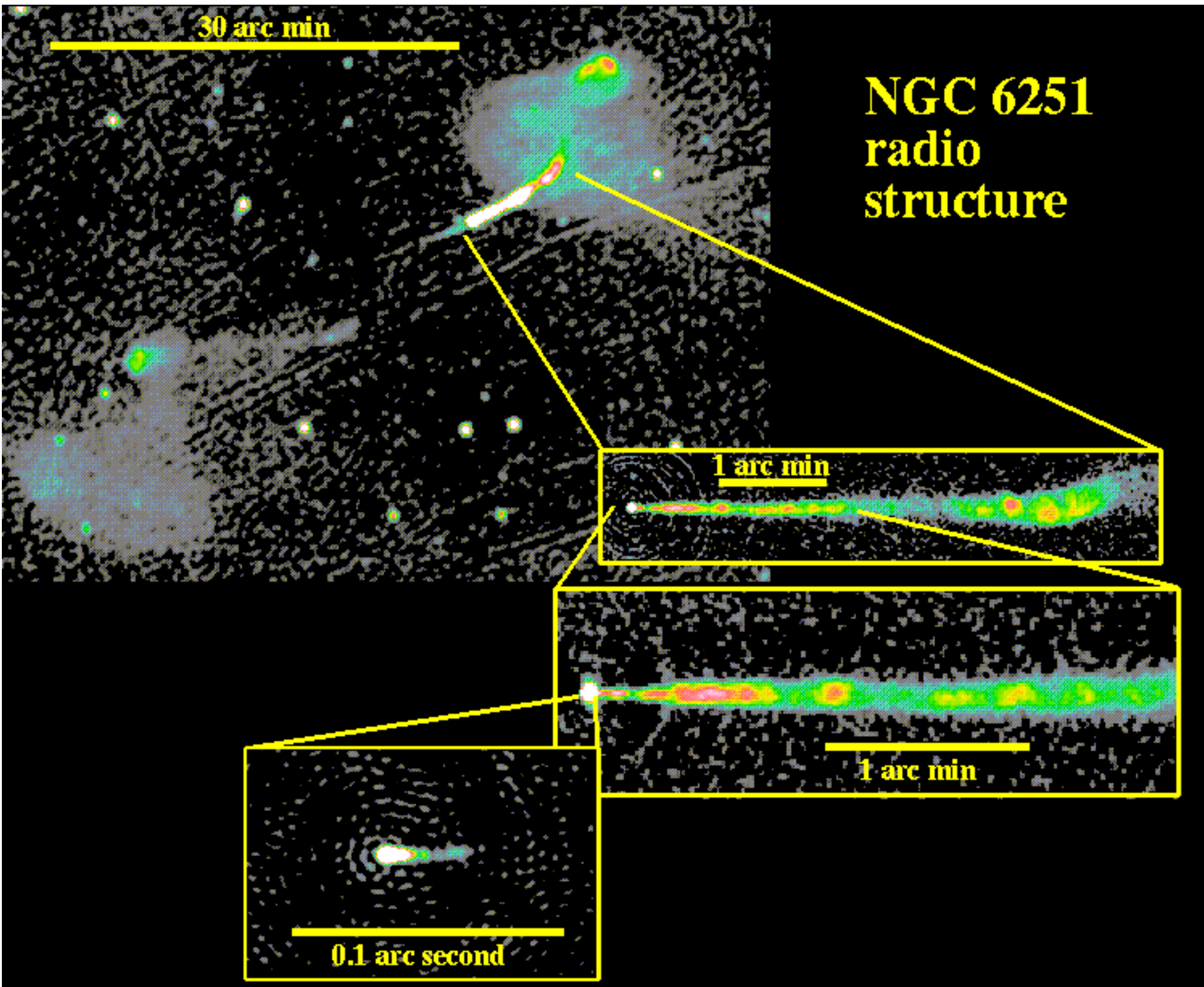
Radio lobes and jets

The strong jet and weak counterjet of the elliptical galaxy NGC 6251.

It is remarkable that the **jet can be traced essentially all the way to the core of the galaxy**.

One important lesson from radio galaxies is that the **central engine continues to eject material in nearly the same direction for at least several million years**, based on the fact that the tiny parsec-scale jets in the core regions point in the same direction as the very extended radio structure which may stretch several million light-years (and thus took at least that many years to form).

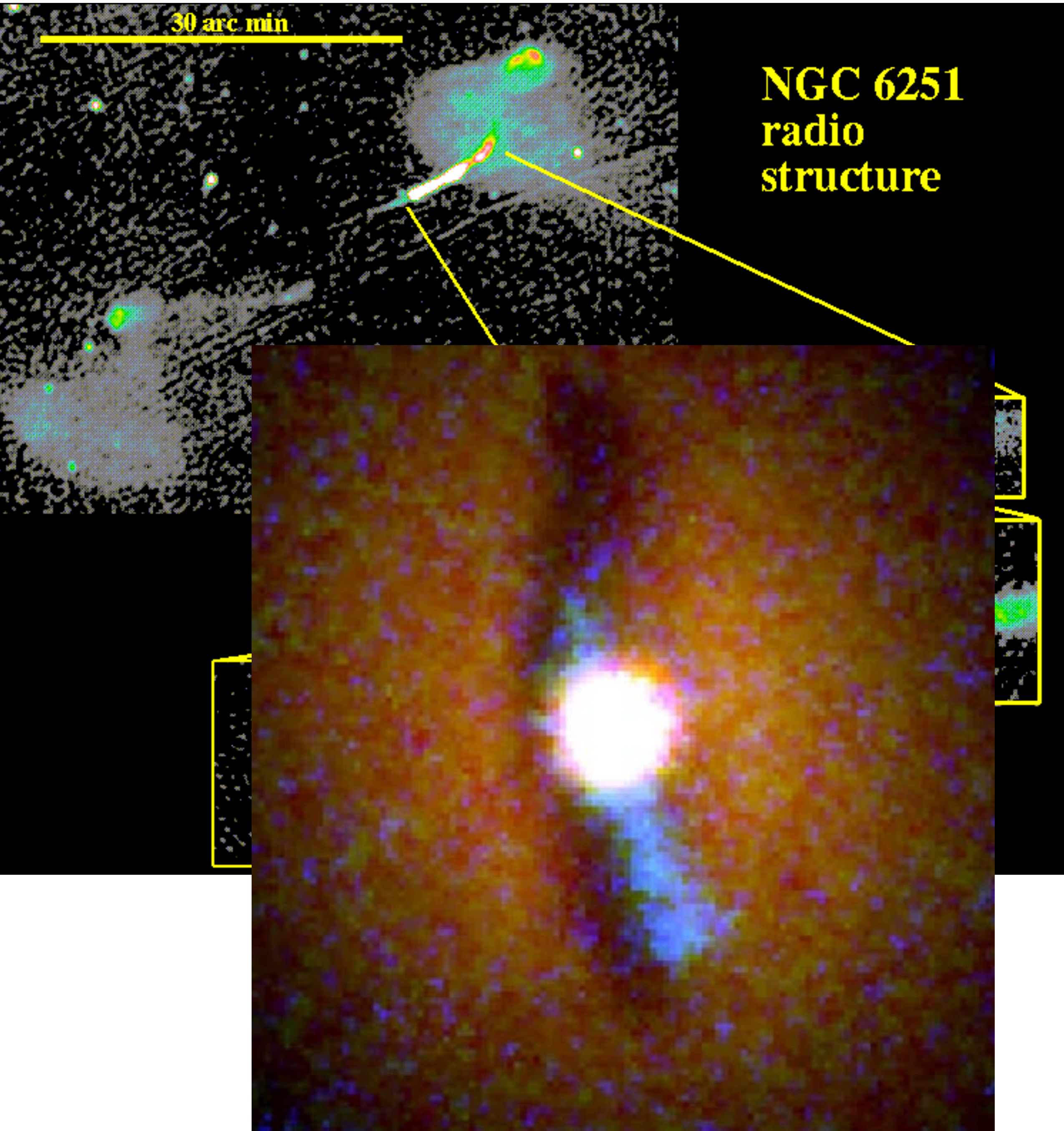
The WSRT map shows the faint counterjet opposite the bright jet; its weakness may indicate that the jet is in relativistic motion more or less toward us, so that **Doppler boosting** makes it appear dramatically brighter than its counterpart.



Radio lobes and jets

Something is lighting up the centre of galaxy NGC 6251. Most likely a large black hole not shrouded by gas and dust typically found near the centre of a galaxy.

Observations taken with the Hubble Space Telescope indicate a new perspective on the centres of galaxies: a **bright central object that is illuminating a surrounding material disk**, shown in blue. The lack of reflection from the upper part of the disk indicates that this **disk is warped in shape**. A huge plasma jet streams out from the central object, perpendicular to the warped disk.



Radio lobes and jets

Other radio jets are not as straight as those of Cyg A or **NGC 6251**.

The windblown appearance of the jets emanating from NGC 1265, produced by that galaxy's motion through the intracluster gas of the **Perseus cluster**.

Galaxy clusters tend to host the **largest elliptical galaxies**. Due to the galaxy density in clusters **interactions and mergers are very frequent** between the galaxies -> **giant elliptical galaxies can form**.

Most galaxy clusters have a giant elliptical galaxy in the centre of the cluster.

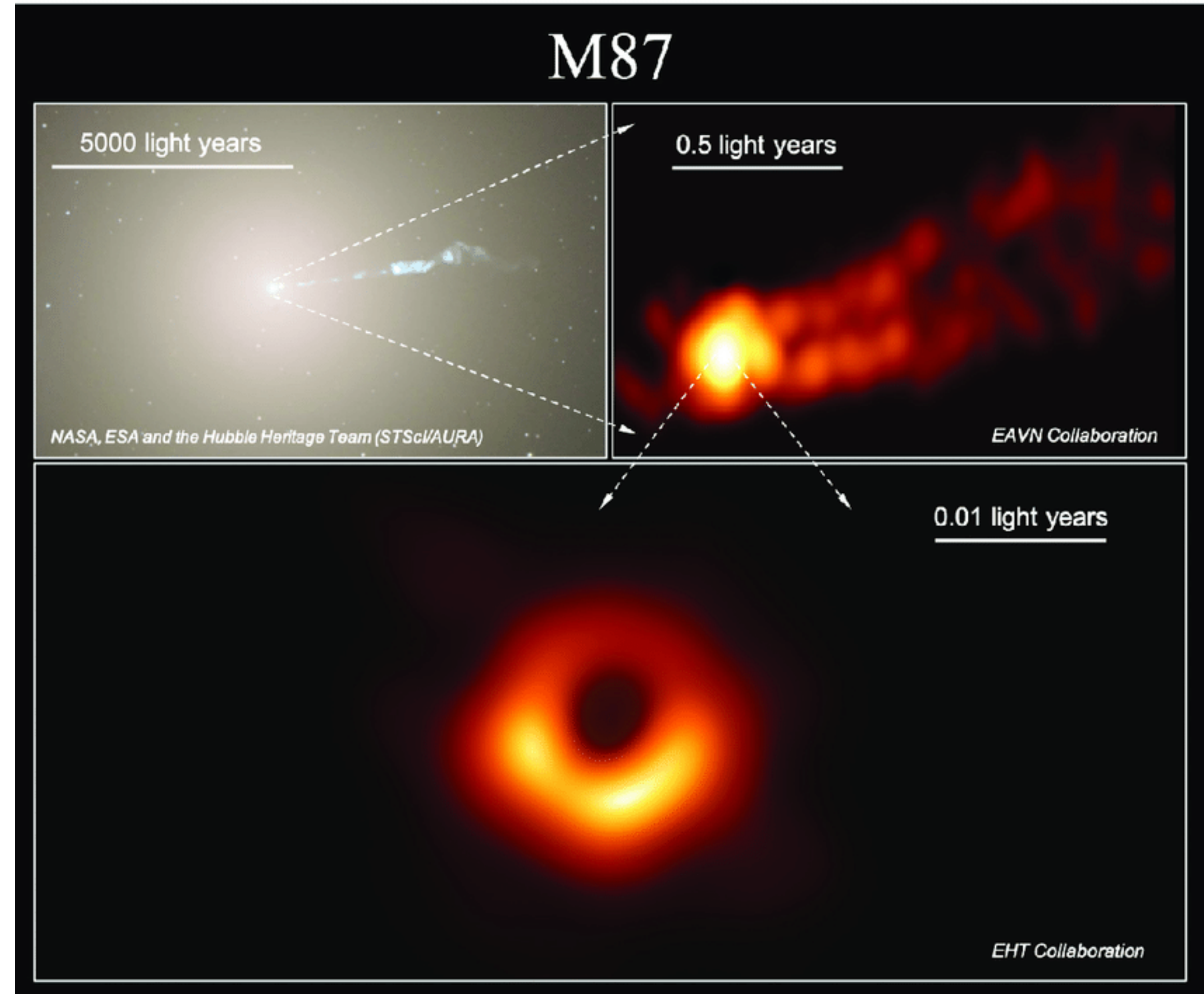


Radio lobes and jets

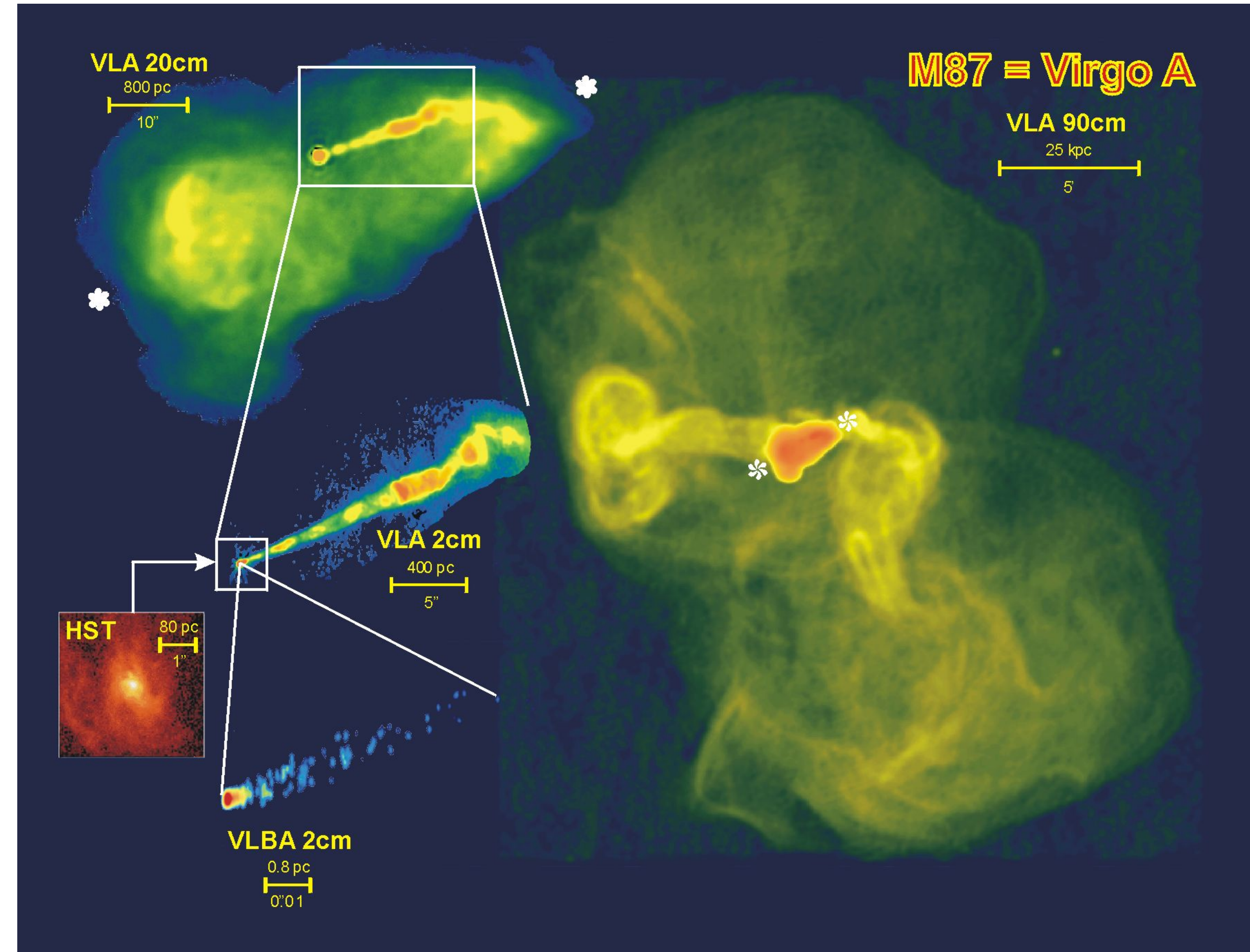
Following Cyg A, many more radio galaxies were discovered. One of these is M87, the **giant elliptical (E1)** galaxy that lies at the **center of the Virgo cluster**. With an apparent visual magnitude of $V = 8.7$, M87 is **one of the brighter-appearing galaxies in the sky**.

The **Virgo cluster** is the **closes galaxy cluster** to us.

HST view of M87, also known as Virgo A to radio astronomers. Its prominent jet, shown at the right, was discovered optically in 1917. The jet extends from the galaxy some 1.5 kpc into one of its radio lobes.



Radio lobes and jets

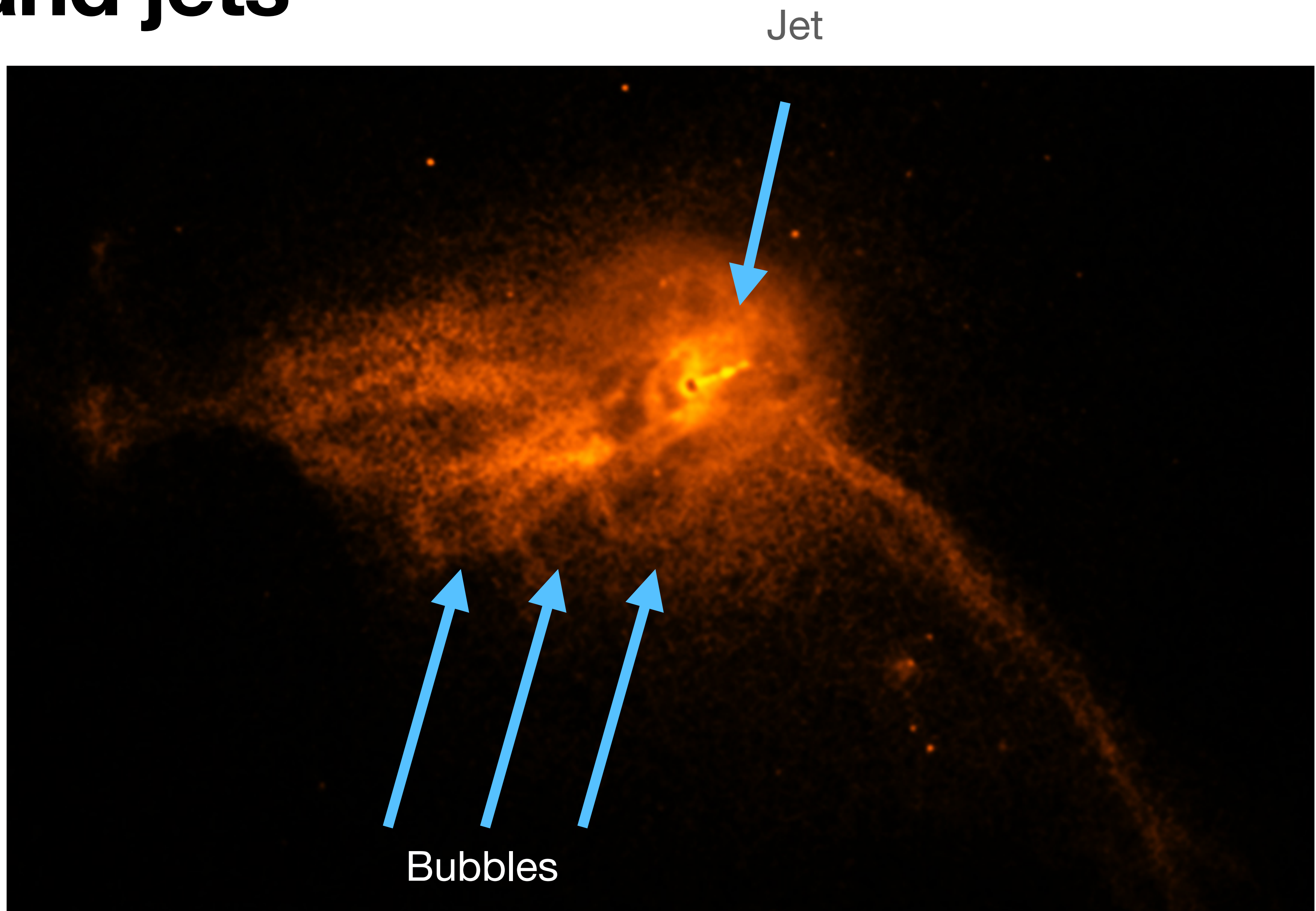


Large scale radio structure of M87.

Radio lobes and jets

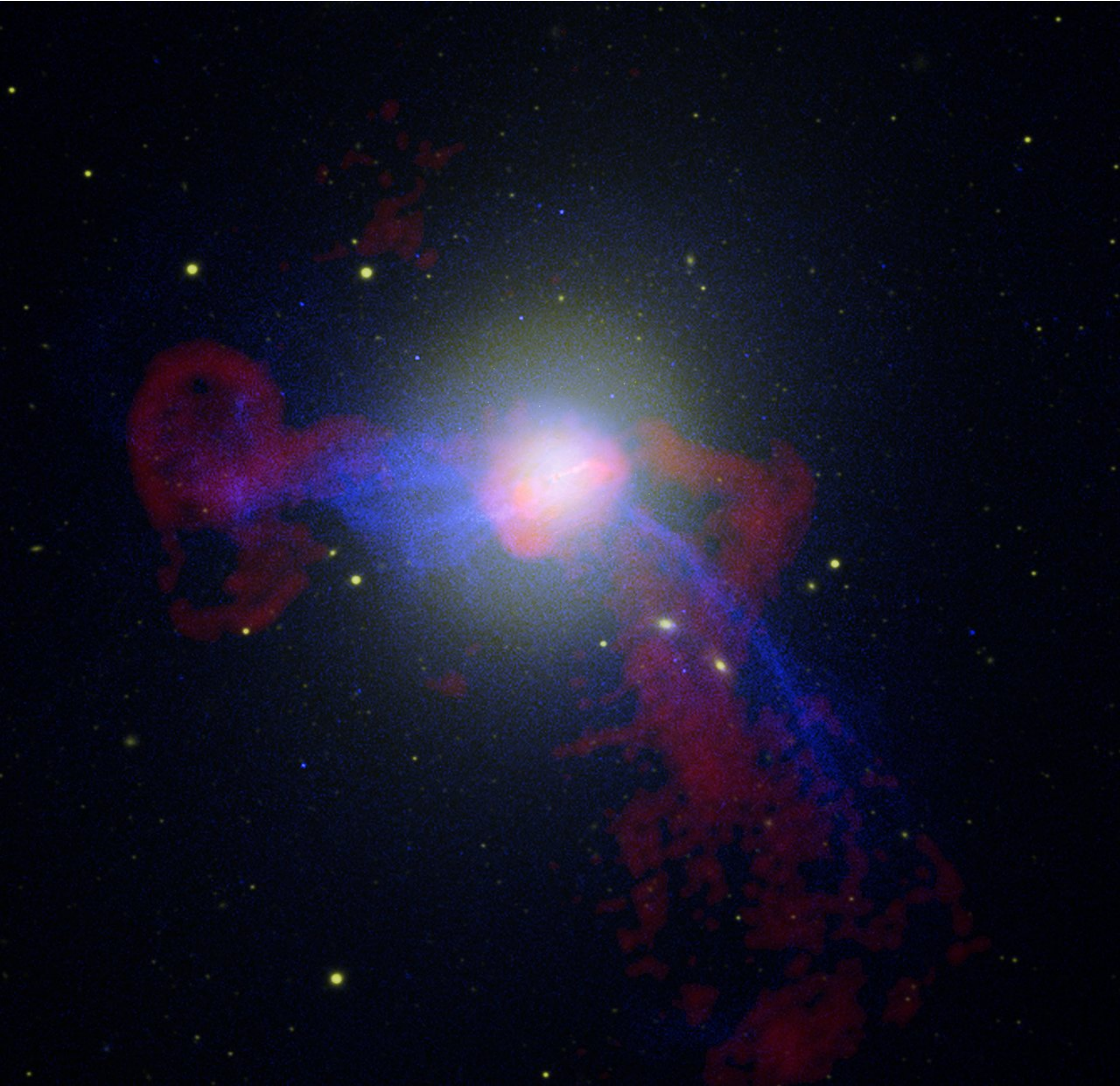
The jet also displays evenly spaced **knots** that are bright at radio, visible, and **X-ray wavelengths**. The X-ray luminosity of M87, including the jet, is roughly 10^{36} W. This is about 50 times greater than M87's radio luminosity.

There is also evidence for a **faint counterjet** extending away from M87 in the direction opposite that of the dominant jet.



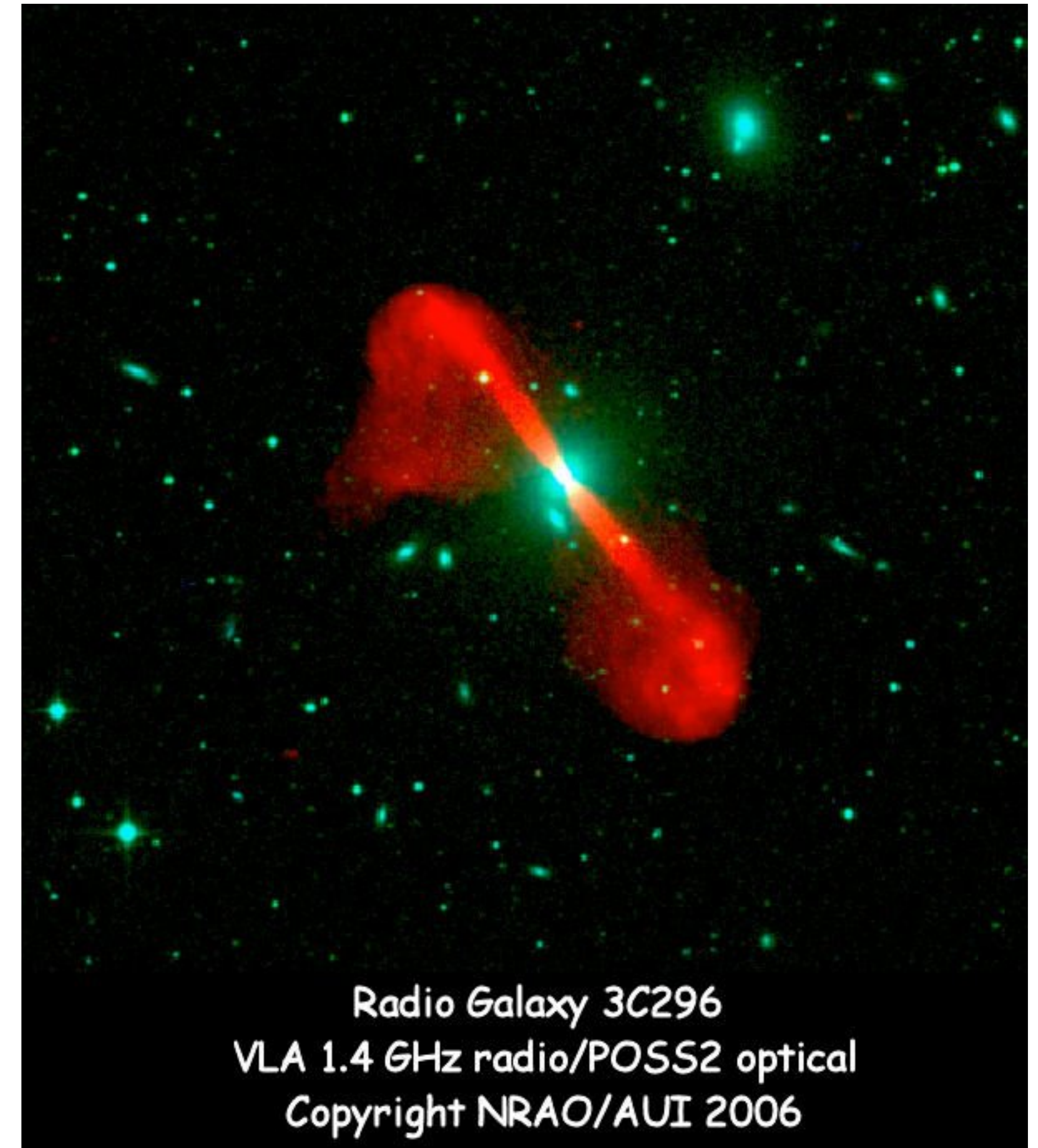
Radio lobes and jets

Radio - red
X-ray - blue
Optical - green



Radio lobes and jets

One of the largest radio galaxies known is 3C 236 (the “3C” designates a listing in the **Third Cambridge Catalog** of radio sources). With a redshift of $z = 0.0988$, its distance is about $280h^{-1}$ Mpc, according to Hubble’s law. The radio lobes of 3C 236 are separated by more than $1.5h^{-1}$ Mpc, projected onto the plane of the sky, while its radio jet is only $400h^{-1}$ pc long.

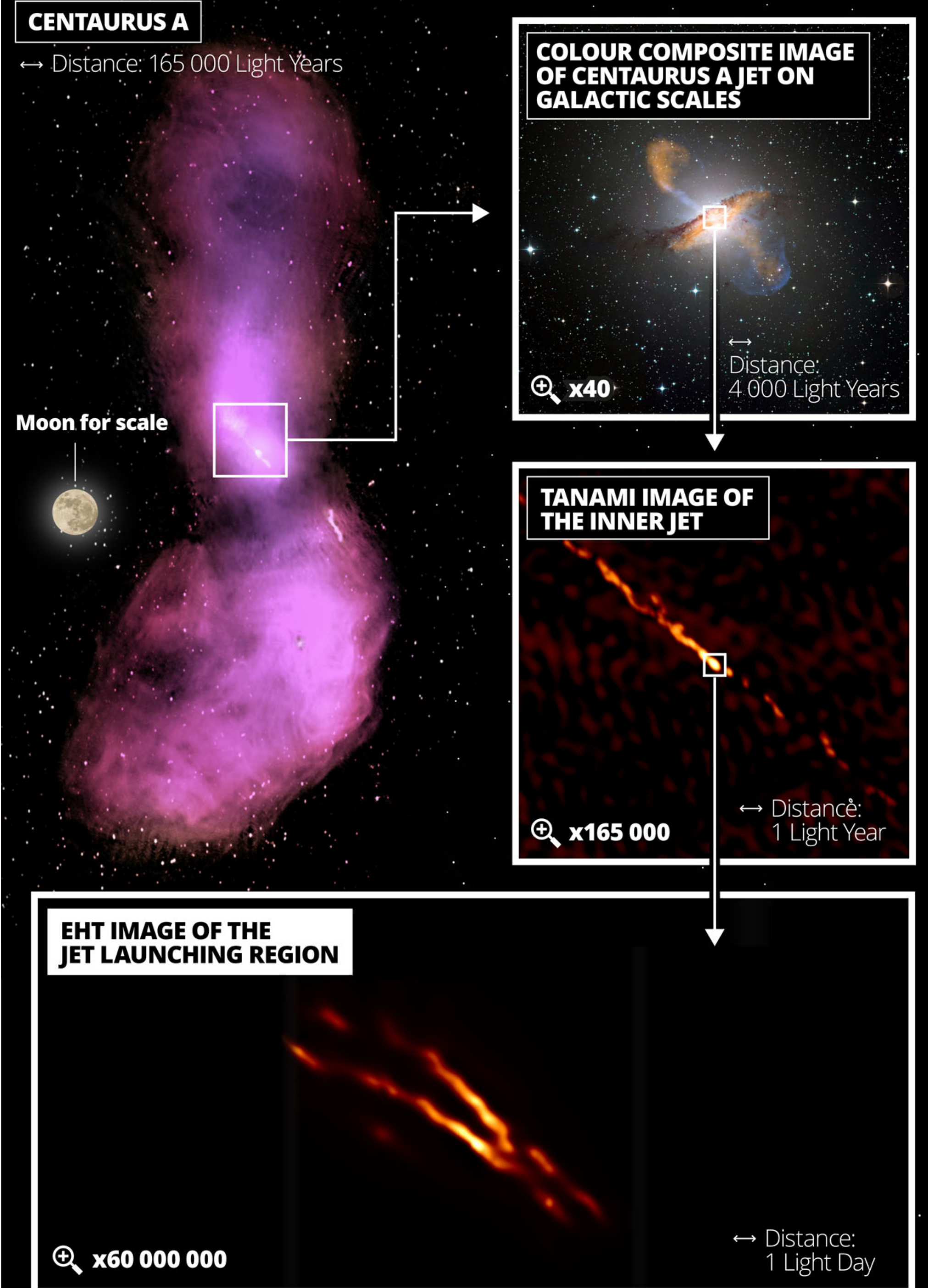


Radio Galaxy 3C296
VLA 1.4 GHz radio/POSS2 optical
Copyright NRAO/AUI 2006

Radio lobes and jets

The closest example of an AGN is **Centaurus A** (NGC 5128), at a distance of $4.7 h^{-1}$ Mpc.

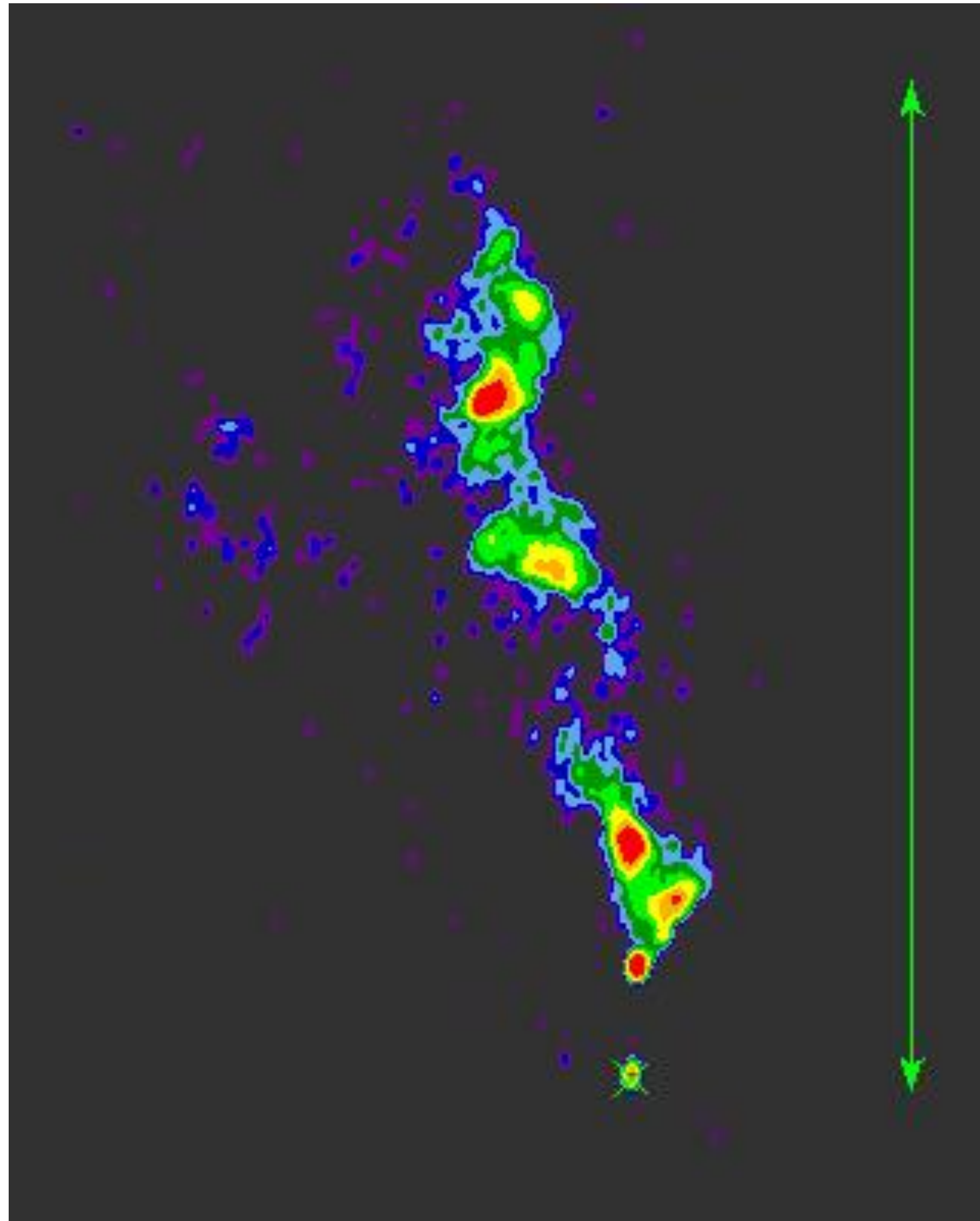
An E2 galaxy girded by a thick dust lane. Superimposed on the photograph is a radio map showing the radio lobes. Like M87, Cen A has a jet extending from its nucleus containing several knots of radio and X-ray emission. Although Cen A is in our astronomical backyard, radio galaxies on average are roughly 100 times less abundant than Seyferts in regions that are nearby in cosmological terms.



Quasars

3C 48 VLBA image (very high angular resolution)

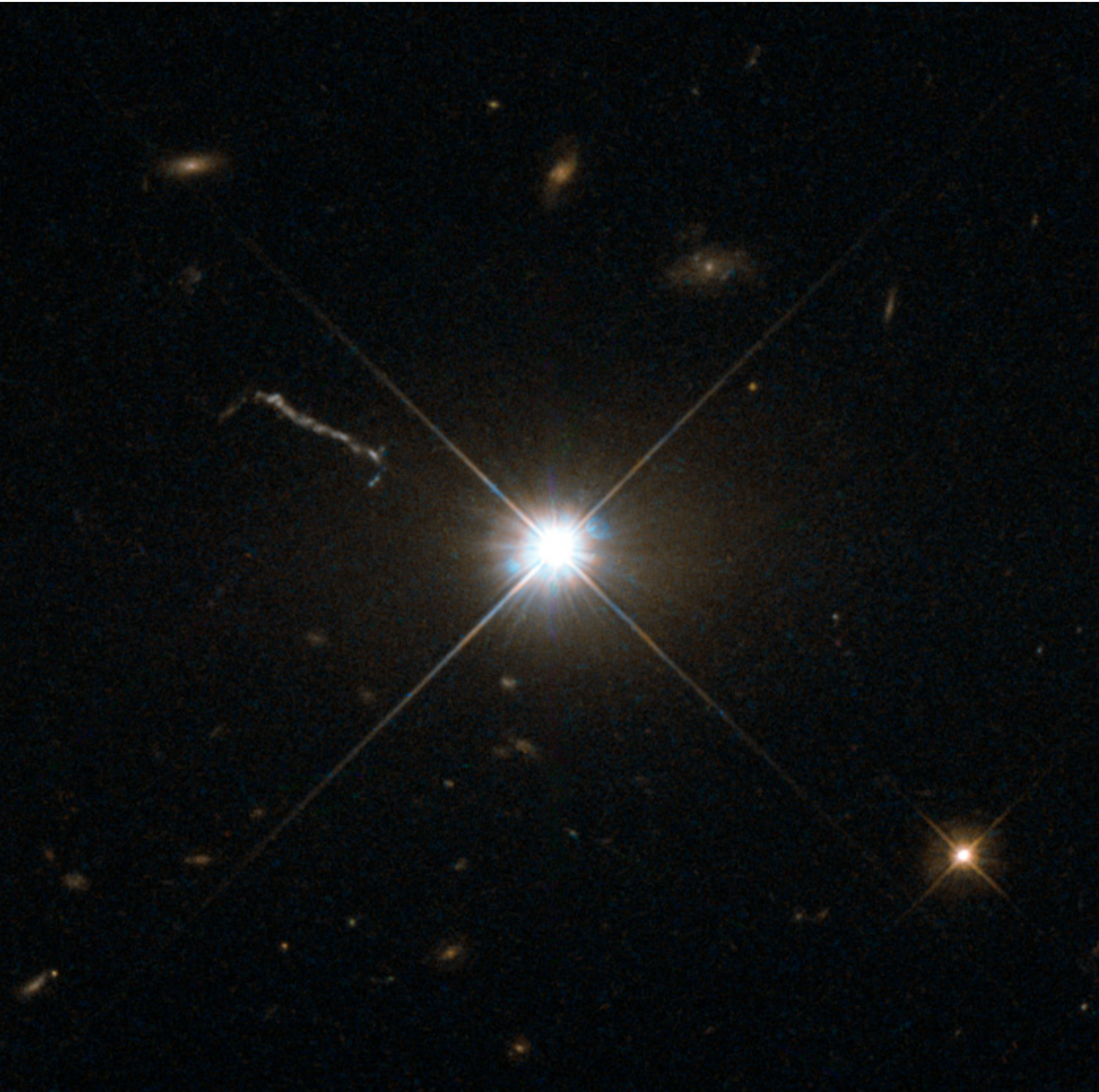
As radio telescopes discovered **increasing numbers of radio sources** in the late 1950s, the task of **identifying these** sources with known objects became more important. In 1960 Thomas Matthews and Allan Sandage were searching for an optical counterpart to another radio source, 3C 48. They found a 16th-magnitude **starlike object** whose unique spectrum displayed **broad emission lines** that could not be identified with any known element or molecule.



Quasars

3C 273 - Hubble image

In 1963 a similarly weird spectrum was found for **another radio source with a stellar appearance**, 3C 273. Figure 12 shows 3C 273 and its jet, which extends a projected distance of $39h^{-1}$ kpc from the nucleus.



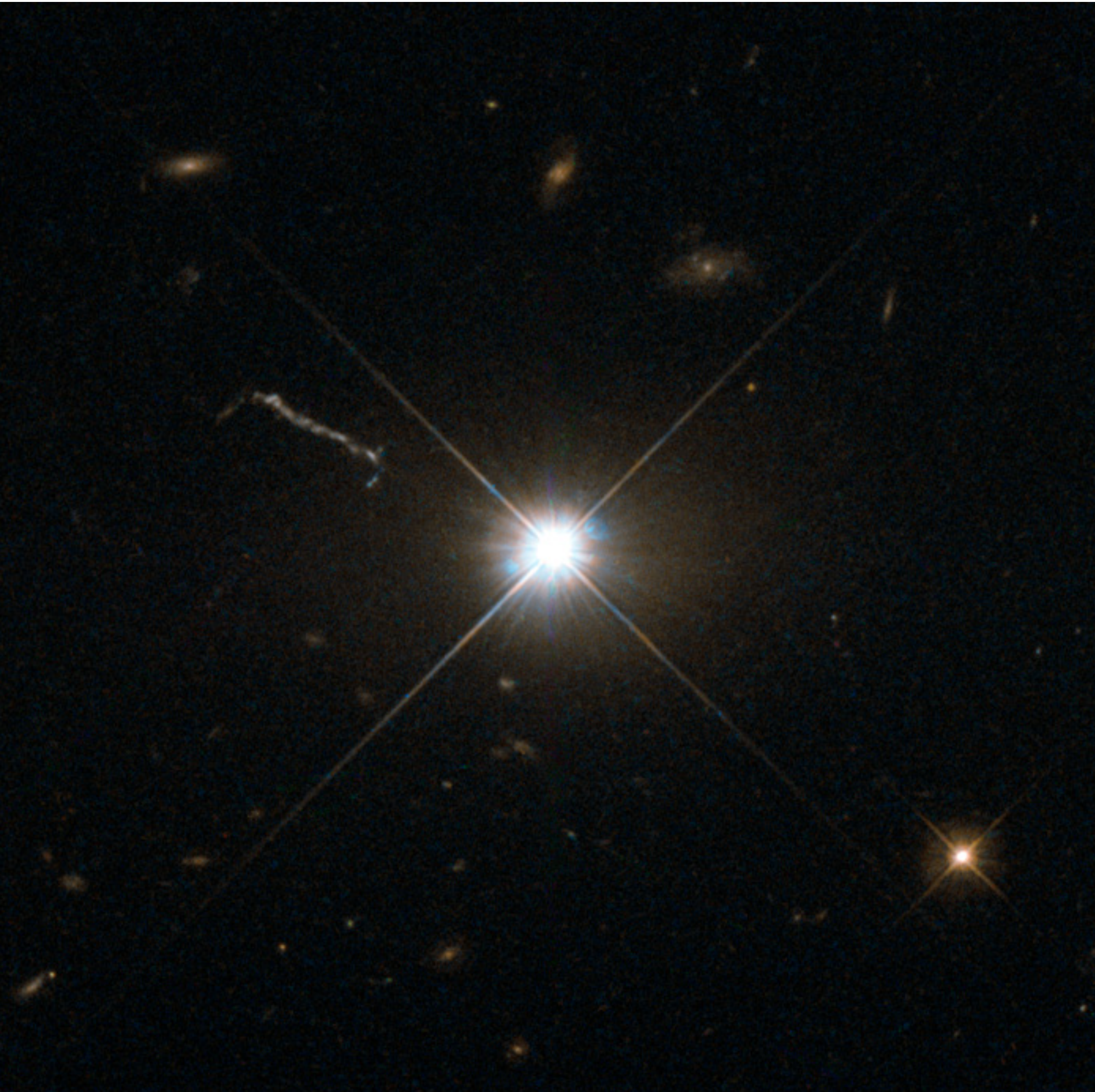
Quasars

3C 273 - Hubble image

In 1963 a similarly weird spectrum was found for **another radio source with a stellar appearance**, 3C 273. Figure 12 shows 3C 273 and its jet, which extends a projected distance of $39h^{-1}$ kpc from the nucleus.

3C 48, 3C 273, and other, similar sources were classified as **quasi-stellar radio sources (QSRs)**, which became known as **quasars**.

Later, the mystery lifted somewhat when astronomers recognized that the pattern of the broad emission lines of 3C 273 was the same as the pattern of the **Balmer lines of hydrogen**. These lines had been **severely redshifted** ($z = 0.158$), making their identification difficult. According to Hubble's law, this places 3C 273 at a distance of about $440h^{-1}$ Mpc.



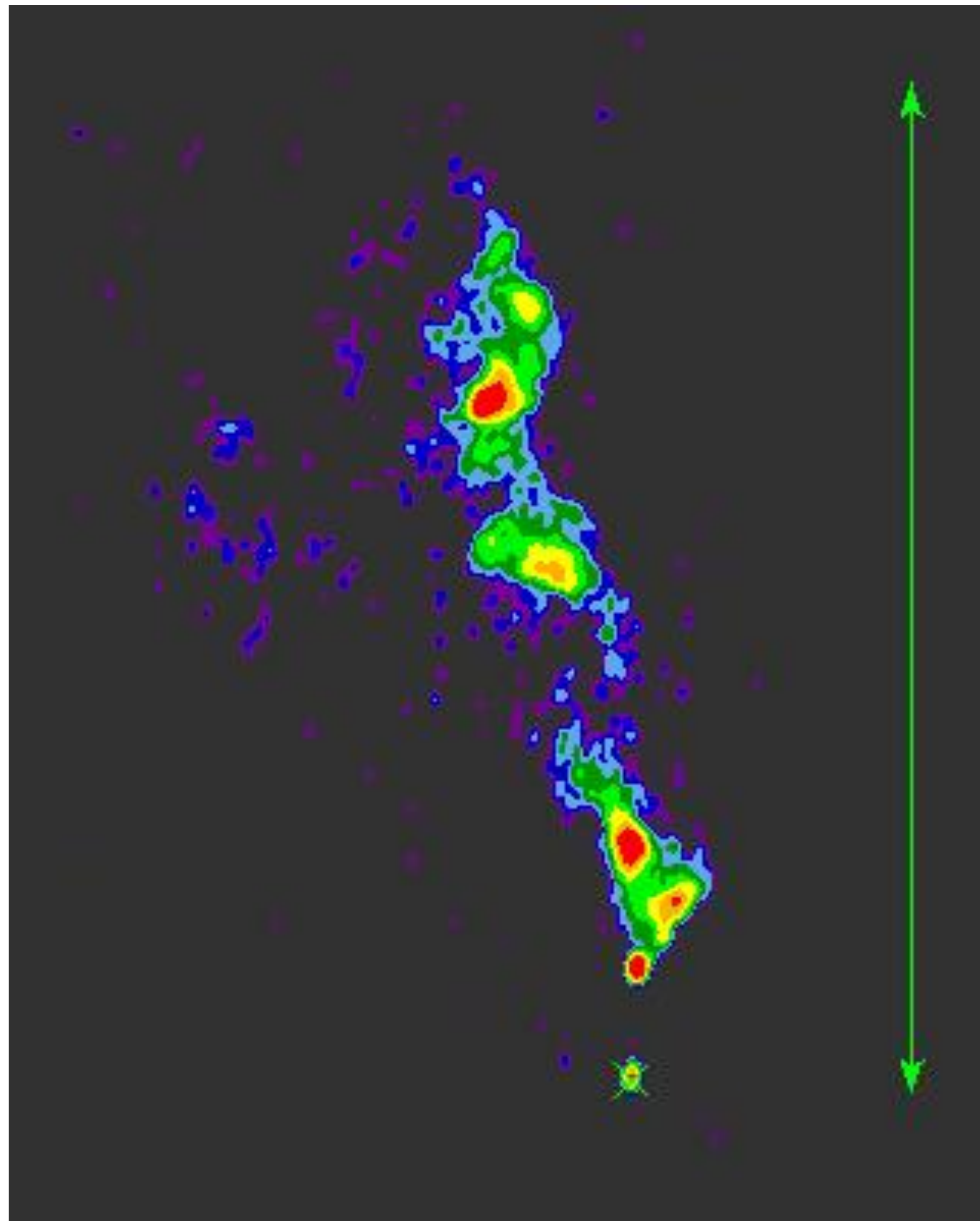
Quasars

3C 48 VLBA image (very high angular resolution)

3C 48 has an even greater redshift, $z = 0.367$, corresponding to a radial velocity of $0.303c$ and a Hubble distance of just over $900h^{-1}$ Mpc.

Astronomers realized that **3C 48 was one of the most distant objects yet discovered** in the universe.

Today we have discovered many more even more distant quasars.



Quasars

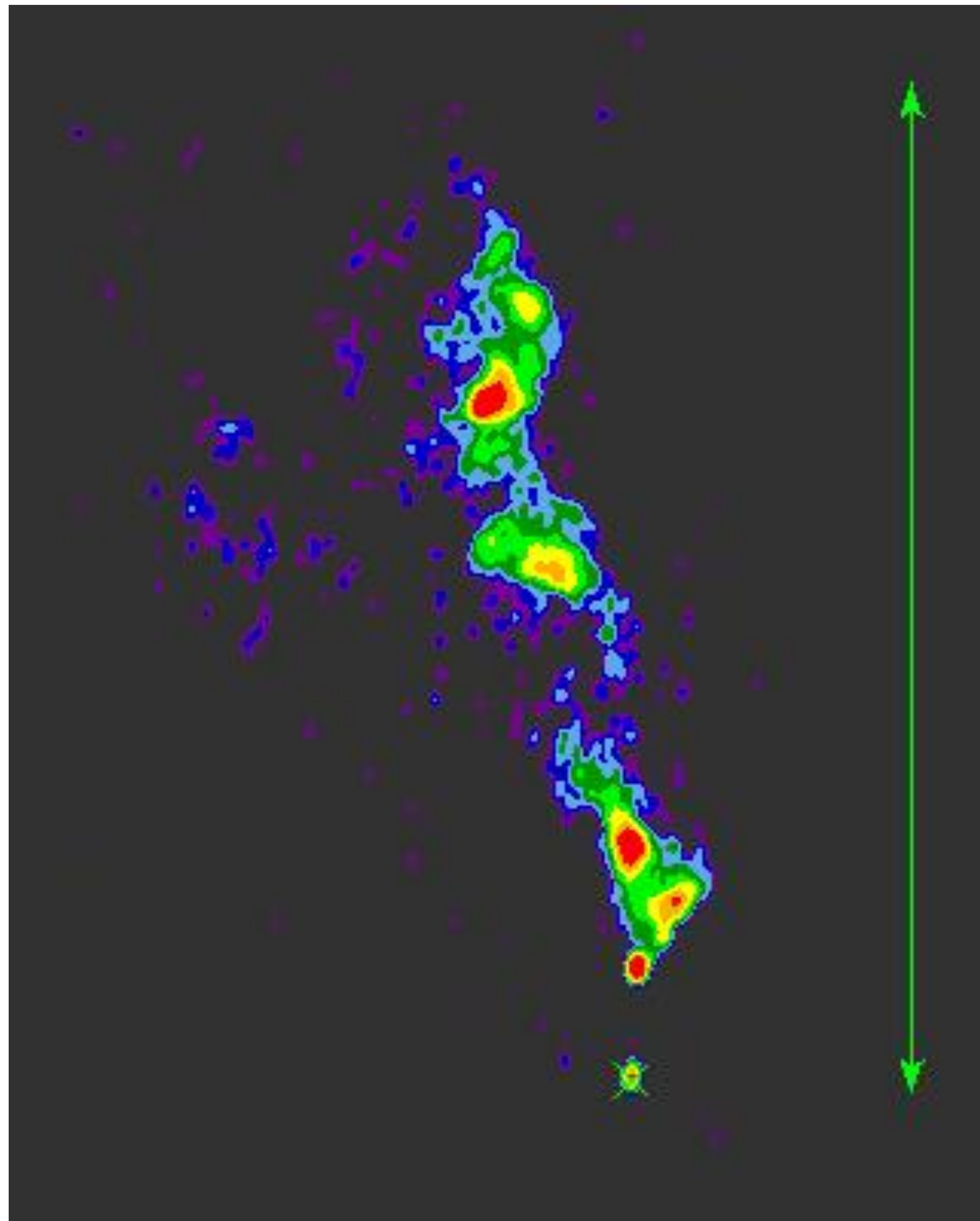
3C 48 VLBA image (very high angular resolution)

3C 48 has an even greater redshift, $z = 0.367$, corresponding to a radial velocity of $0.303c$ and a Hubble distance of just over $900h^{-1}$ Mpc.

3C 48 was one of the most distant objects yet discovered (at the time of the first redshift measurement).

Today the most distant quasars are around $z = \sim 7.6$ and the James Webb telescope is finding objects at $z = \sim 13$.

A quasar's radio emission may come either from radio lobes or from a central source in its core. Quasars are so far away that in optical images most appear as overwhelmingly bright, starlike nuclei surrounded by faint fuzzy halos. In some cases, a fuzzy halo can be resolved into a faint parent galaxy. **To be visible from such great distances, quasars must be exceptionally powerful.**



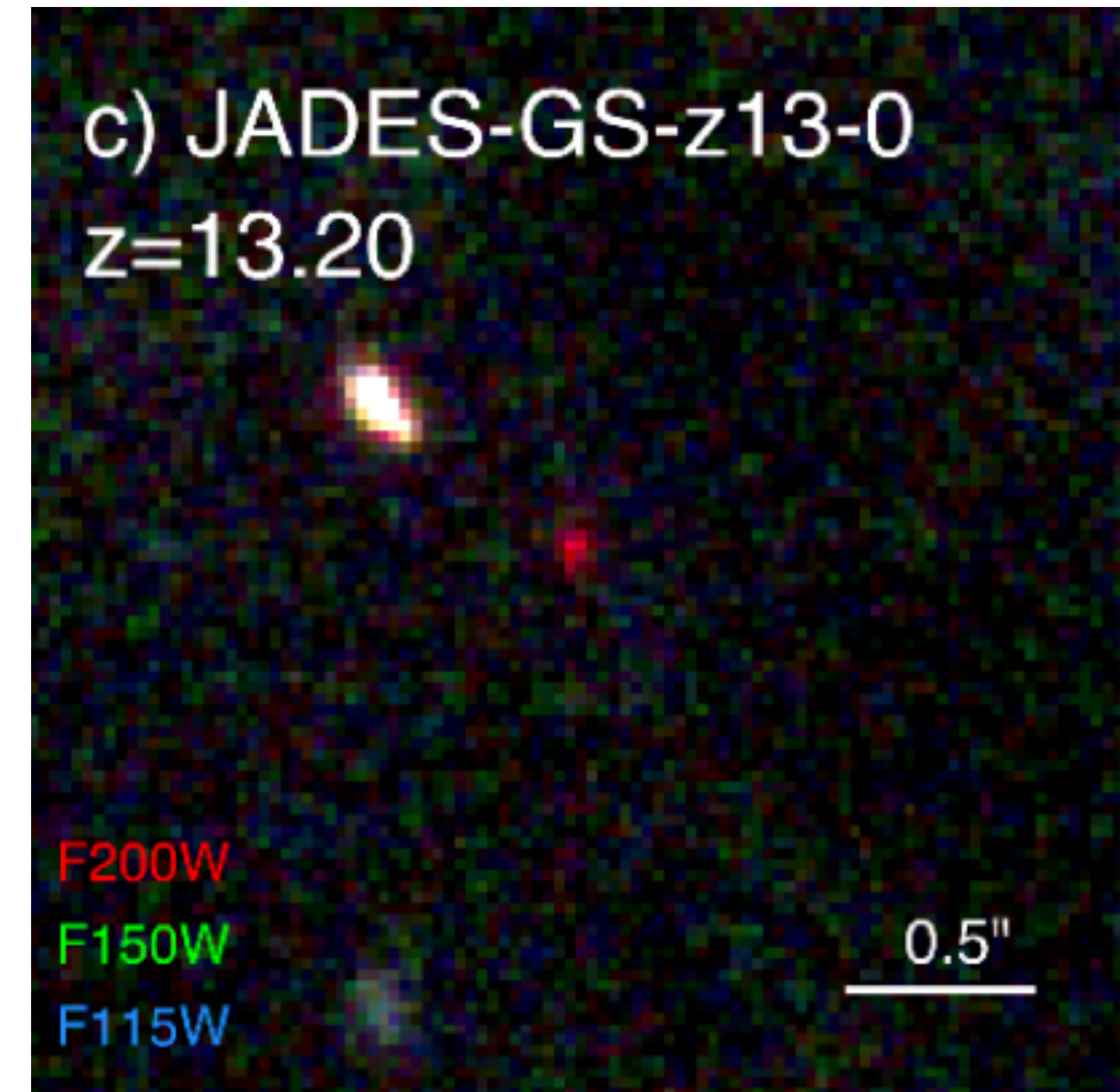
Quasars

This object was detected with the James Webb telescope and has an approximate redshift of $z = 13.20$ (redshift is determined with spectroscopy). The **age of the Universe is estimated to be $z = 13.787$**

Identified as a Lyman-break galaxy. **Lyman-break galaxies are star-forming galaxies at high redshift** that are selected using the differing appearance of the galaxy in several **imaging filters** due to the position of the Lyman limit.

Radiation at higher energies than the Lyman limit at 912 Å is almost completely absorbed by neutral gas around star-forming regions of galaxies. In the rest frame of the emitting galaxy, the emitted spectrum is bright at wavelengths longer than 912 Å, but very dim or imperceptible at shorter wavelengths — this is known as a "dropout", or "break", and can be used to find the position of the Lyman limit. At high redshift galaxies this break is shifted to optical or infrared wavelengths.

The most distant object in the Universe? In 2023.



Quasars

Example 1.2. The following equation can be used to obtain the absolute visual magnitude of the quasar 3C 273, which has an apparent visual magnitude of $V = 12.8$:

$$m - M = 5 \log_{10}(d) - 5 = 5 \log_{10} \left(\frac{d}{10 \text{ pc}} \right).$$

Adopting $[h]_{\text{WMAP}} = 0.71$ yields a distance of $d \approx 620 \text{ Mpc}$, implying that

$$M_V = V - 5 \log_{10} \left(\frac{d}{10 \text{ pc}} \right) = -26.2.$$

This value can be used to obtain an estimate of the luminosity of the quasar at visual wavelengths. Using $M_{\text{Sun}} = 4.82$ for the Sun's absolute visual magnitude gives an **estimate of the quasar's visual luminosity**:

$$L_V \approx 100^{(M_{\text{Sun}} - M_V)/5} L_{\odot} = 2.6 \times 10^{12} L_{\odot} = 1 \times 10^{39} \text{ W}.$$

Quasars

The radio energy emitted by 3C 273 can be estimated from its distance and the value of the monochromatic flux at a radio frequency of 1400 MHz, $F_{1400} = 4.64 \times 10^{-25} \text{ W m}^{-2} \text{ Hz}^{-1} = 46.4 \text{ Jy}$. The radio spectrum follows the power law with a spectral index of $\alpha \approx 0.24$. Integrating the monochromatic flux from $\nu_1 \approx 0$ to $\nu_2 = 3 \text{ GHz}$ gives

$$L_{\text{radio}} = 4\pi d^2 \int_{\nu_1}^{\nu_2} F_{\nu} d\nu = 7 \times 10^{36} \text{ W}.$$

The bolometric luminosities inferred for quasars range from about 10^{38} W to more than 10^{41} W , with $5 \times 10^{39} \text{ W}$ being a typical value.

This implies that the most luminous quasars are on the order of **10⁵ times more energetic than a normal galaxy like our own Milky Way**.

Quasar spectra

The monochromatic flux of 3C 273 is shown in Fig. 14.

This continuous spectrum spans nearly **15 orders of magnitude in frequency**, very broad compared with the sharply peaked blackbody spectrum of a star.

The **decline at the low-frequency end** of the spectrum reflects the larger-than-average spectral index ($\alpha = 0.24$) for 3C 273 in this regime.

->At **low frequencies**, the spectrum is **dominated by radiation from its jet**.

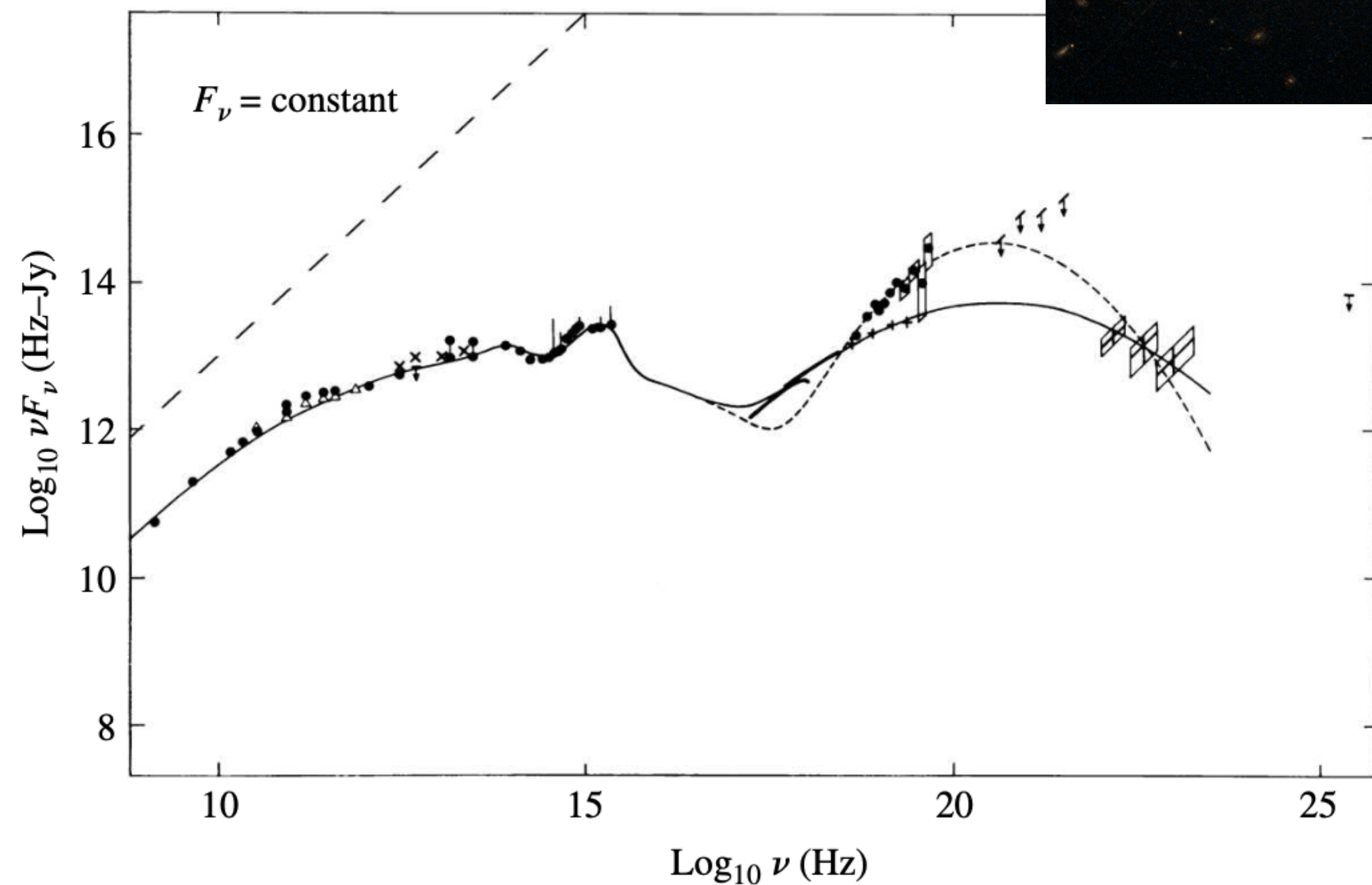
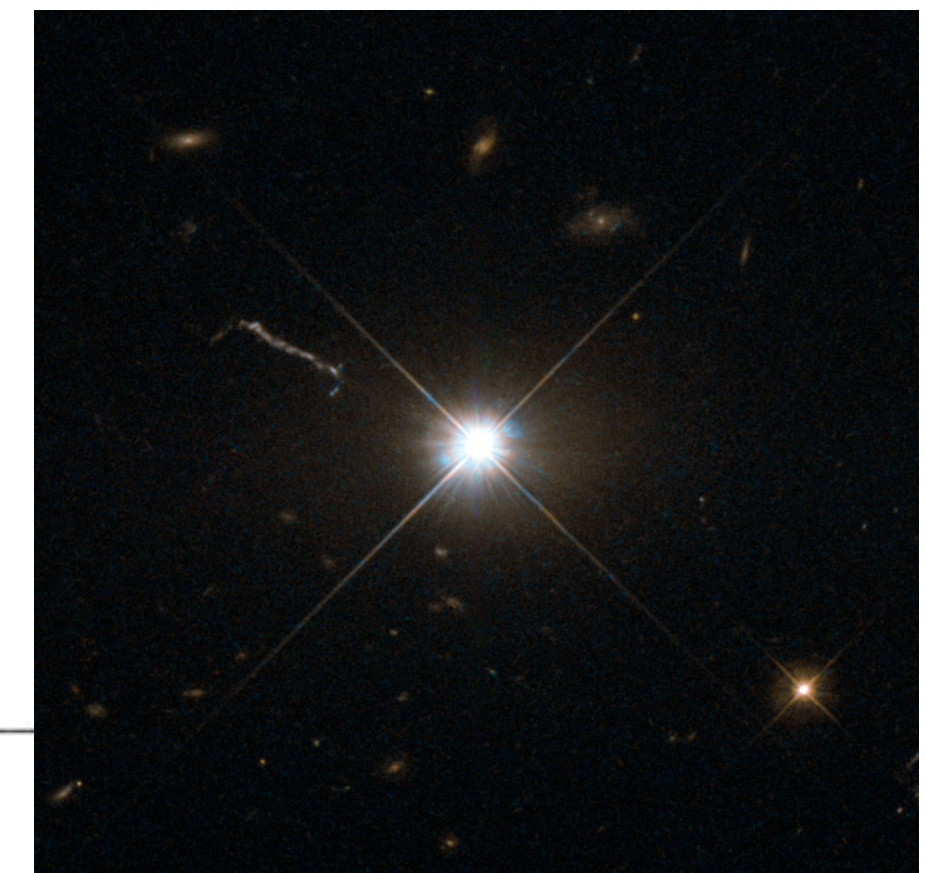


FIGURE 14 The spectrum of 3C 273, after the Doppler shift of the frequencies due to the Hubble flow has been removed. A horizontal line would correspond to a spectral index of $\alpha = 1$; for reference, the diagonal dashed line shows the slope for $F_\nu = \text{constant}$. The two lines on the right correspond to 3C 273 during quiescence and during an outburst. (Figure adapted from Perry, Ward, and Jones, *MNRAS*, 228, 623, 1987.)



Quasar spectra

For **most other quasars**, the spectrum at the low-frequency end falls off more abruptly (**smaller α**). A **typical spectrum turns over in the far infrared** at a frequency of about 5×10^{12} Hz, possibly due to dust and/or synchrotron self-absorption.

Some quasars are most luminous at infrared wavelengths and others peak in **X-rays**.

The peak power output of **3C 273** is in the form of low-energy **gamma rays**.

Quasars emit an excess of **ultraviolet light** relative to stars and so are quite blue in appearance.

In Fig. 14, this ultraviolet excess is indicated by the big **blue bump** between roughly 10^{14} Hz and 10^{16} Hz. A big blue bump is a feature of most (but not all) quasar spectra.

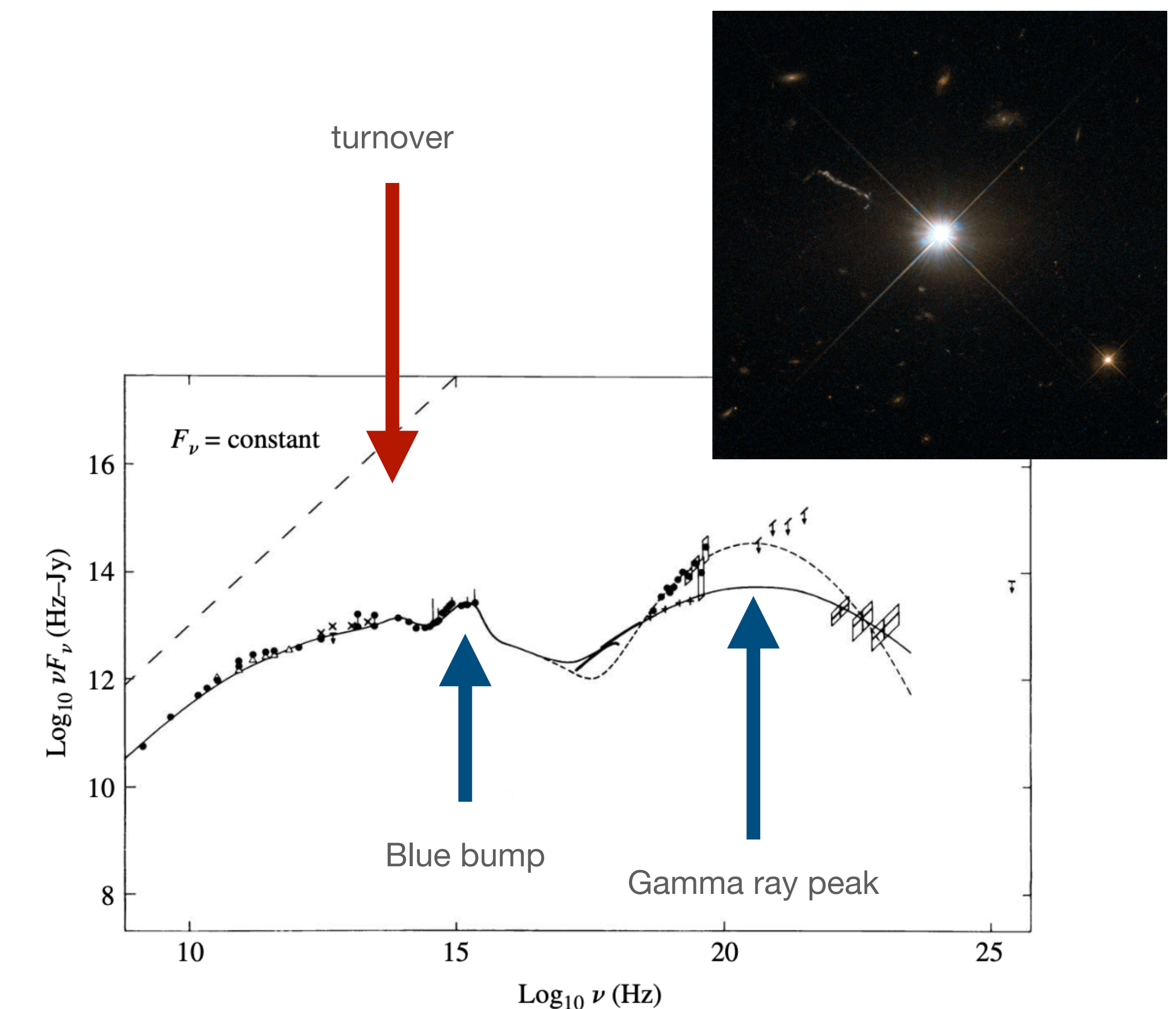


FIGURE 14 The spectrum of 3C 273, after the Doppler shift of the frequencies due to the Hubble flow has been removed. A horizontal line would correspond to a spectral index of $\alpha = 1$; for reference, the diagonal dashed line shows the slope for $F_\nu = \text{constant}$. The two lines on the right correspond to 3C 273 during quiescence and during an outburst. (Figure adapted from Perry, Ward, and Jones, *MNRAS*, 228, 623, 1987.)

Quasar spectra

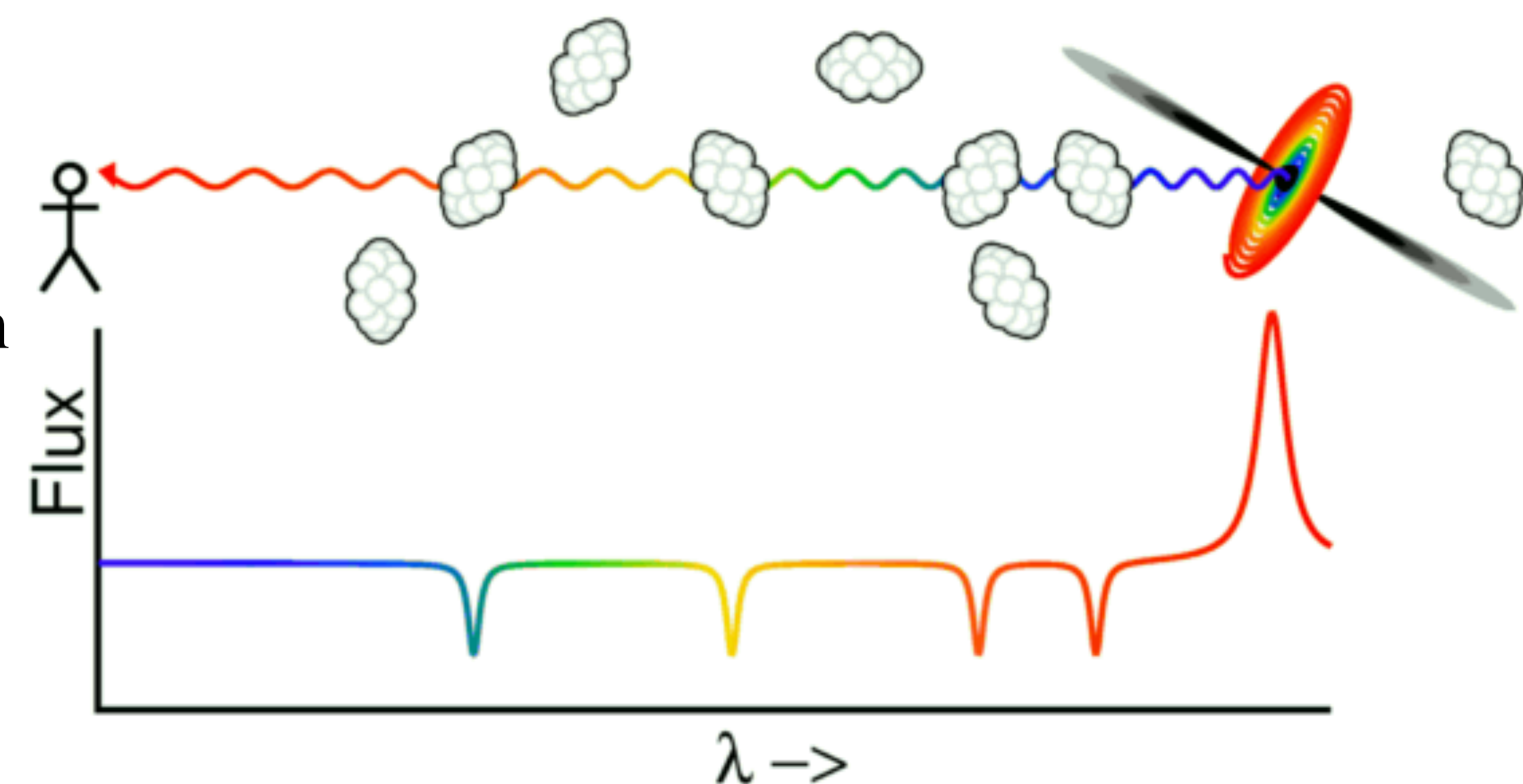
Absorption lines may also be present in some quasar spectra.

In particular, **Doppler-broadened absorption lines**, found in up to 10% of the spectra of quasars, originate from sources with **speeds exceeding 10^4 km s^{-1}** . These lines are believed to be **associated with the quasar itself**.

Many additional **narrow absorption lines** are typically seen in the spectra of quasars with high redshifts ($z > 2.2$) due to the **Lyman series of hydrogen** and metals such as **C IV and Mg II**.

These lines would normally appear at ultraviolet wavelengths but have been **redshifted into the visible spectrum** by the recessional velocity of the absorbing material.

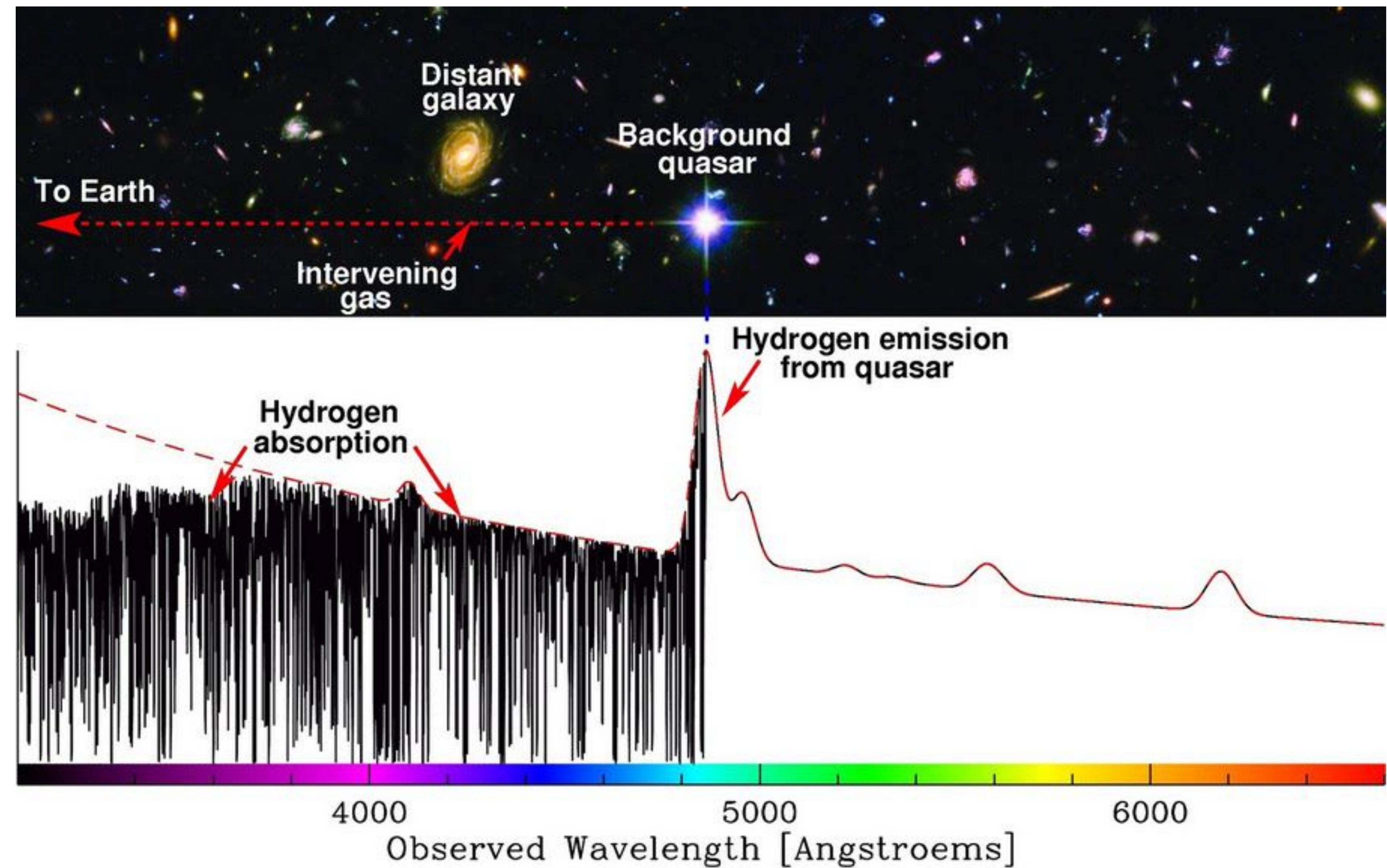
The absorption lines of a given quasar can be placed into **different groups that share common redshifts**. The various groupings of lines are thought to arise from **clouds of intervening material** that lie between the quasar and Earth.



Quasar spectra

The Lyman alpha forest:

In astronomical spectroscopy, the Lyman-alpha forest is a series of absorption lines in the spectra of distant galaxies and quasars arising from the Lyman-alpha electron transition of the neutral hydrogen atom. As the light travels through multiple gas clouds with different redshifts, multiple absorption lines are formed.



Quasi-Stellar Objects

The distinctive appearance of quasars, **starlike with an excess of ultraviolet light**, led astronomers to search for more objects fitting this description. In fact, choosing those objects with $U - B < -0.4$ (blue in colour) results in a nearly complete list of possible quasars (those at very high z are redder), which must then be confirmed by a spectroscopic analysis.

Researchers discovered that about 90% of the confirmed quasar candidates, and **AGNs in general, are relatively radio-quiet**. For this reason, most of these objects are technically referred to as **quasi-stellar objects** (QSOs), rather than quasars (QSRs). These objects tend to have very faint radio emission mostly only detectable through stacking.

Today, the term *quasar* has come to be used almost universally for both radio-loud QSRs and radio-quiet QSOs. As a result, it is common to encounter the descriptions **radio-loud quasars** and **radio-quiet quasars**. However, it is also sometimes the case that **QSO is used as an abbreviation for quasar**.

The terminology can be confusing in the literature.

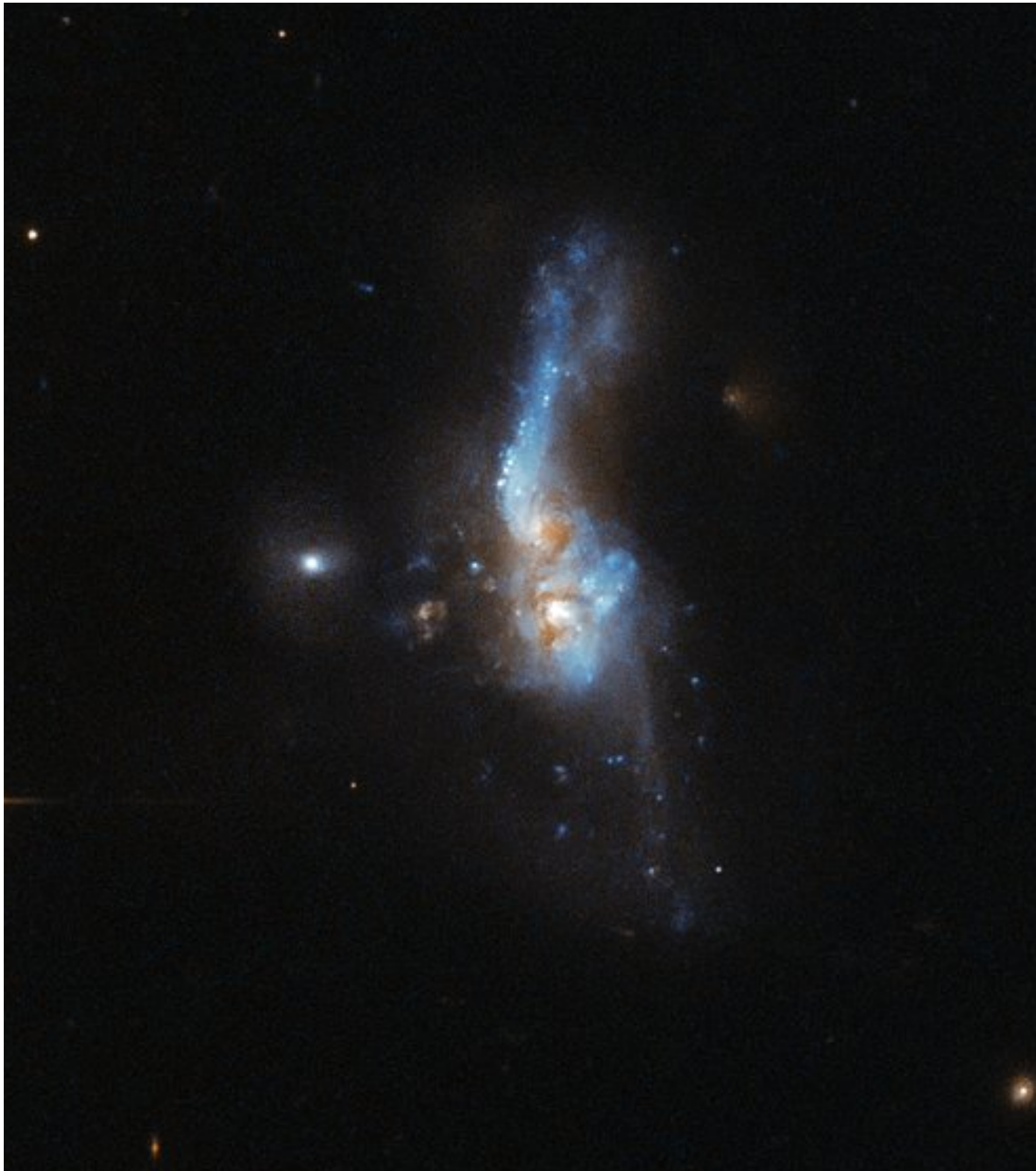
Ultraluminous inferred galaxies

Nearly all **quasars have spectra similar to those of broad-line radio galaxies and Seyfert 1s**, with bright power-law continua and broad emission lines.

Seyfert 2 spectra, with their narrow emission lines, appear to have no counterparts among the quasars. However, some astronomers argue that a subset of the galaxies that were cataloged by the IRAS satellite as being ultra-luminous at infrared wavelengths, known as **ultraluminous infrared galaxies (ULIRGs)**, should be **considered quasars of type 2** rather than **starburst galaxies**. It is suggested that the infrared light results from dust that absorbs and reradiates the light from the quasar nucleus.

According to one study a ULIRG is just part of an **evolutionary galaxy merger scenario**. In essence, two or more spiral galaxies, merge to form an early stage merger. After that, it becomes a late stage merger, which is a ULIRG. It then becomes a quasar and in the final stage of the evolution it becomes an elliptical galaxy.

IRAS 14348-1447 is an ultraluminous infrared galaxy, located over a billion light-years away.



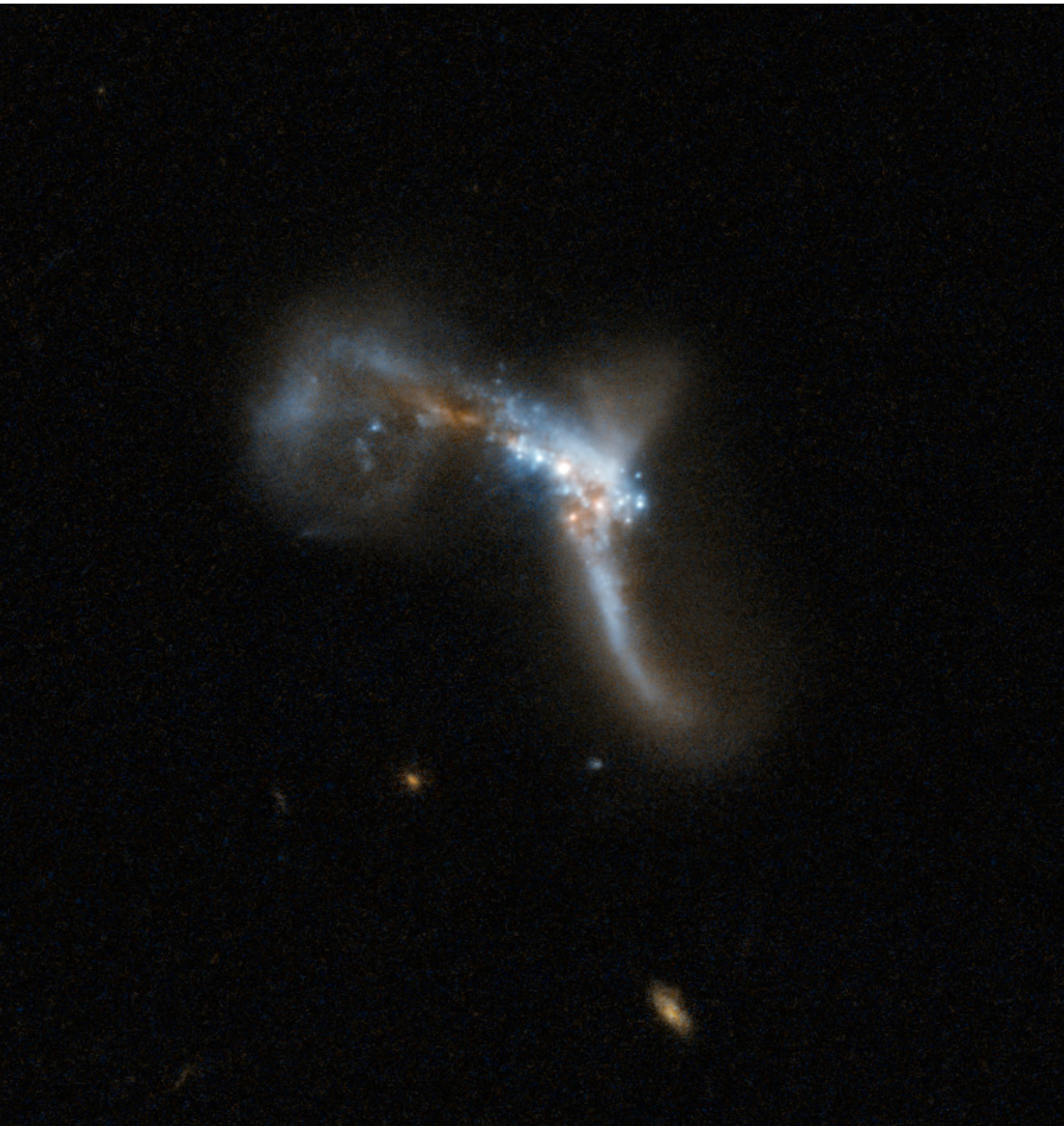
Ultraluminous inferred galaxies

The reason for this **intense infrared emission** lies in an **episode of strong star formation activity**, which was set off by a **collision** between two interacting galaxies.

In this image the twisted shape hides a number of features. In the central region, we can **distinguish two nuclei**, remains of the two different galaxies that are currently colliding.

IRAS 22491-1808 is amongst the most luminous of these types of galaxies, and is considered to be mid-way through its merging stage. The centre also shows several intense star-forming knots. Other traces of the galactic collision are the three very noticeable tails in the image — two linear and one circular.

IRAS 22491-1808, also known as the **South America Galaxy**. It is an ultraluminous infrared galaxy (ULIRG)



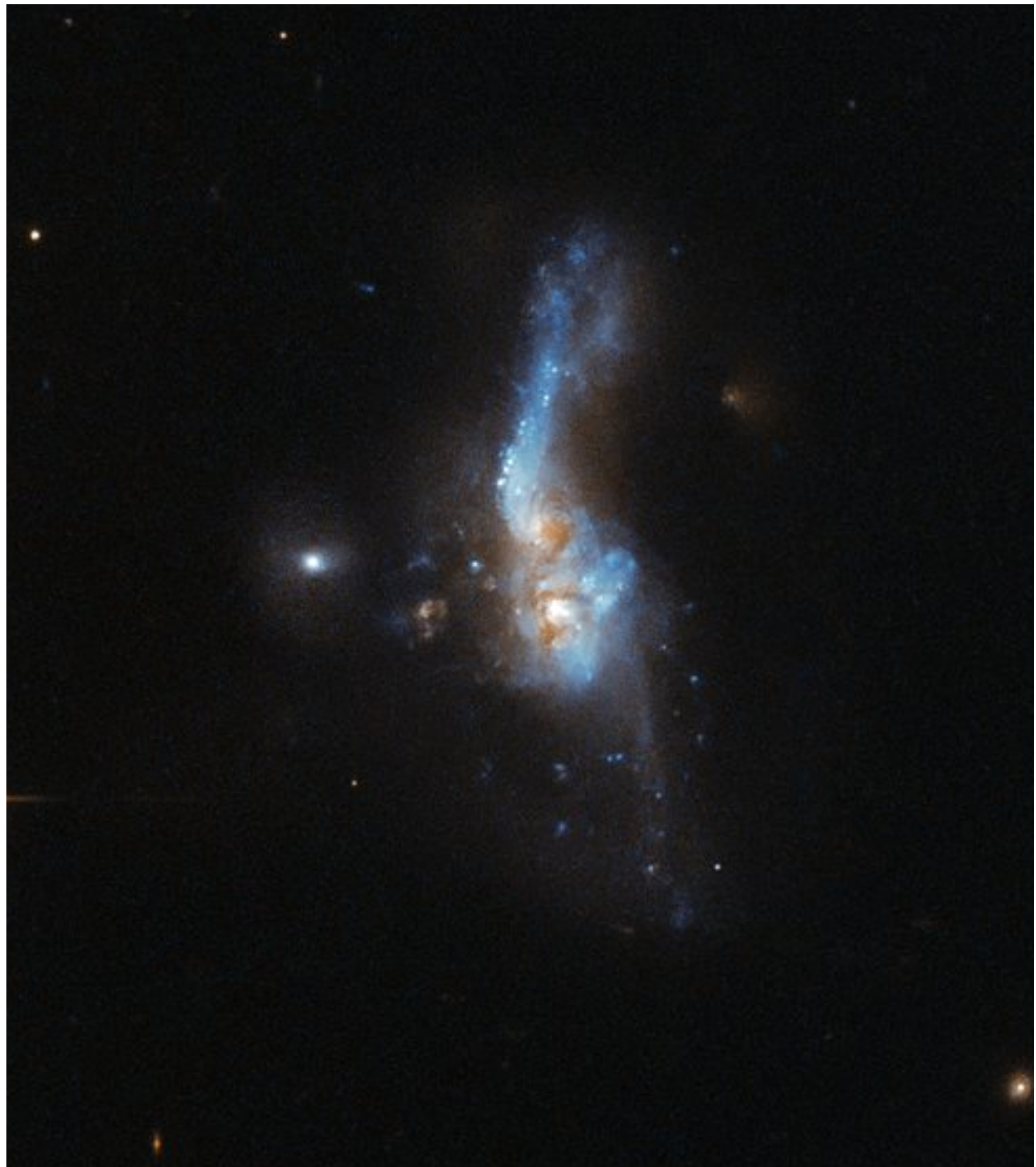
Ultraluminous inferred galaxies

Luminous infrared galaxies or LIRGs are **galaxies** with **luminosities**, the measurement of brightness, above $10^{11} L_\odot$. They are also referred to as **submillimeter galaxies (SMGs)**.

- Galaxies with luminosities above $10^{12} L_\odot$ are ultraluminous infrared galaxies (ULIRGs).
- Galaxies exceeding $10^{13} L_\odot$ are hyper-luminous infrared galaxies (HyLIRGs).
- Those exceeding $10^{14} L_\odot$ are extremely luminous infrared galaxies (ELIRGs).

Many of the LIRGs and ULIRGs are showing **interactions, disruptions and intense star formation**.

IRAS 14348-1447 is an ultraluminous infrared galaxy, located over a billion light-years away.



High redshift

The **Sloan Digital Sky Survey** (SDSS) has cataloged 46,420 quasars.

The brightest entry in the catalog in the i band (centered on a wavelength of 748.1 nm) is the object SDSS 17100.62+641209.0 at a redshift of $z = 2.7356$, having $M_i = -30.242$.

The most distant quasar in the catalog is SDSS 023137.65–072854.4 at a redshift of $z = 5.4135$, implying a recessional velocity of more than $0.95c$. In fact, there are 520 quasars in the SDSS catalog with redshifts greater than $z = 4$.

For such large cosmological redshifts, we must abandon using the Hubble law to determine distances.

Cosmological redshifts are caused by the expansion of the space through which the light travels, so for extremely large distances the total elongation of the wavelength depends on how the expansion of the universe has changed with time. The rate of expansion is changing in response to all of the matter and energy in the universe.

For this reason, it is customary to quote the redshift, z , rather than an actual distance determination.

High redshift

You should keep in mind, however, that the fractional change in wavelength for a cosmological redshift is the same as the fractional change in the size of the universe, R , since the time when the light was emitted.

$$z = \frac{\lambda_{\text{obs}} - \lambda_{\text{emitted}}}{\lambda_{\text{emitted}}} = \frac{R_{\text{obs}} - R_{\text{emitted}}}{R_{\text{emitted}}},$$

which gives

$$\frac{R_{\text{obs}}}{R_{\text{emitted}}} = 1 + z.$$

Thus a redshift of $z = 3$ means that the universe is now four times larger than when the light was emitted.

Evidence for Quasar evolution

The regions that are cosmologically close to us make up “today’s universe.” In observing these regions, astronomers can study galaxies as they appear here and now in the present epoch. When looking deeper into the universe, however, we see photons that have been traveling for a long time from a source that may have changed significantly since the light began its journey. This essentially means that looking farther into space implies peering farther into the past. Thus telescopes serve as time machines, providing a window to the early universe.

Bright quasars were more common at earlier epochs than they are now, as evidenced by observations at large and small z , respectively.

Several factors could contribute to the greater space density of luminous quasars in the past. **Both the total number of quasars and their luminosities may have been different** then, and it is obviously a difficult task to disentangle these influences. A further complication is introduced by the **expansion of the universe**. The universe is larger today than it was at a redshift z by a factor of $1 + z$, so **the space density of quasars would be greater in the past** even if their numbers and luminosities have remained constant.

To avoid confusion caused by the expansion of the universe, we have defined a **comoving space density** that mathematically removes the effect of the expanding universe. The number of objects per Mpc^3 at a redshift z is divided by $(1 + z)^3$, scaling the space density down to the value it would have today (at $z = 0$).

Evidence for Quasar evolution

The comoving space density of a constant number of nonevolving objects does not change as the universe expands, and so a **change in this density implies that the number of objects is varying or that the objects are evolving (or both)**.

Statistical studies indicate that there are more than **1000 times as many** quasars per Mpc^3 (comoving space density) **brighter** than $M_B = -25.9$ at $z = 2$ than there are today ($z = 0$). However, there is strong evidence that the **total number of quasars has *not* changed significantly** from the present ($z = 0$) back to roughly $z = 2$. Figure 15 shows several luminosity functions.

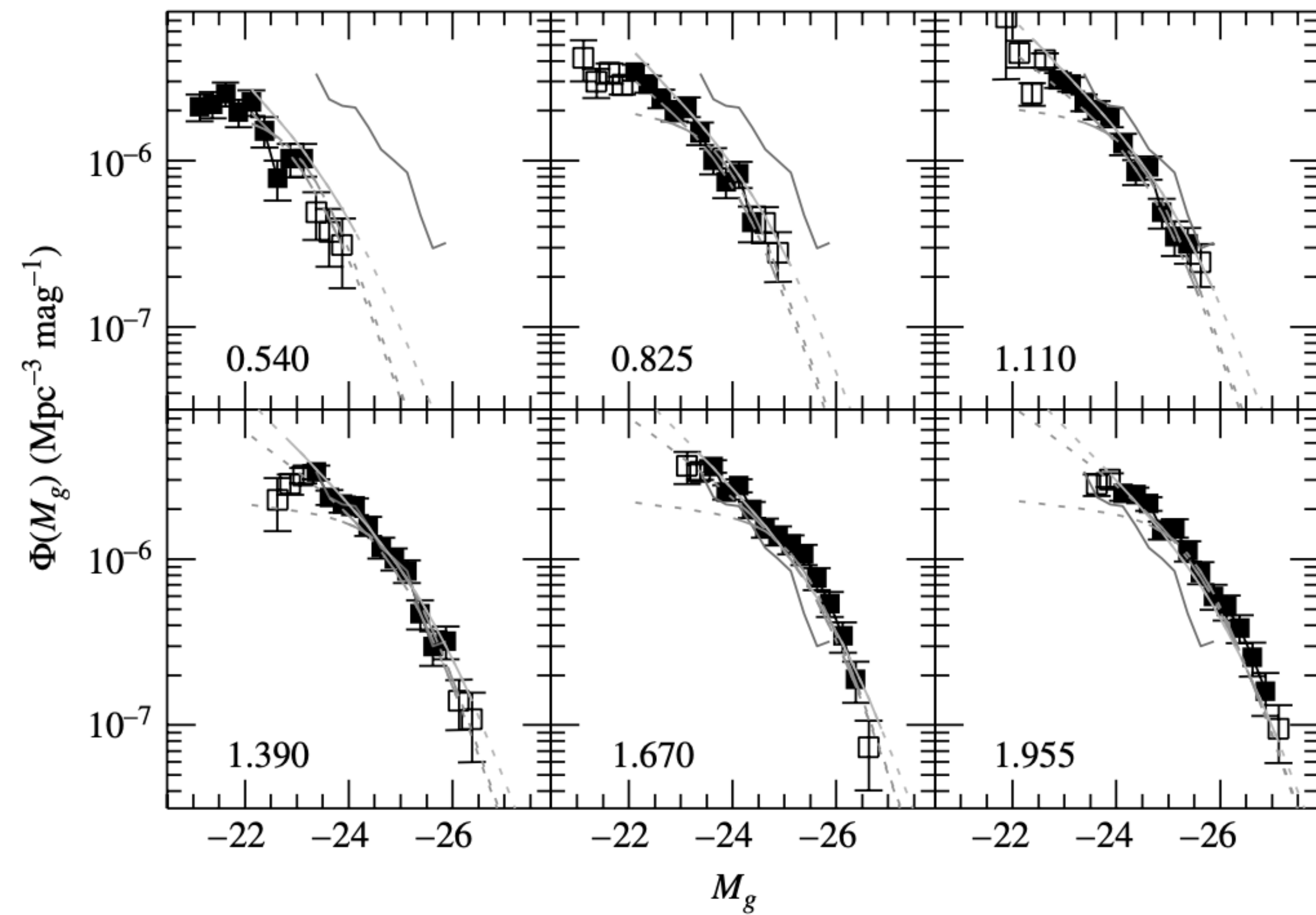


FIGURE 15 Luminosity functions for quasars with different redshifts. The redshifts are indicated in each frame; for instance, in the upper-left-hand frame, $z = 0.540$. The jagged line that is present in every frame (upper right in $z = 0.540$) represents the data for $z = 1.390$. Note that the population is brighter at greater redshifts. Data are from the Sloan Digital Sky Survey (SDSS) and the 2-degree Field survey (2dF) for 5645 quasars. The g band is centered on 480 nm. (Figure adapted from Richards et al., *MNRAS*, 360, 839, 2005.)

Evidence for Quasar evolution

luminosity functions, Φ , for quasars in different redshift intervals, where $\Phi(M_g)$ is the number of quasars per Mpc^{-3} (comoving) that have an absolute magnitude between M_g and $M_g + d M_g$.

Note that for $z < 2$, the curves would overlap if they were shifted horizontally along the M_g -axis. **This indicates that for $z < 2$, the populations of quasars with different redshifts differ only in their luminosities, not in their comoving space densities.**

Then the lack of bright quasars today is an evolutionary effect, caused by a decrease in their luminosities with time.

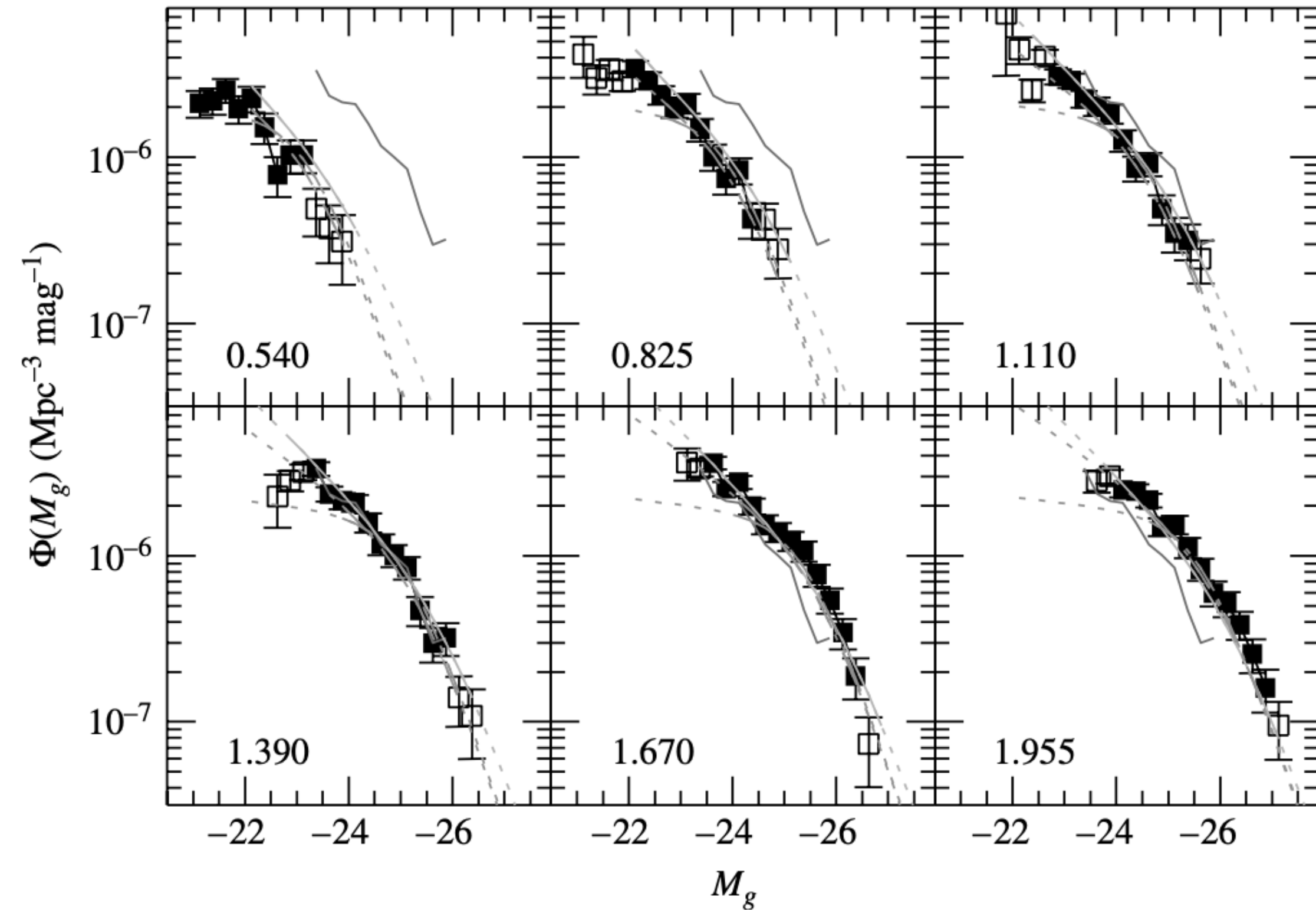


FIGURE 15 Luminosity functions for quasars with different redshifts. The redshifts are indicated in each frame; for instance, in the upper-left-hand frame, $z = 0.540$. The jagged line that is present in every frame (upper right in $z = 0.540$) represents the data for $z = 1.390$. Note that the population is brighter at greater redshifts. Data are from the Sloan Digital Sky Survey (SDSS) and the 2-degree Field survey (2dF) for 5645 quasars. The g band is centered on 480 nm. (Figure adapted from Richards et al., *MNRAS*, 360, 839, 2005.)

Evidence for Quasar evolution

This luminosity evolution of quasars is shown in Fig. 16. Apparently, a picture in which a constant number of quasars grows dimmer as the universe expands is consistent with the observations for $z < 2$.

The situation becomes more complicated between $z = 2$ and $z = 3$.

We can study the birth and evolution of quasars out to $z \sim 6$. Statistical surveys at both optical and X-ray wavelengths show that the comoving space density of AGNs peaks at a redshift of approximately $z \approx 2.5$ and then drops off for $z > 3$.

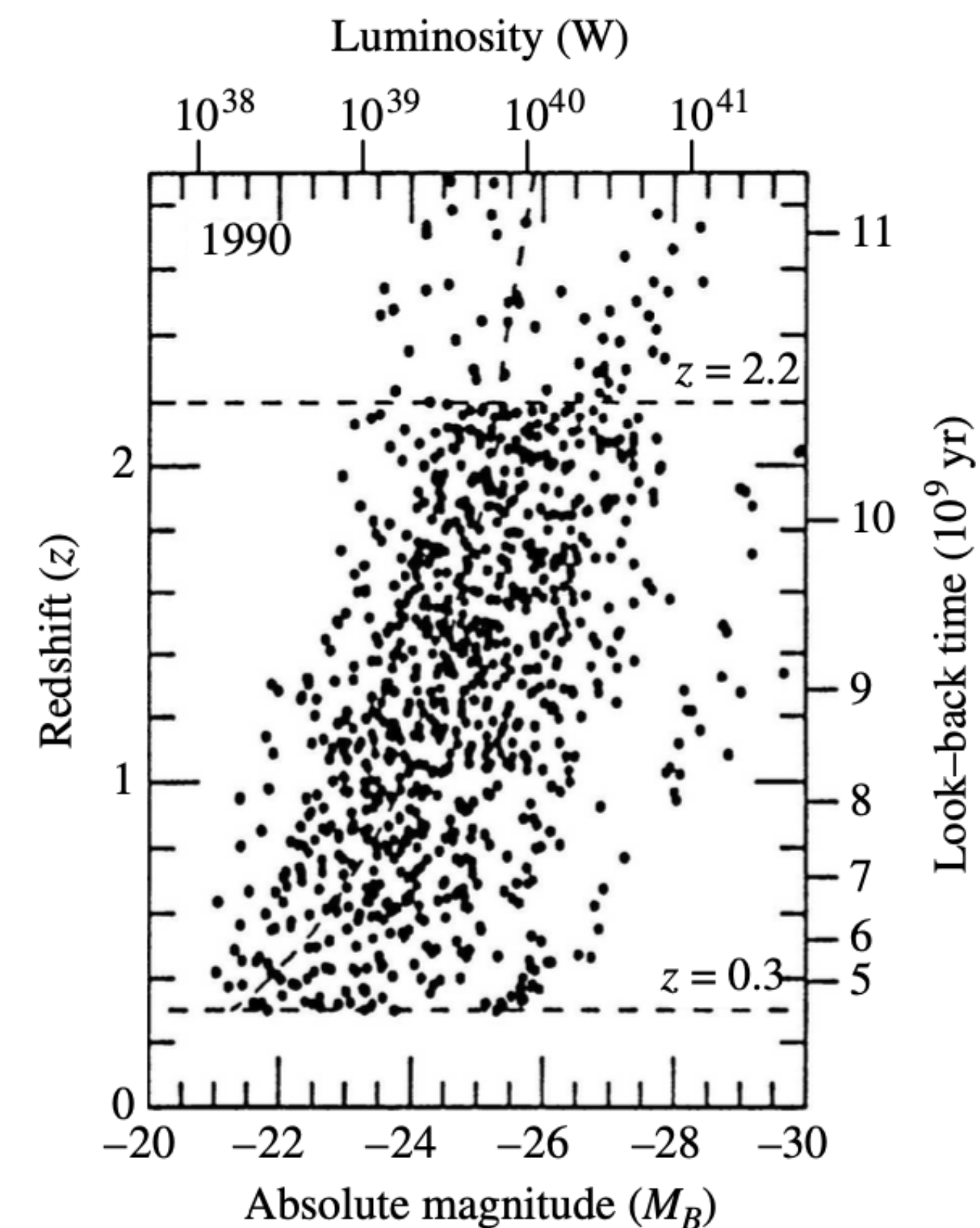


FIGURE 16 The dimming of quasars with time. For $z < 0.3$, there are too few nearby objects to provide an adequate sample for this figure. The empty region at the upper left has not been sampled by observations in this study. (Figure adapted from Boyle, *The Environment and Evolution of Galaxies*, Shull and Thronson (eds.), Kluwer Academic Publishers, Dordrecht, 1993.)

Evidence for Quasar evolution

the comoving space density of AGNs peaks at a redshift of approximately $z \approx 2.5$ and then drops off for $z > 3$; see Fig. 17. These studies indicate that the comoving space density declines by roughly a factor of 10 from its peak value by $z \approx 4$.

This high- z deficit in the number of quasars could reflect a growth phase of supermassive black holes that power the nascent AGN. A well-defined **relationship exists between the mass of a supermassive black hole and the velocity dispersion of the spheroid of a galaxy**, suggesting that **as the mass of the galaxy grows and the velocity dispersion of its spheroid increases, so does the mass of the central supermassive black hole**.

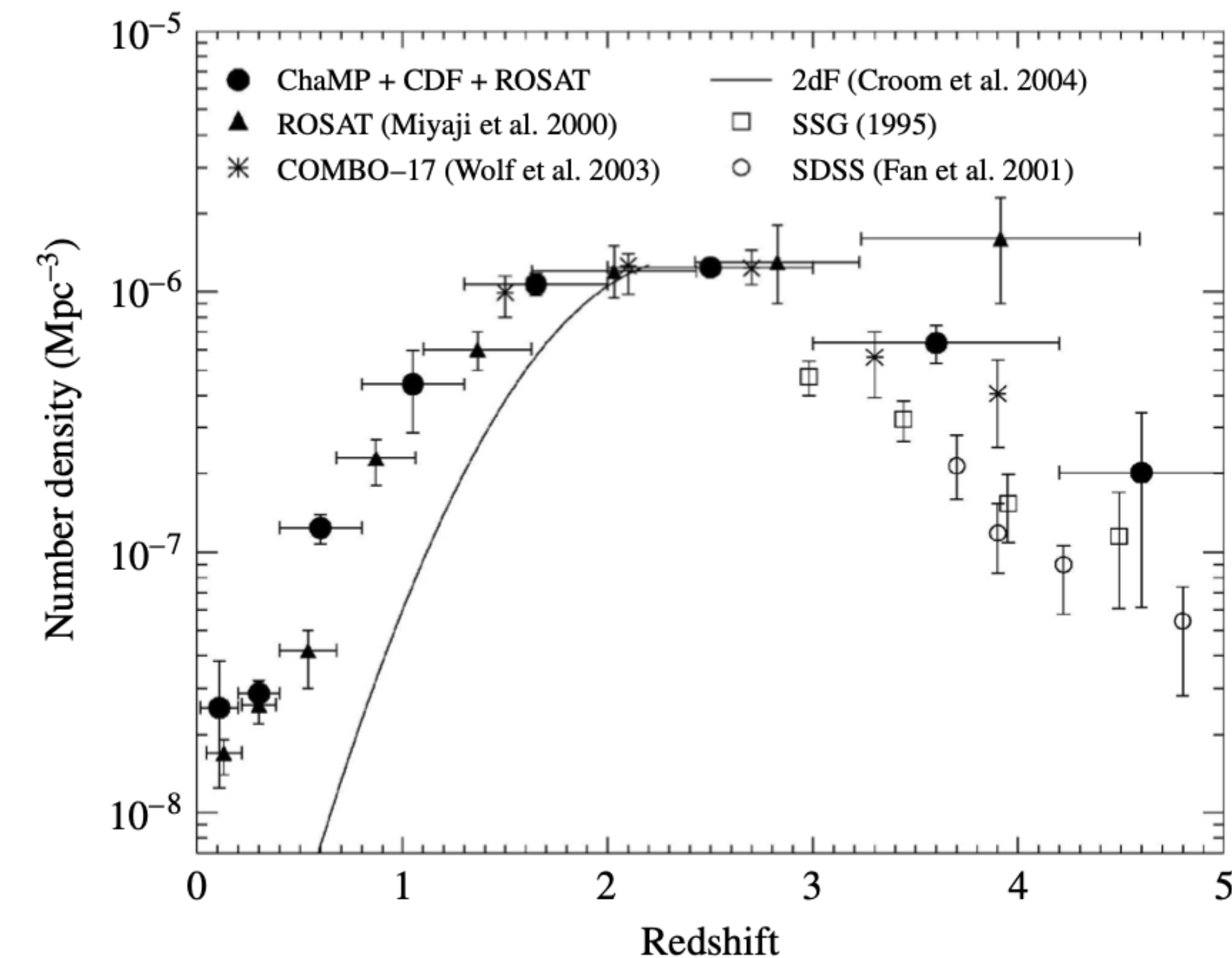


FIGURE 17 The comoving space density of active galactic nuclei (number per cubic megaparsec) as a function of redshift. (Figure adapted from Silverman et al., *Ap. J.*, 624, 630, 2005.)

Evidence for Quasar evolution

There is **evidence, including interactions in observed quasars**, suggesting that an individual quasar “event” lasts only for a galactic dynamical timescale (the dynamical timescale, essentially the characteristic free-fall or orbital time).

Figure 18 shows the quasar PKS 2349–014 and a companion galaxy about the size of the LMC (the small bright spot just above the quasar). The thin curved wisps that almost surround the quasar are probably the result of a tidal interaction between the quasar and the companion galaxy. The companion is so close that it will probably merge with PKS 2349–014 in the near future.

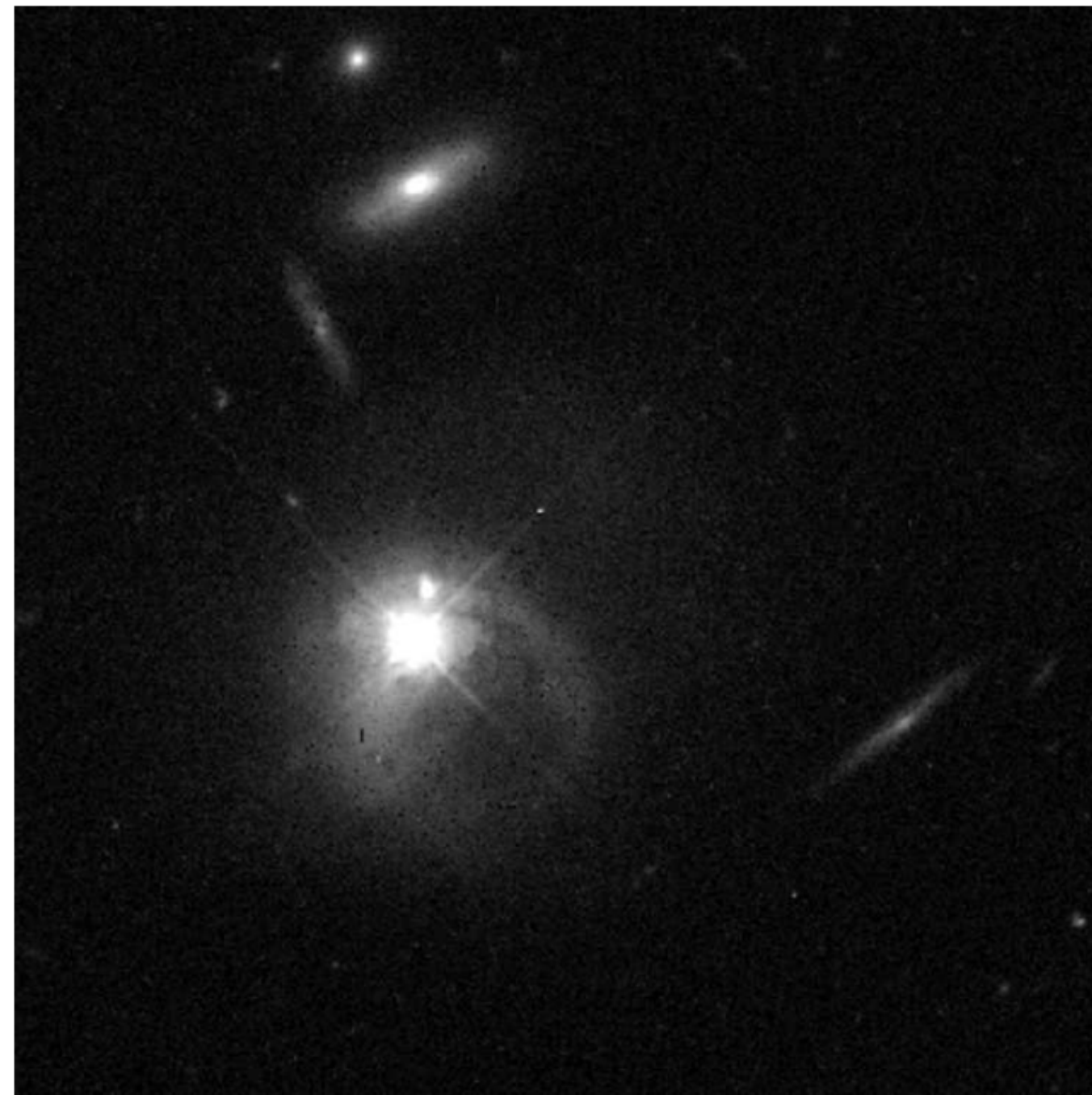
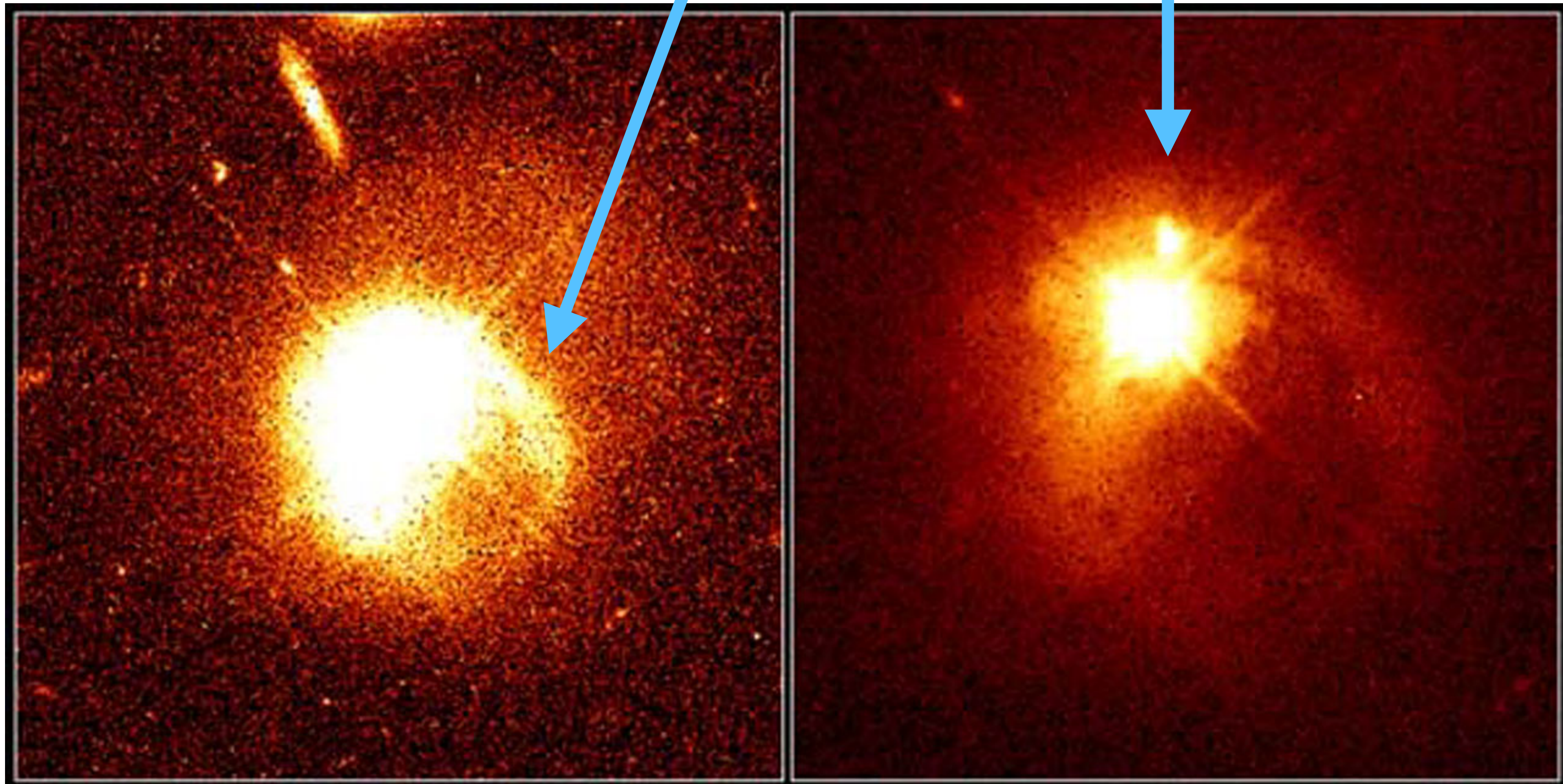


FIGURE 18 The quasar PKS 2349–014 in a gravitational interaction with a companion galaxy. (Figure from Bahcall, Kirhakos, and Schneider, *Ap. J. Lett.*, 447, L1, 1995. Courtesy of J. Bahcall, Institute for Advanced Study, NASA.)

Evidence for Quasar evolution

Zoom in on the previous image.



Quasar PKS 2349

PRC96-35b • ST Scl OPO • November 19, 1996

J. Bahcall (Institute for Advanced Study), M. Disney (University of Wales) and NASA

Companion galaxy

Tidal features

Evidence for Quasar evolution

In 2003, an extensive study of the morphology of the host galaxies of 33 radio-loud quasars, radio-quiet quasars, and radio galaxies in the redshift band $0.1 < z < 0.25$. The study was conducted by using the Hubble Space Telescope in combination with VLA radio imaging. The research team was able to conclude that **all of the galaxies in their sample associated with radio-loud quasars or radio galaxies are massive ellipticals. Of the 13 radio-quiet quasars in the sample, 9 are hosted by massive ellipticals while the remaining 4 are in disk/bulge systems.**

Of the 4 disk/bulge systems, the luminosities of 2 of them are dominated by their bulge components, implying that **11 of the 13 radio-quiet quasars (or ~ 85%) are associated with galaxies that are predominantly spheroidal.**

In addition, the 2 disk-dominated galaxies are the sites of the lowest-luminosity AGNs in the sample by far, and they may be more appropriately considered Seyfert 2 galaxies. From the systems investigated in this study, it appears that all of the true quasars and radio galaxies in the sample are hosted by massive ellipticals that are nearly indistinguishable from lower-z quiescent **galaxies typically found near the centres of rich clusters.**

Evidence for Quasar evolution

The study also revealed that all of the radio-loud quasars contained central supermassive **black holes of at least $10^9 M_\odot$** and that the radio-quiet quasars contained black holes with masses in excess of **$5 \times 10^8 M_\odot$** .

It appears from this work that **radio-loud systems are much less abundant than radio-quiet systems** (10% vs. 90%) simply because the **radio-loud systems require more massive central black holes** to power the strong radio energy emission. However, although the investigation did find a broad correlation between increasing black hole mass and increasing radio luminosity, **the most luminous radio sources cannot be attributed to black hole mass alone**. Black hole rotation also may be required to power the strongest radio sources.

In a second, statistical study of 12,698 quasars with redshifts in the range $0.1 < z < 2.1$, considered the evolution of black hole masses with increasing redshift. They found that **black hole masses sufficient to power quasars were in place by $z \sim 2$** . They further determined that all of the central black holes had masses in the range $10^7 M_\odot < M_{bh} < 3 \times 10^9 M_\odot$, where the upper limit corresponds to the most massive black holes yet found in the local universe (specifically, in M87 and Cygnus A).

The SDSS quasar study was also able to point out that quasar **bolometric luminosities increase steadily with redshift** from roughly $0.15L_{Ed}$ at $z \sim 0.2$ to $0.5L_{Ed}$ at $z \sim 2.0$, where L_{Ed} is the Eddington luminosity. It is also evident from the data that the **Eddington luminosity limit remains valid at the high-z end of the study**.

Evidence for Quasar evolution

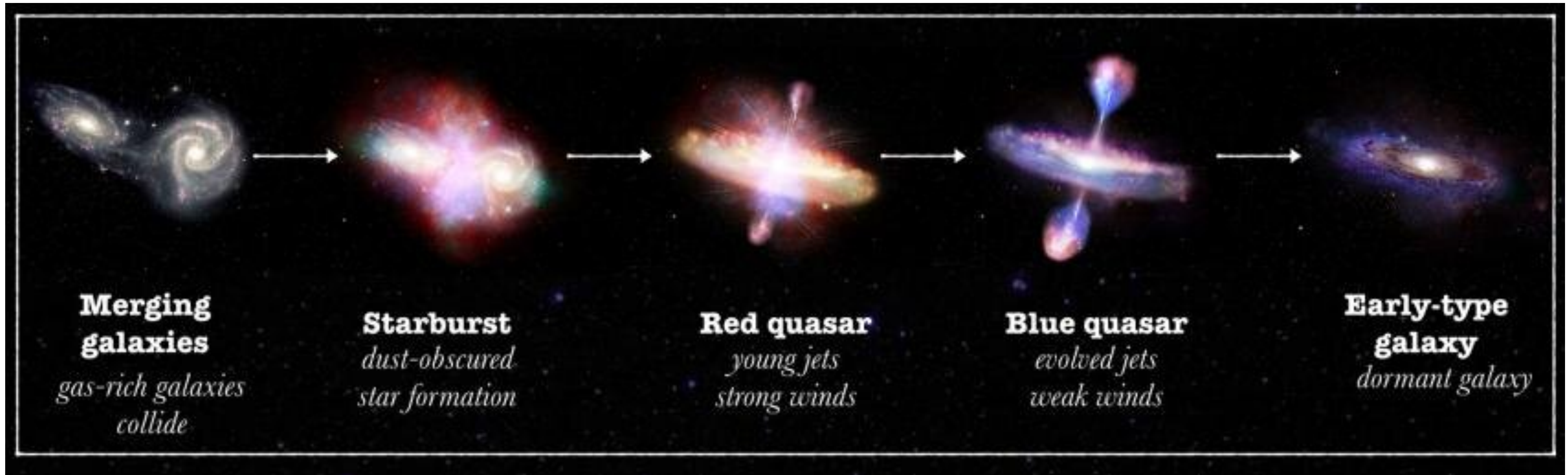
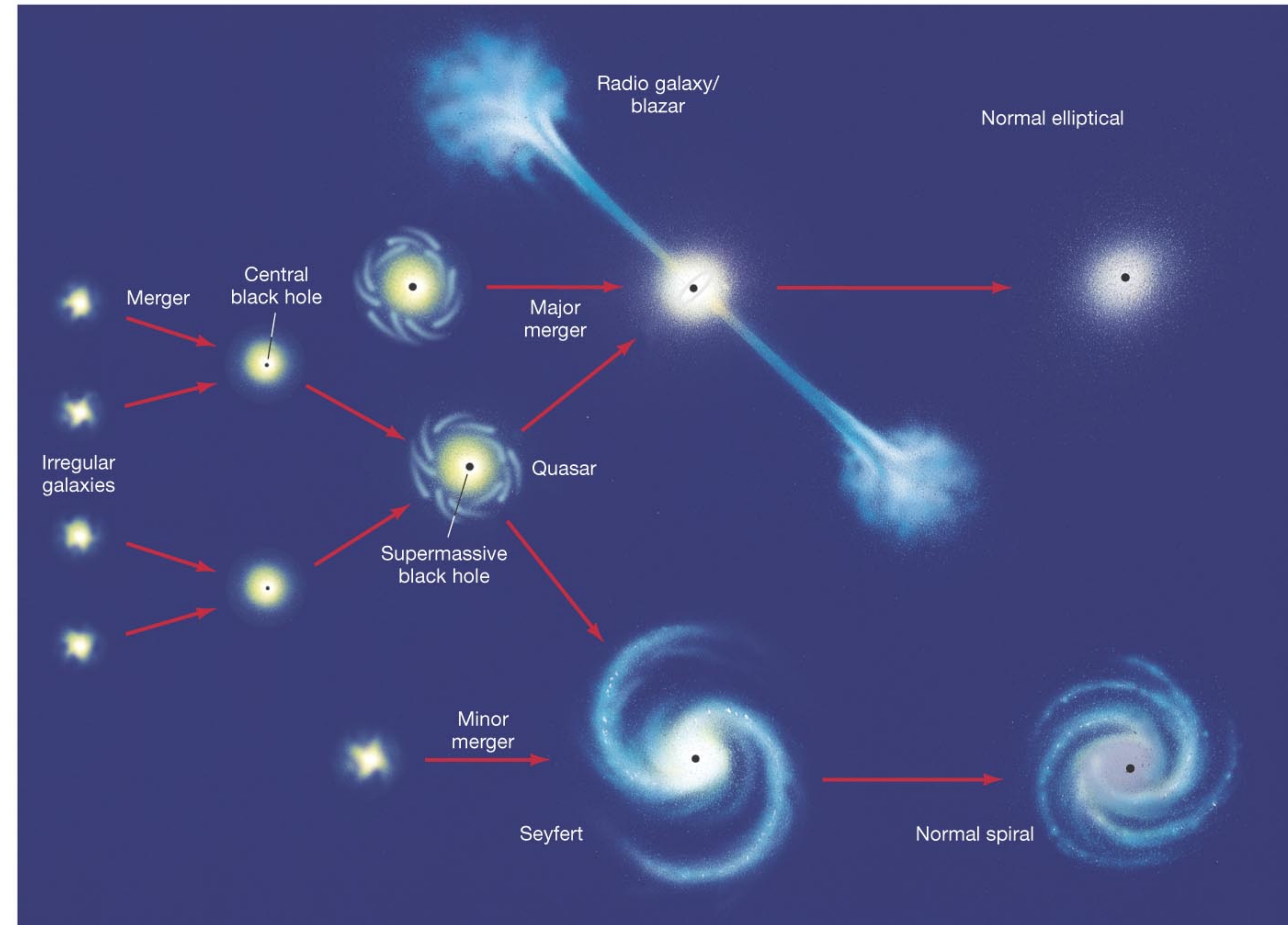


Illustration on how galaxy mergers can trigger starburst and quasar activity.

Evidence for Quasar evolution

Illustration of a possible scenario:

- Major mergers producing radio galaxies and
- minor mergers producing Seyfert galaxies



AGN variability

The energy produced by many of the AGNs discussed above (excluding NLRGs and Seyfert 2s) **can vary on short timescales**. The luminosity of the broad emission lines and continuum of some Seyfert 1 galaxies and quasars can change by a **factor of 2 within a few months, weeks, or even days**, although there is little or no corresponding variation in the narrow lines.

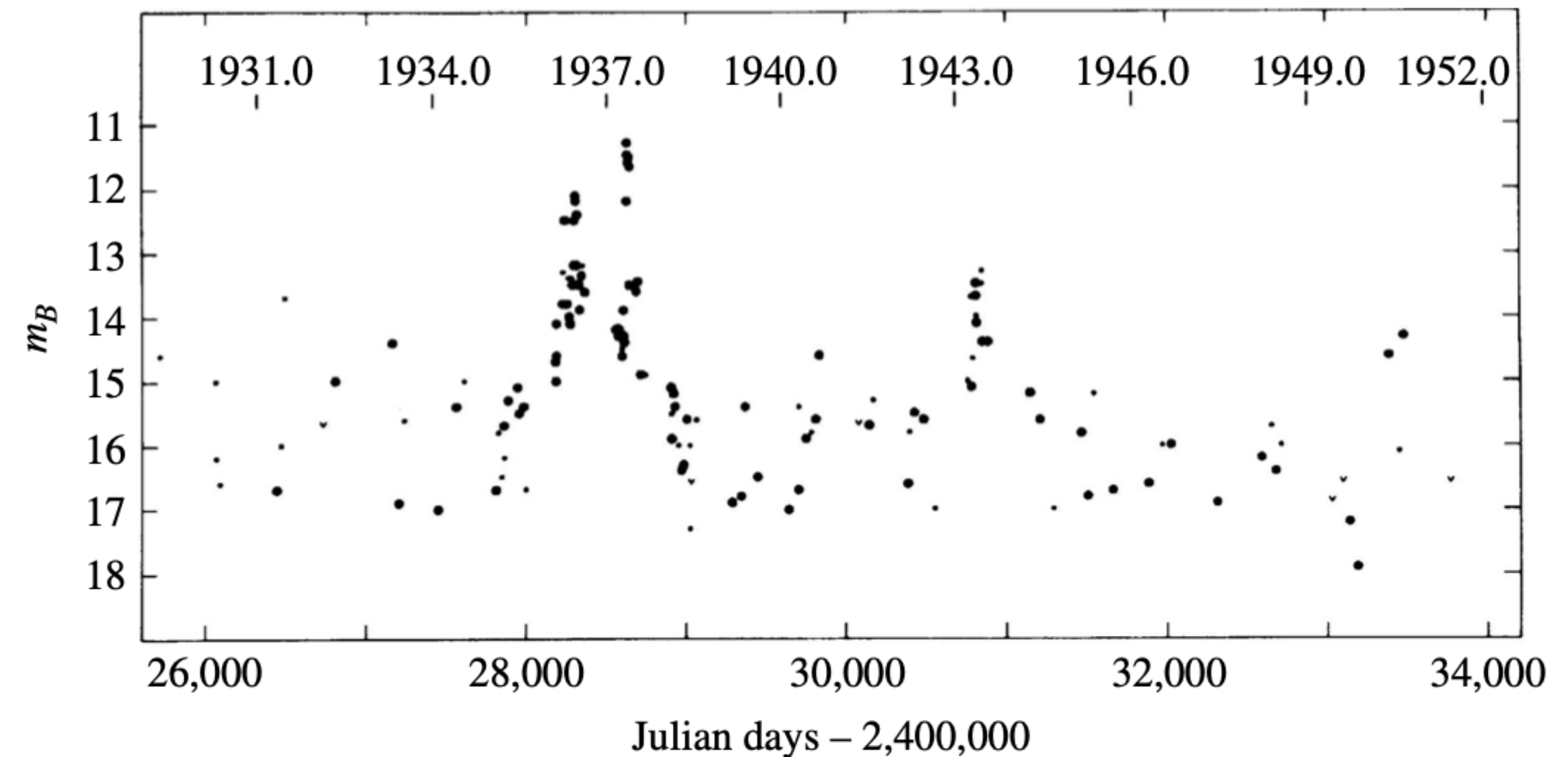


FIGURE 19 The variation in the apparent magnitude of the quasar 3C 279, based on an examination of archival astronomical photographs. (Figure adapted from Eachus and Liller, *Ap. J. Lett.*, 200, L61, 1975.)

AGN variability

The variation in broad emission lines typically lags behind the continuum variation over similar timescales. There are also variations of a few percent in the visible and X-ray output of Seyfert 1s and quasars on timescales as short as a few minutes, with X-ray fluctuations typically the most rapid. At the other end of the scale, **there may be changes of a longer duration.**

For example, Fig. 19 shows that around the year 1937, the quasar 3C 279 brightened by a factor of 250 at visible wavelengths during an outburst that lasted for several years.

Small scale variation -> small region of emission

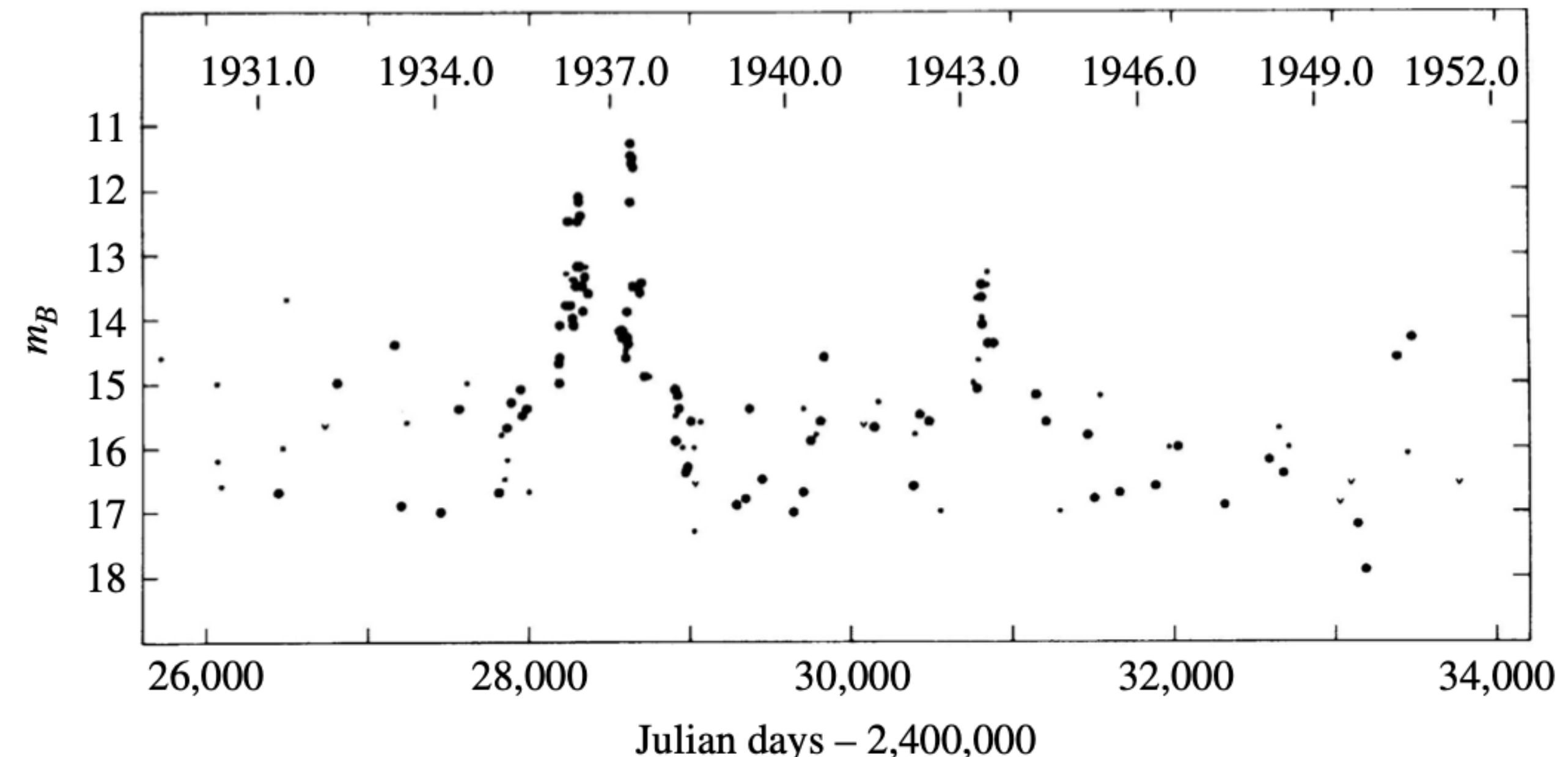


FIGURE 19 The variation in the apparent magnitude of the quasar 3C 279, based on an examination of archival astronomical photographs. (Figure adapted from Eachus and Liller, *Ap. J. Lett.*, 200, L61, 1975.)

Polarisation

Quasars typically show **low degrees of polarization**. At visible wavelengths, the degree of **linear polarization** is usually less than 3% for both radio-quiet and radio-loud objects, although it **may reach up to 35%** polarization for a few objects.

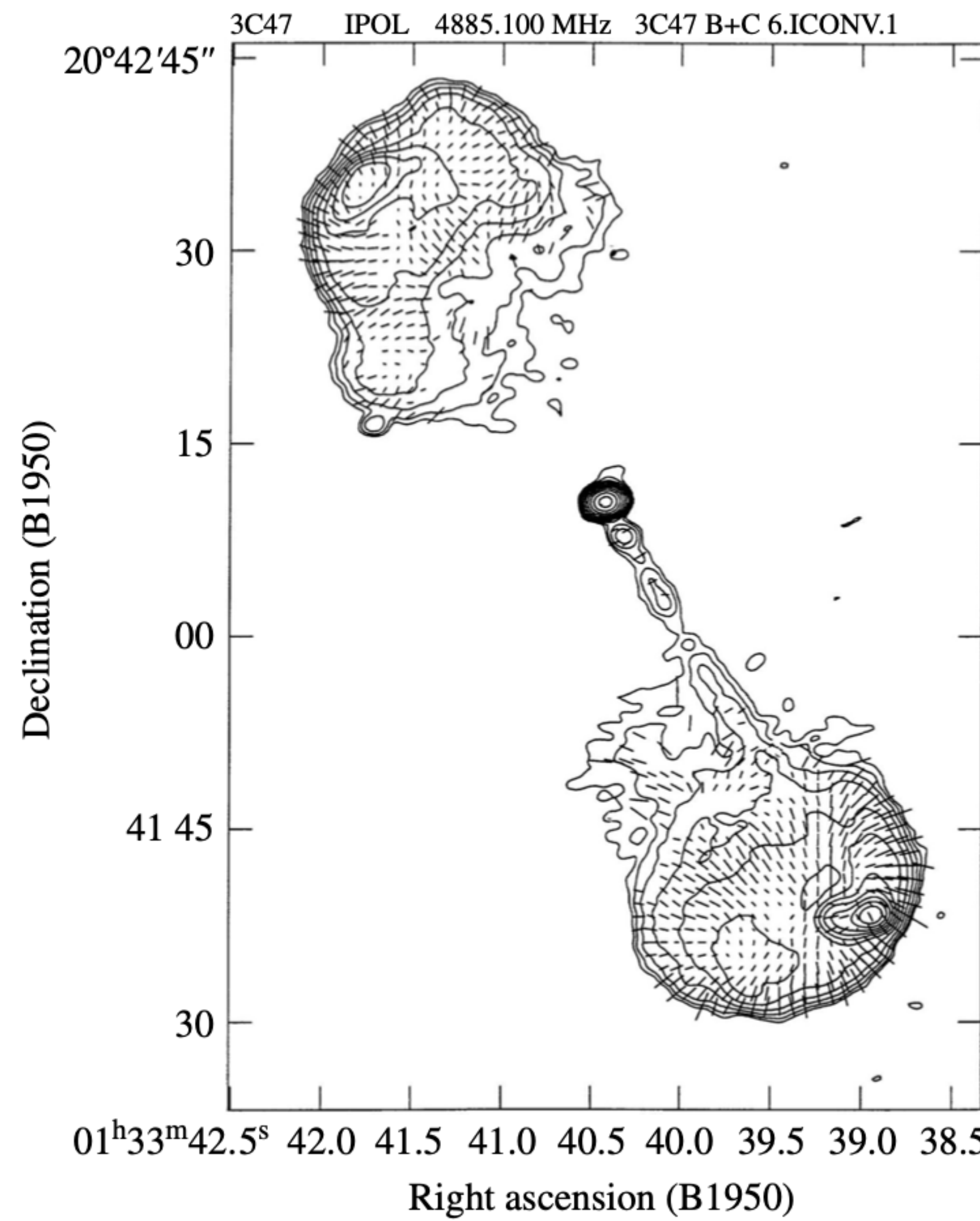


FIGURE 20 Polarization mapping of the magnetic field of the quasar 3C 47. Both lobes are highly polarized. (Figure adapted from Fernini et al., *Ap. J.*, 381, 63, 1991.)

Polarisation

The radio emission from high-polarization quasars comes mostly from a compact core; such quasars are called **core-dominant radio sources** (and also **compact sources**). These quasars are less polarized at radio wavelengths than the **lobe-dominant sources**, which may **reach up to 60% linear polarization**. The degree of **linear polarization of AGN radio jets is typically 40% but may exceed 50% within a small region**. (Synchrotron radiation is highly linearly polarized. The lower polarization of the core-dominant sources is probably due to synchrotron self-absorption.)

Figure 20 shows the orientation of the magnetic field of the quasar 3C 47, as obtained from polarization measurements.

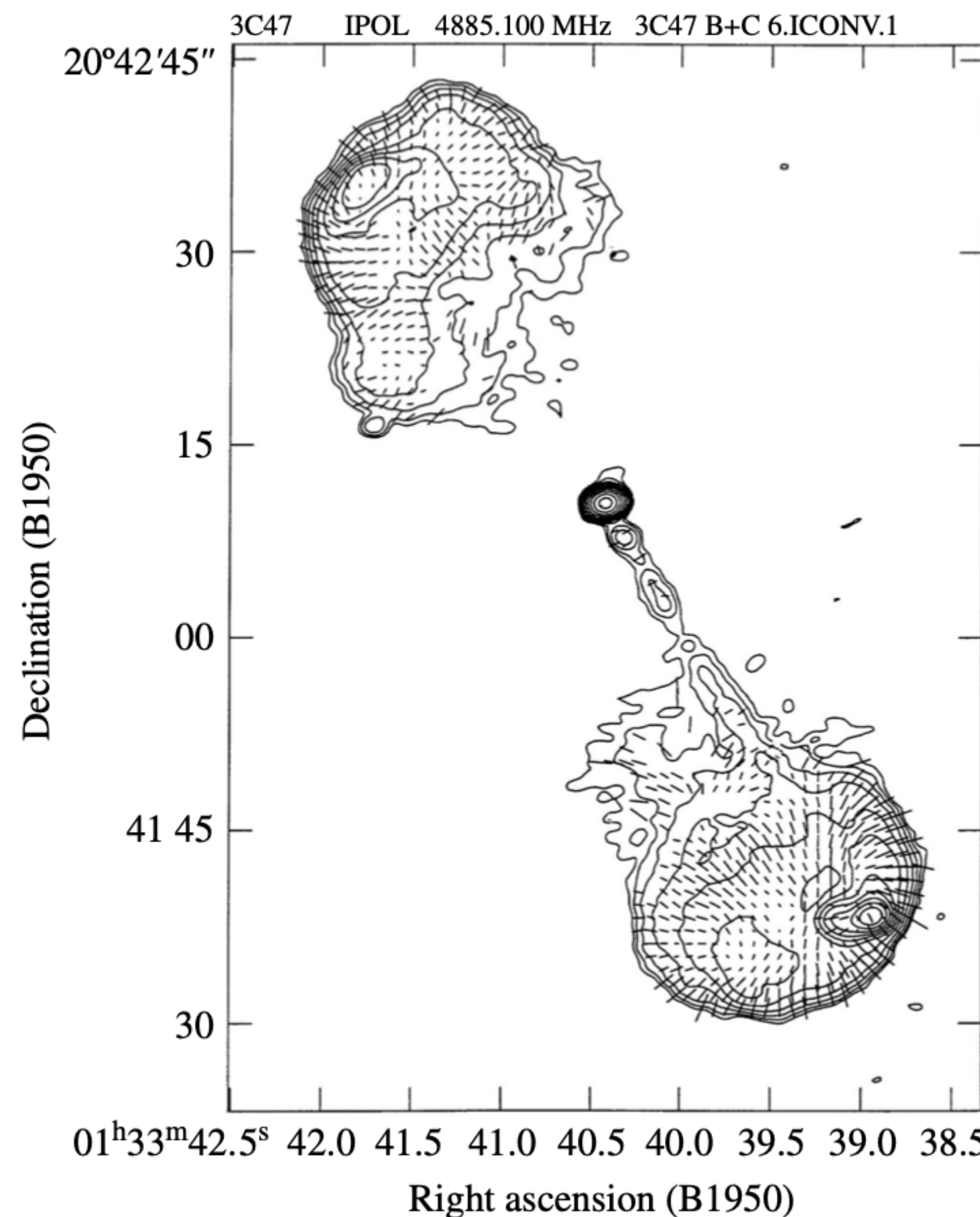


FIGURE 20 Polarization mapping of the magnetic field of the quasar 3C 47. Both lobes are highly polarized. (Figure adapted from Fernini et al., *Ap. J.*, 381, 63, 1991.)

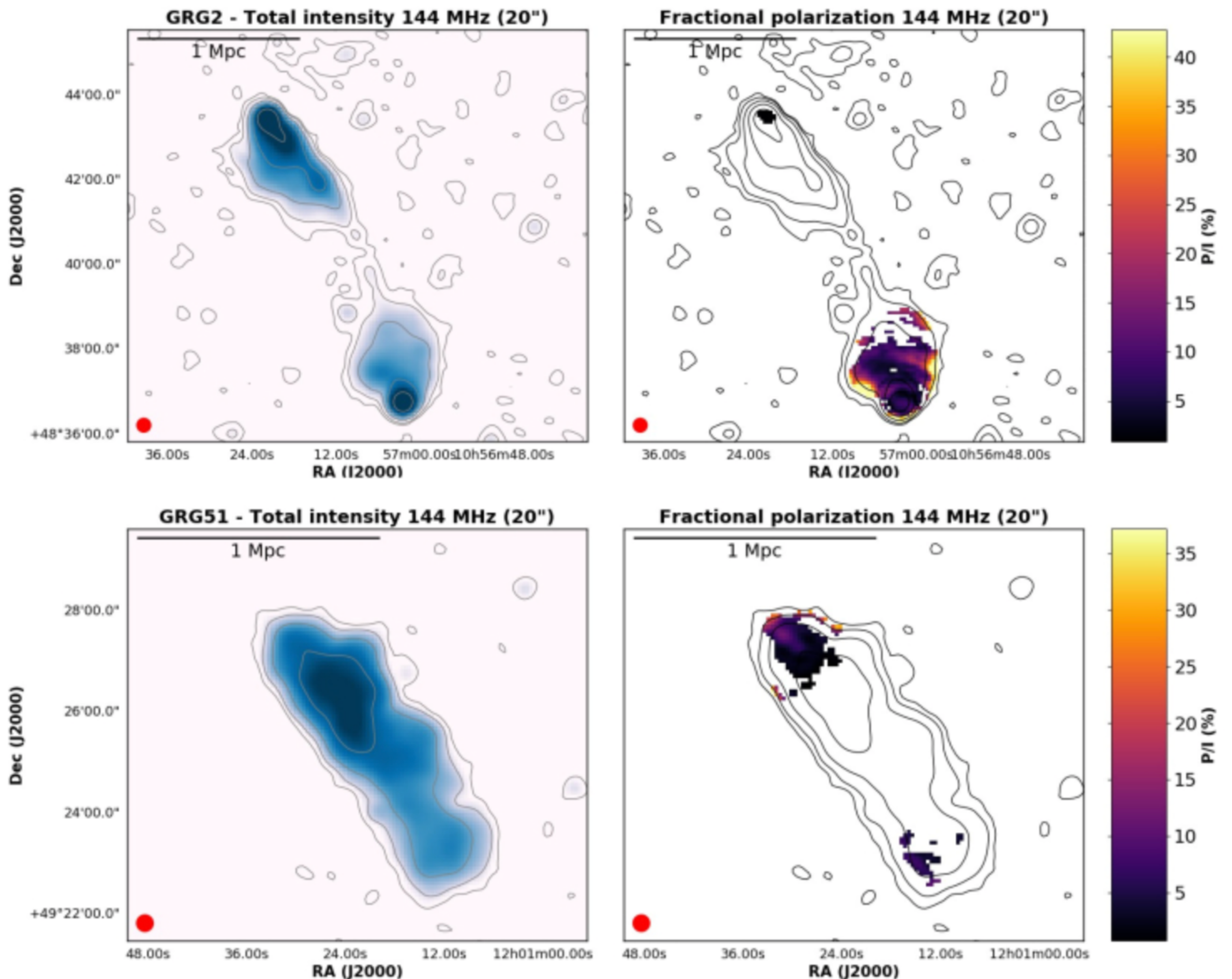
Polarisation

Giant radio galaxies are formed from relativistic jets of matter and energy, emanating from the central regions of active galactic nuclei.

Synchrotron radiation is often polarized, from the radio jets and lobes of these objects.

The low-energy electrons responsible for the low-frequency emission can propagate large distances from their origins in the central core or lobe hot spots, and large radio cocoons are expected to surround many objects.

The figure shows two giant radio galaxies observed by the LOFAR telescope. The right hand side shows the fractional polarization of the radio lobes.



Using the polarization properties of a sample of giant radio galaxies (i.e. sources with a physical size of about 1 Mpc) we probed intergalactic magnetic fields outside galaxy clusters. ([Stuardi et al. 2020](#))

Fanaroff-Riley Luminosity classes

FR I - NGC 1265
The centre is the brightest

In 1974, B. L. Fanaroff and J. M. Riley suggested that the radio-loud AGNs could be categorized into **two general luminosity classes**.

- **Class I objects:** those for which the ratio of the distance between the brightest spots of radio emission on either side of the centre (excluding the central source) to the full extent of the radio source is less than 0.5;
- **Class II objects:** have a ratio greater than 0.5.

FR II - Cyg A: the **two ends are the brightest**



Fanaroff-Riley Luminosity classes

FR I - NGC 1265
The centre is the brightest

FR I sources have diminishing radio luminosity with increasing distance from the center of the jets,

while FR IIs tend to be most radio-bright at the ends of the lobes.

It is also common that FR I galaxies have two **recognizable radio jets**, while FR II galaxies often exhibit only a single identifiable jet (the counterjet is either very weak or undetectable). Furthermore, **FR I galaxies may have curved jets**, while FR II jets tend to be straight.

FR II - Cyg A: the two ends are the brightest



Fanaroff-Riley Luminosity classes

FR I - NGC 1265
The centre is the brightest

There is also a rather clear demarcation between FR I and FR II classes in terms of the specific luminosity. Sources having a specific luminosity at **1.4 GHz of less than $10^{25} \text{ W Hz}^{-1}$ are identified as FR Is**, and those with greater specific luminosities are inevitably classified as FR IIs.

FR II - Cyg A: the two ends are the brightest



Blazars

The properties of **rapid variability** and a **high degree of linear polarization at visible wavelengths** define the class of AGNs known as **blazars**.

A blazar is an active galactic nucleus (**AGN**) with a **relativistic jet directed very nearly towards an observer**. **Relativistic beaming** (relativistic Doppler effect + relativistic aberration) of electromagnetic radiation from the jet makes blazars **appear much brighter** than they would be if the jet were pointed in a direction away from Earth.

Blazars are powerful sources of emission across the electromagnetic spectrum and are observed to be sources of **high-energy gamma ray photons**. Blazars are **highly variable sources**, often undergoing rapid and dramatic fluctuations in brightness on short timescales (hours to days). Some blazar jets appear to exhibit superluminal motion, another consequence of material in the jet traveling toward the observer at nearly the speed of light.

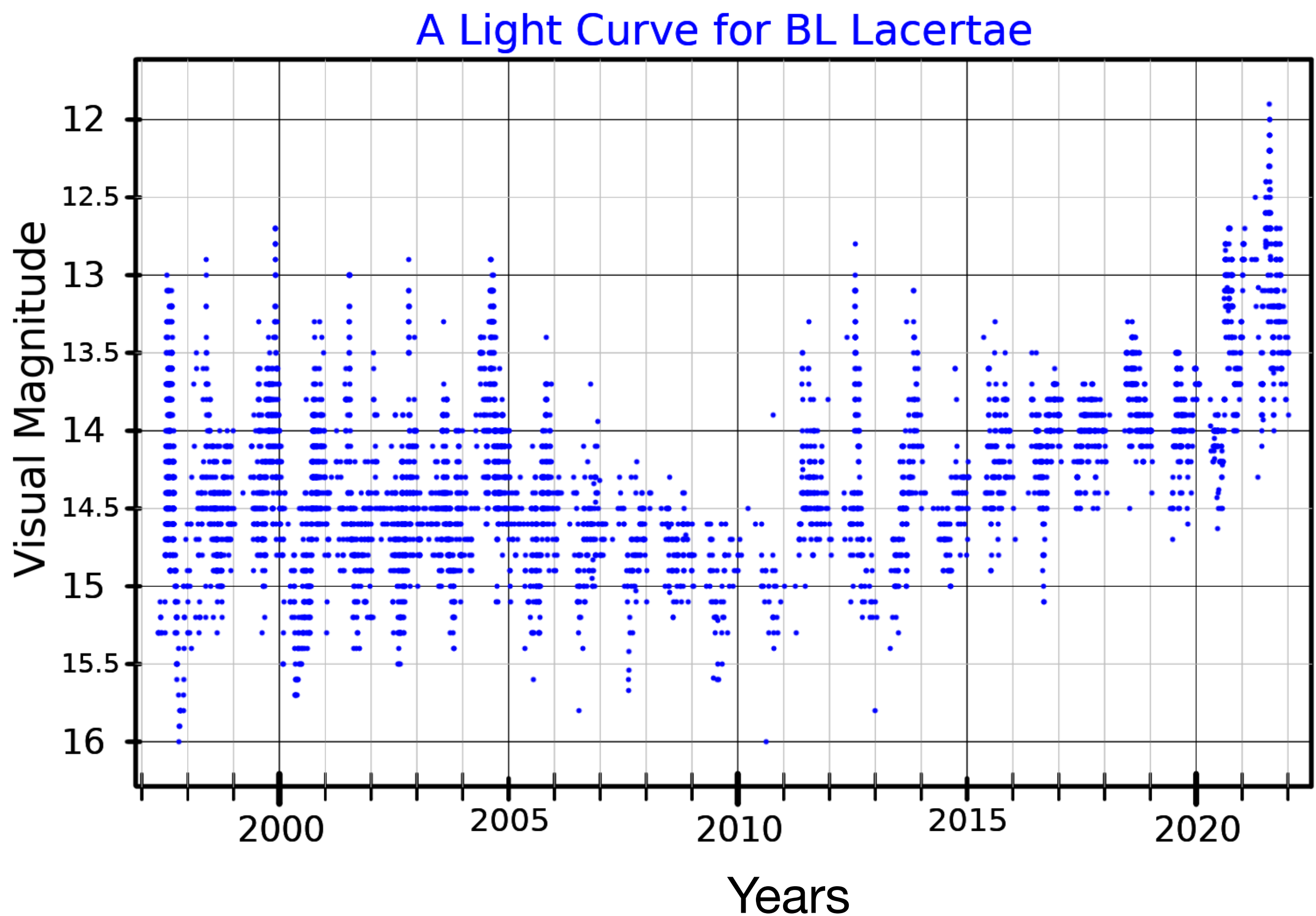
The blazar category includes BL Lac objects and optically violently variable (OVV) quasars.

Mrk 421



Blazars

The most well-known object in this class is **BL Lacertae**, found in the northern constellation of Lacerta (the Lizard). BL Lac was **originally classified as a variable star** because of its irregular variations in brightness; hence the variable star type of designation. In a week's time BL Lac would double its luminosity, and it would change by a factor of 15 as the months passed. But although BL Lac has a stellar appearance, **its spectrum shows only a featureless continuum with very weak emission and absorption lines**. Careful observations reveal that the bright, starlike nucleus of BL Lac is surrounded by a fuzzy halo that has a spectrum similar to that of an **elliptical galaxy**.



Blazars

BL Lac objects are a **subclass of blazars** that are characterized by their **rapid timevariability**. Remarkably, their luminosities may change by up to 30% in just 24 hours and by a factor of 100 over a longer time period. BL Lacs are also distinguished by their strongly **polarized power-law continua** (30–40% linear polarization) that are **nearly devoid of emission lines**.

However, observations of a few faint spectral lines have revealed **high redshifts**, so that, like quasars, BL Lacs are at cosmological distances. Of those BL Lacs that have been resolved, about **90%** appear to reside in **elliptical galaxies**. Joining the BL Lac objects in the blazar classification are the **optically violently variable quasars** (OVVs). They are similar to the BL Lacs except that they are typically much more luminous, and their spectra may display broad emission lines.

M94

LINERs

A final class of objects worth mentioning consists of the so-called **Low Ionization Nuclear Emission-line Regions (LINERs)**. These galaxies have very **low luminosities in their nuclei**, but with fairly **strong emission lines of low-ionization species**, such as the forbidden lines of [O I] and [N II]. The spectra of LINERs seem **similar to the low-luminosity end of the Seyfert 2 class**, and LINER signatures are **detected in many** (perhaps a majority of) **spiral galaxies** in high-sensitivity studies. These low-ionization lines are **also detectable in starburst galaxies and in H II regions**, and so it is unclear whether LINERs truly represent a low-luminosity limit of the AGN phenomena.



M104



Summary of AGN

TABLE 1 A Summary of AGN Classes.

| Class | Sub-class | Description |
|----------------|-------------------|---|
| Seyferts | Type 1 | broad and narrow emission lines, weak radio emission, X-ray emission, spiral galaxies, variable |
| | Type 2 | narrow emission lines only, weak radio emission, weak X-ray emission, spiral galaxies, not variable |
| Quasars | Radio-loud (QSR) | broad and narrow emission lines, strong radio emission, some polarization, FR II, variable |
| | Radio-quiet (QSO) | broad and narrow emission lines, weak radio emission, weak polarization, variable |
| Radio Galaxies | BLRG | broad and narrow emission lines, strong radio emission, FR II, weak polarization, elliptical galaxies, variable |
| | NLRG | narrow emission lines only, strong radio emission, FR I and FR II, no polarization, elliptical galaxies, not variable |
| Blazars | BL Lacs | almost devoid of emission lines, strong radio emission, strong polarization, rapid variability, 90% in ellipticals |
| OVV quasars | | broad and narrow emission lines, strong radio emission, strong polarization, rapid variability, much more luminous than BL Lacs |
| ULIRGs | | possibly dust-enshrouded quasars, alternatively may be starburst phenomena |
| LINERs | | similar to low-luminosity Seyfert 2, low-ionization emission lines, in many (perhaps majority of) spiral galaxies, alternatively may be starburst phenomena or H II region emission |